CRANFIELD UNIVERSITY

J HOWARD

SUB-IDLE MODELLING OF GAS TURBINES: ALTITUDE RELIGHT AND WINDMILLING

SCHOOL OF ENGINEERING

Eng.D THESIS

CRANFIELD UNIVERSITY

J HOWARD

SUB-IDLE MODELLING OF GAS TURBINES; ALTITUDE RELIGHT AND WINDMILLING

SCHOOL OF ENGINEERING

Eng.D THESIS

CRANFIELD UNIVERSITY

SCHOOL OF ENGINEERING

Eng.D THESIS

2003-2007

J HOWARD

Sub-Idle Modelling of Gas Turbines; Altitude Relight and Windmilling

Supervisors: Prof. P. Pilidis (School of Engineering),
G. Clarke (School of Management)
Industrial Supervisors: Mr. A. Rowe (Rolls-Royce plc)
Dr. P. Naylor (Rolls-Royce plc)

5th October 2007

This thesis is submitted in partial fulfilment of the requirements for the Degree of Engineering Doctorate.

Abstract

Gas turbine sub-idle performance modelling is still in an early development stage and this research aims to provide and improve present techniques, for modelling of windmilling and transient windmilling relights, through to groundstart simulations. Engine ATF data was studied and used to align models created within this research for low and high bypass engines, and compare these models simulation results.

Methods for the extrapolation of component characteristics are improved and performed in linearised parameter form, and the most efficient approach discussed.

The mixer behaviour is analysed and recommendations of off-design mixer behaviour representation in a sub-idle model are proposed and performed within the modelling.

Combustion at sub-idle conditions is investigated with regards to the loading parameter definition, and also its representation for the influence of evaporation rate being limiting to overall combustion efficiency. A method is proposed on extrapolating and representation of the combustion characteristic.

Compressor behaviour and the blade torques at locked rotor and windmilling conditions are studied using 3D CFD, producing insight and discussion on CFD suitability and what it can offer at these operating conditions. From the CFD studies generic loss coefficients were created for all compressor blades, from which a zero speed is created for the whole compressor, from a theoretical stage stacking calculation. This zero-speed curve is shown to allow interpolation of component characteristics to the sub-idle region, improving the definition and a predictive approach. A windmilling conditions cascade test rig is proposed, designed and built for validating the CFD loss coefficients.

The findings and discussions within this thesis provide useful reference material on this complicated and little documented area of research. The modelling and methods proposed, provide great advancement of the research area, along with further integration of the Cranfield UTC in performance with Rolls-Royce.

Table of Contents

List of figures

List of tables

Acknowledgements

The funding of this research has been jointly from Rolls-Royce and Engineering and Physical Sciences Research Council, therefore my thanks and appreciation, whom without, this research would not have been possible.

The research itself and the period has been such a large and diverse undertaking, it has enveloped a large wealth of people. Therefore there are many people to thank for their support.

For his guidance, understanding and advice throughout the research, my greatest thanks goes to my academic supervisor Prof. Pilidis. Also I would like to thank Dr Ramsden, Prof. Singh and Mr Hales for their support and invaluable advice.

Within Rolls-Royce my special thanks goes to my industrial supervisors Arthur Rowe and Stephen Brown for their time and continued advice, with the all important technical direction. My thanks to Phil Naylor, for his continued friendship and support, John Keen and Owen Cumpson for their help and valued assistance in developing the modifications to the Sub-idle code. I have many thanks to people within Rolls-Royce who have devoted time for conversations and or providing me very needed data to continue my research, so my thanks go out to, Richard Tunstall, Phil Curnock, Dave Lambie, Fran Bragg, Andy Stewart, and Martin Cox. I would like to thank Stephen Harding and Marco Zedda for their interest and support in providing combustion data.

I would like to thank my parents and my sister for their continued support and their understanding.

My friends, without which I would either had gone mad without someone their to listen to my ranting of ideas and just support as friends, so thanks to Alessandro, Marco, Phil, Robin, Kevin, Karl, Greg, Frank, Marco, Pavlos, Vassilios, Arjun, Bobby, and Adam.

Nomenclature

A	Area (in^2 or m^2)
ATF	Altitude Test Facility
B	Mass Transfer number
BD19	A gas turbine sub-idle simulation model
BDD	Basic Design Data
C	Velocity (m/s)
C_p	Coefficient of Specific Heat, at constant pressure (kJ/kg.K)
Comb	Combustion
D, d	Diameter (m)
Eta	Efficiency
ESS	Engine Section Stator {core duct stator at entry to IPC or HPC)
FAR	Fuel Air Ratio
FADEC	Full Authority Digital Electronic Control
H	Total Enthalpy (chu/lb.K)
HP	High Pressure
HPC	High Pressure Compressor
I	Inertia
IP	Intermediate Pressure
IPC	Intermediate Pressure Compressor
ISA	International Standard Atmosphere
Isen	Isentropic
k	Thermal conductivity
K	Pressure loss constant
LP	Low Pressure
LPC	Low Pressure Compressor
$\dot{m}$	Mass flow (kg/s, lb/s)
M	mean
Mn	Mach number
MTO	Maximum Take Off

n	Number of blades
N	Rotational speed (rpm)
NGV	Nozzle Guide Vane
OGV	Outlet Guide Vane
p	static pressure (psia)
P	Total Pressure (psia)
PR	Pressure Ratio
Q	Flow Function
R, r	Radius (m), square root
Re	Reynolds Number
Rho	Density (kg/m^3)
S	space of pitch (m)
SFC	Specific Fuel Consumption (kg/h.N)
SLS	Sea Level Static
SMD	Sauter Mean Diameter (m)
SMPR	Static Mixer Pressure Ratio
t	time (s), Static temperature (K)
T	Total temperature (K)
V	Velocity (m/s)
W	mass flow (kg/s, lb/s)

Symbols

α	Air Angle (degrees)
β	Blade angle (degrees), Beta line
Δ	Delta
η	Efficiency
γ	Ratio of Specific Heats
ρ	Density (kg/m^3)
θ	Combustion Loading parameter
$\bar{w}$	Mean total pressure loss

ω	radians

Subscripts

a	Axial
A	Area (m^2, in^2)
b	Blade
c	Combustor
F	Fuel
g	Gas
p	Polar moment
ref	reference or design
res	residence time
th	Theoretical

1. Introduction

1.1. CRANFIELD UTC IN GAS TURBINE PERFORMANCE ENGINEERING

The Rolls-Royce University Technology Centre (UTC) at Cranfield was created in March 1998, of which this work is part of a continued programme of research into the area of altitude relight and windmilling.

All research within the scope of this EngD is sponsored by Rolls-Royce Plc and all data herein is commercially confidential. The reader should have sought the necessary permissions and adhere to the confidentiality agreement before continuing.

The structure of the thesis is such, that the literature review pertaining to each research subject area is contained within that subject's chapter.

1.2. SUB-IDLE GAS TURBINE PERFORMANCE

1.2.1. INTRODUCTION

Traditional performance modelling of gas turbines has concentrated on the design point and typically off-design operation to idle. Therefore sub-idle performance modelling of a gas turbine engine is not a typical design process within a company. Two main reasons designate this position, one is that the design point and the engine efficiency and thrust rating are the most desired specifications for the company to meet, and although contractually the company has to meet engine relight requirements, unfortunately, with exception of the combustion design department, these are not of prime importance. That is until the engine is not able to relight on testing. The second reason is the difficulties in producing a performance model and the engine data required by the model, for these extreme off design conditions the engine components have to operate at and their behaviour at these conditions. These engine operating conditions in

which an engine will experience these extreme sub-idle conditions, are described in the following two chapters.

Much knowledge of engine relight behaviour is gained within companies on engine test beds, with little ability to predict the relight performance. It is on the test bed where changes to the control system and in some circumstances, changes to engine components are made to improve the engine light-up performance.

As an introduction to this area of research the following two chapters describe the phenomenon of the prime concern, where sub-idle modelling becomes applicable in the scenarios of windmilling relights and also describes the on runway starting of engines thus termed groundstarting.

1.2.2. WINDMILLING RELIGHT

1.2.2.1. Introduction

Windmilling relight is an extreme and typically rare occurrence in aircraft engine operation. The typical situation of requirement for windmill relight is when in flight the engine flames out. The engine spool speeds decelerate rapidly, to a rotational speed which is maintained by the aircraft forward speed, producing a ram pressure at the front face of the engine inlet. The momentum of this air imparts force onto the compressor blades like the effect on a windmill, thus causing the spools to rotate in the same direction as in normal lit operation. There is typically a pressure drop across the engine compressor, combustor and turbine, exhausting through the exhaust nozzle and balancing with the atmospheric pressure (or nacelle wake and drag pressures). A relight procedure, instigated by the aircraft pilot, applies fuel into the combustor and then lights the igniters to re-start the engine. Upon successfully relighting, the engine will accelerate and return propulsive thrust to the aircraft.

It should also be noted that industrial engines can also windmill, from the effect of wind passing into the engine inlet and any suction effect across the top of the exhaust stack (the Author has actually witnessed this with a free power turbine aero-derivative engine, on an offshore installation, though the engine rotational speeds were very small).

The ram pressure produced at the engine intake, from the aircraft forward velocity, is a combination of increase in total and static pressure from the ambient pressure. An increase in total from the ram pressure and an increase in static, as the stream-tube into the intake acts as a diffuser. In addition to the above effects, spillage occurs at the front face of the intake as defined by the stream in Figure 1. b), and therefore results in a spillage drag on the engine nacelle. These losses have been studied in-depth by ESDU [13] and [14].

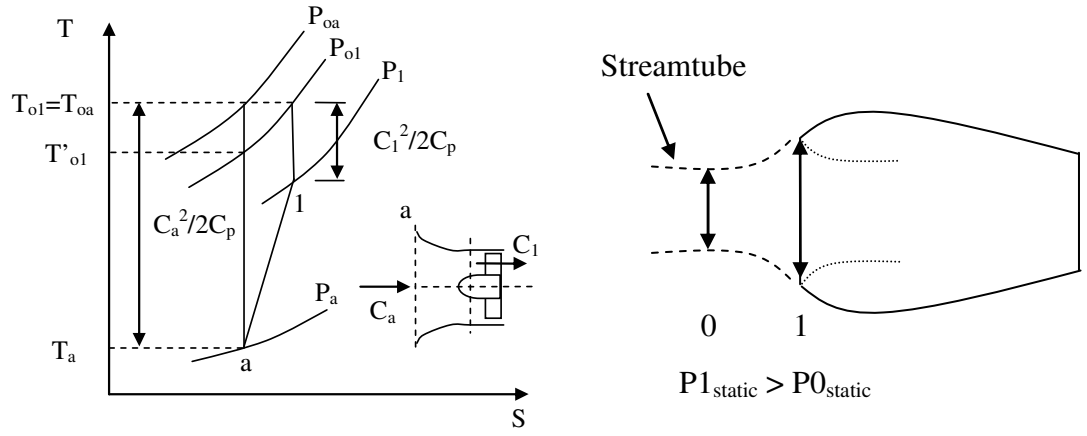

Figure 1. a) Intake ram pressure effects at design. b) Windmilling stream tube.

Aircraft engines are required by the airframe manufacturer to meet certain windmill relight operational boundaries. These are defined in an operating range defined like in Figure 2. The engine is required to relight at a range altitude and flight speeds, and the ability of the engine to successfully relight at these conditions produces limit lines. There are two main relight areas, windmilling relight and assisted windmill relight. The latter is described in the following chapter 1.3.

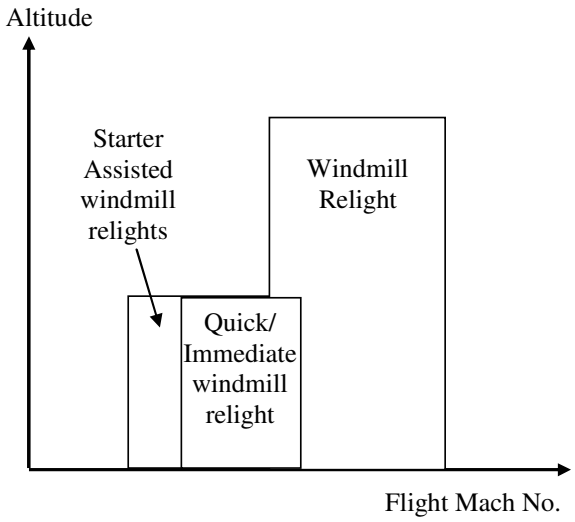

Figure 2. Typical Relight Envelope.

To describe the varied windmilling operations and situations imposed by the flight conditions, these subjects are split into the following descriptive chapters.

1.2.2.2. Steady State Windmilling

A windmilling engine is never truly operating at a steady state condition. The assumption the windmilling engine is steady state is reasonable and analysis at these conditions maybe the most simplistic, however, it is the one of the most useful. On such aircraft as the Nimrod in surveillance mode, two of the four engines are switched off to conserve fuel during cruise. The situation could also occur on other aircraft where, for some operating reasons, the engine has been left a long time after flame-out before trying the relight procedure. In this instance the steady state speed will only remain constant if the aircraft other engines are capable of sustaining a constant flight Mach number and altitude, otherwise the rotational speed will be varying as a function of these flight conditions.

The Nimrod aircraft with two of the engines windmilling, if unlit for long enough, the engines will be cold soaked. In that the carcass and components have cooled to the ambient conditions, thus not imparting heat into the gas path flow. To summarise, the measurement of cold windmilling conditions provides the most accurate data to analyse and investigate.

1.2.2.3. Windmilling Relight

From a steady state windmilling condition, as described in the above chapter, the fuel flow is added and igniters then lit, thus relighting the engine, to start and accelerate from the windmilling spool speed. It is the HP spool which first receives the energy provided by the combustor to the HPT thus this leads the acceleration of the other spools. The IP spool acceleration lags the HP, and the LP lags the IP.

Analysis of windmill relight ability, allows the engine manufacture to present the envelope of flight conditions at which the engine will relight. The engine tests to derive this relight envelope, are performed in an Altitude Relight Facility (ATF), a test bed designed to simulate the air inlet conditions in flight and altitude.

1.2.2.4. Quick Windmilling Relight

A more typical relight situation, where the engine after a flameout is required to be relit in the time whereby the spools are still decelerating, is called a quick or immediate relight. The relight is problematic due to a number of reasons, the inertia of deceleration spool speed as to be overcome to accelerate the engine, thus the power input required is much higher. Also the flows are extremely turbulent so losses are high, and the components will have a large source of heat energy stored within them, which has not had the time to dissipate through convection. This heat energy is thus transferred to the gas path flows and tends to cause compressors to move towards stall, the surge line to reduce and the non-dimensional speed will be altered, as discussed by

Howard [24] and Naylor [44]. Heat soakage in quick windmill relights is not really covered in this work, but results within the modelling shall be studied.

1.2.2.5. Pullaway

Where the engine has relit successfully the engine spool speeds will accelerate, with the LP spool speed lagging the HP. The time the engine takes to accelerate is important as the quicker the engine can accelerate the quicker it will achieve an operating condition where useful thrust is being produced by the engine, thus returning power to the aircraft.

1.2.3. GROUNDSTARTING AND ASSISTED RELIGHTS

One of the most important and daily needs of an engine, is to start on the runway when the aircraft is stationary. These starts are called groundstarts, which are typically from zero speed from which the engine HP spool is initially accelerated, by an attached starter motor, to a light-up spool speed, Curnock [10] provides a good insight into engine starting. At which point fuel is added and igniters turned on. Once lit and the engine has enough energy to self sustain acceleration, the starter motor is turned off (for air turbine starters the air supply valve is shut off). The engine continues to accelerate to idle where it will wait to thermally soak prior to acceleration to full power.

Assisted starts follow the same procedure, however, at conditions of a low flight mach number at which the spool speed is typically not zero (although much lower rotational speed than normal windmill relights).

1.3. REQUIREMENT FOR SUB-IDLE PERFORMANCE MODELS

The need for a sub-idle performance model is for two main requirements which can be described as predictive and analytical. The first is the requirement to predict new engine design performance for light-up boundaries within the aircraft flight envelope, to meet the airframe/ customers requirements and Aviation authorities. The second is the ability to analyse an engines performance, where changes may be made to components

and the effect on the relight behaviour/ response times is required either for studies or for actual changes required. An example of this second requirement would be studying the effect of increasing a hydraulic pumps load, to provide more hydraulic power for aerialion control, on the engine windmilling and relight performance.

A reliable sub-idle performance model would in the first instance offer financial rewards of time saved on test beds. The construction of control software prior to engine testing would be aided and again save time on test beds. Sensitivity studies of changes to component on the relight performance could be simulated. A sub-idle model would also be useful to other departments, particularly the combustion team. Data from this model would result in removing the need for spare built in safety margin at the design stage, by providing engine specific predicted flows and pressures entering the combustor at light-up, which would enable reduction in combustor size.

The information from a model, which matches well with the engine, can provide intrusive analysis at stations on the engine, which otherwise cannot be measured on actual engines. The benefit of the model, is that it can calculate the transient conditions and explain these to the user, such as heat soakage effects and their influence.

1.4. RESEARCH AND TOPIC AREAS

The research topic covers the sub-idle performance of gas turbines, this research is particularly positioned towards aircraft engines, however, most modelling principles are applicable to all engines.

The aim of this research is to improve the knowledge in the area of sub-idle performance modelling, techniques for creating models and relationships to produce reliable and repeatable techniques with the ultimate aim of predicting sub-idle engine performance.

Methodology approach was to cover particular areas of relight performance of an interest to the sponsor, producing investigations and the findings to increase the knowledge in this area of performance.

Primarily the research focused on the problems involved with sub-idle performance modelling of two-spool turbofan engines, their assembly, and the issues involved in running such models. Additionally, the research utilises an extrapolation method, with making improvements and suggesting alternative techniques and parameters.

Within the first month of the research, a meeting was convened at Rolls-Royce Derby with the sponsor's performance department leaders, to outline the research activities for this EngD and the following research areas were proposed to be covered.

Research Areas;

- Sub-idle model of a two-spool Engine A, a low bypass ratio military mixed engine.
- Sub-idle model of a two-spool Engine B, a high bypass ratio civil mixed engine.
- Comparison of component characteristics in the sub-idle region.
- Combustion light-up efficiencies.
- Locked rotor studies in CFD, this developed in the 2nd year where the sponsor requesting that a test rig be built to study the losses.

The subject areas defined above set the principle of this research to investigate the problems of sub-idle modelling particularly with reference to two-spool engines, as previous research within Rolls-Royce had already been undertaken on three spool sub-idle engine modelling.

As the research project developed and evolved, it became clear that there was a real lack of knowledge and understanding in the open community and within the sponsoring company of the influencing changes in map construction and affect on the engine sub-idle performance. Most previous studies and research, if at best, had achieved a model to run with attempts to align the model to test data. However, no investigative analysis had been undertaken on the influence of various components and that in fact within one technique of extrapolating characteristics there are many variances that can achieve similar results.

The real research and contribution to knowledge from the model simulations, is utilising the model in an adaptive approach to create and align the engine component characteristics in the sub-idle operating region. From this adaptive study, sensitivity analysis and changes to configurations would be simulated and thus gain a better understanding of these influences in an engine operating at windmill relights and in the sub-idle region. Many previous studies have only considered steady state windmill modelling, whereas this research also simulates transient windmill relights.

Additionally it was also found that the pretence of many extrapolation methods were that the characteristics were predicted, whereas in fact the extrapolations depended on test data to align the extrapolations, instead of a fully predictive technique. Therefore studies were performed in an attempt to produce techniques and a method to meet this need. In particular a technique was produced for a generic calculation of a zero speed curve from which interpolation would predict sub-idle characteristics.

This research also provides insight and guidance to modelling problems as well as simulations at engine conditions other than the typical windmilling study, such as assisted windmill relights and quick windmill relights. The research follows on from previous research by Geoff Jones [29] and also work by Howard [24].

Due to confidentiality reasons, any engines referenced, are done so by a particular letter. A separate report within the UTC by Howard [26] defines the actual engine name and parameters used in this thesis. There are 7 engines referenced within this thesis, an overall description of each of this engines configuration is given below in Table 1.

Engine	Description
Engine A	Two-Spool Military Low Bypass Ratio Turbofan, Mixed Exhausts.
Engine B	Two-Spool Civil High Bypass Ratio Turbofan, Mixed Exhausts.
Engine C	Three-Spool Civil High Bypass Ratio Turbofan.
Engine D	Two-Spool Turbojet.
Engine E	Three-Spool Civil High Bypass Ratio Turbofan, Mixed Exhausts.
Engine F	Three-Spool Civil High Bypass Ratio Turbofan.
Engine G	Three-Spool Civil High Bypass Ratio Turbofan.

Table 1. Engines referencing within report, and description.

Most of the simulation model research was based around Engine A and B, whilst most of the CFD modelling was based on Engine A, C and D. The Mixer studies were concentrated around engine A.

2. Altitude Test Facility Data Analysis

2.1. INTRODUCTION

One of the most important aspects of this research is to compare the results of simulations (see chapter 3), theoretical methods (see chapters7, 8 and 9) and CFD (see chapter 9) approaches to actual engine data. The author of this thesis believes this topic to be very important as many studies fail to compare sub-idle results with actual engine test data. Therefore this chapter describes the methods used to analyse data, calculate mass flows, and tackling issues with test data or missing data.

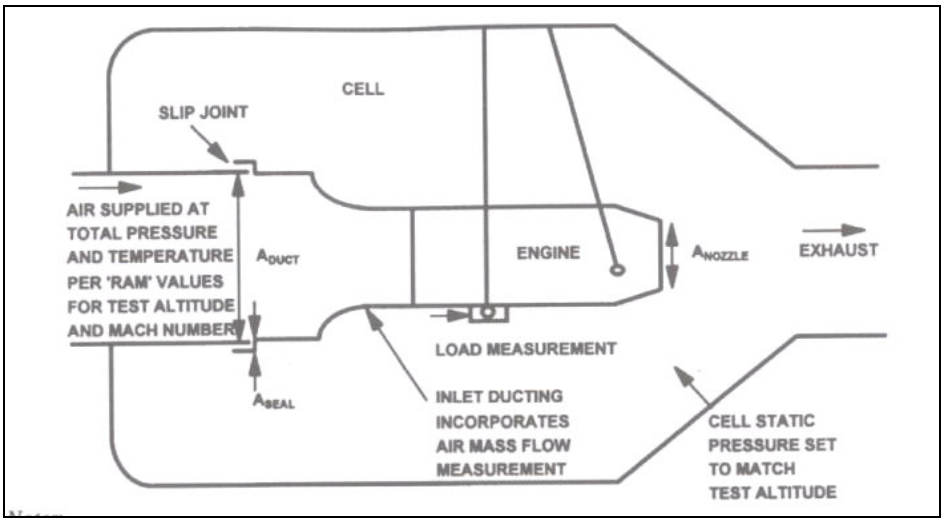

Figure 3. Diagram of an Altitude test Facility, Walsh [59].

The Altitude Test Facility (ATF) shown in Figure 3. allows the simulation of flight conditions for operating tests of the engine. In particular the facility allows testing of the engine for windmilling relight and many other operating conditions. Therein ATF engine data analysis is used in this thesis for analysis and comparison of results. The ATF engine test only provides the inlet conditions directly to the intake of the engine, no intake affects are therefore represented or nacelle flows, therefore the test cannot

represent installed thrust. In particular the test cannot indicate the spillage losses around the nacelle, thus the drag and forces accounting around the nacelle cannot be realised.

With the inlet conditions of altitude and flight Mach number set at entry to the engine, the altitude conditions of static pressure also require to be set within the cell to impose the relevant exit conditions for the nozzle. However, the test does not include for free stream velocity interaction with the engine nozzles as would be in flight. Therefore following ATF tests, the engine will be flight tested within its nacelle.

2.2. LITERATURE REVIEW

Walsh [59] extensively describes the ATF test bed and the types of measurement employed typically and by the sponsor. The pressure and temperature instruments within a rake are positioned, based upon area weighting. While the direction they point is based on trying to represent a wide range of operating conditions. For measurements at the far off design conditions, at an incidence of up to +/- 25^{o}, the dynamic head can still be recovered for pressure measurement if a 'Kiel head' is used. Even this range of incidence may not be large enough for flow directions in the wide range of off-design conditions of windmilling.

An interesting report in the open literature is the discussion of an in flight tests of altitude relight of the Eurofighter 2000, by Bragagnolo [5]. This provides an interesting insight into the actual application for an aircraft and the test pilot interaction.

The effect of power offtake on a turbojet test engine is described by Walker [58], in which the torque (to simulate an increasing load) was applied by a dynamometer. To understand what percentage of the offtake torque is provided by the compressor, the

turbine was removed. It is one of the few tests where the compressor and turbine have been separated. The results show the maximum in power offtake available for a given flight Mach number is at a particular corrected non-dimensional speed. Thus the inverse of this would be to say that changing the power offtake required from the engine at a windmilling condition will change the spool speed, resultantly this will change the pressure losses through the components. As a result of the testing method of applying torque, the windmilling torque to zero speed is shown. In this representation of torque there is no maxima or minima as with power curves, instead a slightly curved to almost straight line is produced as torque accounts for the momentum. This is discussed further in chapter 9.1.

Another influencing parameter on the windmilling performance and relight of engines is the control bleed flow. As discussed by Rebeske [50] not only does the control bleed flow effect light up but it also affect the windmilling spool speed. He explains that variable bleed could be used providing faster light-up times and that increasing the bleed flow area by 22% increased acceleration times by 2.65 times and moved the accelerating working line further away from surge as one would expect. Therefore the bleed valve flow area and conditions have a very significant effect on acceleration times.

2.3. METHODOLOGY/ ANALYSIS

2.3.1. CALCULATIONS

In a designated engine station, the typical instrument measurements are Total Pressure, Static Pressure and Total Temperature. These can be recorded on steady state or high response transient probes. Other instrumentation such as the FADEC instrumentation are not good for fast response indication in highly transient operations, due to the

thickness of the thermocouple around the temperature probe or the thickness of a pitot tube disturbance on the air flow.

A number of pressure and in some cases temperature probes at a particular station are aligned on a rake. The average values of these probes, provides a measurement of the average station conditions. Averaging of the instrument probes in a rake is possible as they are positioned based on area weighting.

The isentropic flow calculations, deriving the Q flow values and Mach numbers are used to derive the station massflow. Alternatively the design point information with an approximation of the inlet Mach No. (i.e. 0.5 for a compressor) can be used to determine for example, the inlet flow area of a compressor (shown by Eq. 1). However, when working with test data rake pressures and temperatures the area required to derive mass flow, is that area at the probe position. Therefore the design point calculation of area will not suffice, although is useful as a first approximation.

$$Q = \frac{W\sqrt{T}}{PA} \text{ ; assume compressor inlet Mach No. } \approx 0.5 \qquad \text{Eq. 1}$$

A dynamic head pressure probe is typically at the HPC entry and exit on most engine tests. This instrument is a useful alternative to the typical static pressure reading, although it applies the pitot pressure (P*) definition for incompressible flow as shown in Eq.2. To that of the measured averaged static pressure probe, the author observed from ATF engine data it has typically slightly lower values of pressure and does not increase as rapidly on acceleration of the engine.

$$p_s = P_T^* - 0.5\rho V^2 \qquad \text{Eq. 2}$$

(Static Pressure = Total Pressure – Dynamic Pressure)

The calculation of mass flow and any number of other calculable parameters can be made of test data or model data in the Rolls-Royce ALICE, these are called 'Lets'. Deltas and Factors may be known for the relevant instrument rake and therefore these can be applied to the let calculation.

2.3.2. DEALING WITH POOR DATA

Poor ATF engine data maybe from a probe failure within a rake or produce erroneous, and in some cases for temperature probes, negative values. Therefore all probe data used on a rake were compared against each other, and manually sorted to remove erroneous probes from the rake averaging.

Also probes cannot be aligned to the actual exit flow direction of each component as these vary widely, though the instrumentation has to record for a wide range of operating conditions from windmilling, groundstarting, to idle and design point. A typical example would be the compressor exit angles deviation and large wakes created behind them.

In conversations, Rowe [52] recommended a thorough approach to handling windmilling ATF data is to ensure the instrumentation offsets are included in the calculations. To achieve understanding the instrument offsets an ATF case of zero shot is used at the beginning of the day or test where the instrument readings are recorded, however, the engine is static, and the engine will have no heat soakage. The deltas of the pressure and temperature instruments values to that of the ambient air conditions, can be applied to correct the offset of the instrument measurements. At windmilling conditions a small delta can still have a significant effect on results as the engine operating pressures are also small.

Uncertainty of the calculation of massflow is one of the greatest concerns, as this parameter is crucial in the analysis of the engine performance and validation of the model. The pressures are so small that even a small delta in an instrument reading would have a very adverse affect on the resulting calculated flow. If the total massflow entering the engine is assumed reasonably accurate, then by deducting the sum of the calculated core and bypass flows, the overall flow error can be calculated. Table 2. below presents the possible error, where the error is calculated as in Eq.3.

$$Error_{mass\ flow} = W_{engine\ total} - W_{core} - W_{bypass} \qquad \textbf{Eq. 3}$$

% Fan Non-dimensional speed	Error in the sum of the calculated core and bypass mass flow. % of Engine total inlet mass flow
21.59547	13.36333
8.873901	14.03491
15.51089	-7.42254
14.48542	-10.9521
10.34178	-5.96958
10.38055	-5.90381
12.13241	-8.64005
14.73589	-12.0463
21.59547	-15.2425

Table 2. Error on calculating core and bypass mass flows, for Engine A.

The uncertainty of whether it was the bypass or core which has the largest error can be analysed by considering separate duct massflows, in the useful analogy of the fan outer

and core flows having a choking representation of distributed flow. It is important to understand that the flow error was added to the core and then the bypass flow, as described below.

Engine B measurement pressures have a very large uncertainty due to the rakes only consisting of two probes. Therefore these measurements have insufficient definition of the pressure profile and thus average station pressure, which has to be considered when studying the data.

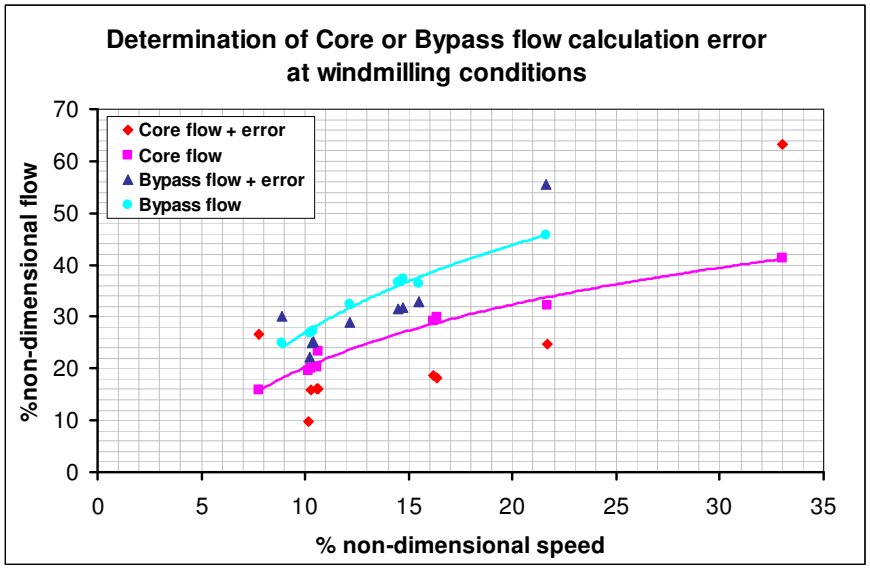

Figure 4. The error on calculation of core and bypass mass flows Engine A.

From studying Figure 4. the distribution of the error fits well around the bypass flow calculation, as the %error around the core would seem far too high. A probable cause of the error in the bypass duct is that the flow leaving the fan may posses some swirl or other secondary losses that are affecting the probe results at these far off-design conditions. The result of this investigation was that bypass flow was calculated by using the total ATF engine inlet mass flow minus the core calculated mass flow. Also it can be said that if the error was removed from the core flow, this would have significant change and no longer create a smooth choking profile with respect to non-dimensional

speed. Applying all the error around the bypass flow in itself is an approximation, as the core flow calculation may be responsible for some proportion of this error, however, this was the assumption used.

What is also found by analysing the data in this way is the confirmation of how the compressors in windmilling perform, with respect to spool speed, which is a function of flight Mach Number, as highlighted in chapter 2.3.3.

Also a useful assumption is that there is approximately 1/3rd pressure loss in HPT which was confirmed from the test data. It is more difficult to assess pressure loss over LPT turbine on a mixed engine as it was found when studying the effect of the mixer, where the LPT exit pressure is resultantly higher than the LPT inlet. The pressure increase effect reduces as the engine accelerates towards idle.

Data for the turbines is limited to only T6 temperature being available, and pressures are limited to only total pressures at each Turbine NGV's. As a result a total pressure loss may be found, though this is little use on the linearised characteristics if there are no temperatures to derive the turbine work.

As will be made apparent in the later chapter 5.1.4, the fuel schedule is required from zero flow to the Light Up Fuel Flow (LUFF) and the accelerating fuel flow. The engine fuel flow representation should be shown versus NH spool speed as versus time provide no relationship to the response of the engine.

Fan exit measured pressures were in doubt as there would be a large change in swirl angle even though it is approximately half way in the OGV structural duct. This would also satisfy the argument that the calculated flow at this station is in error.

2.3.3. ANALYSING DATA

For all windmilling steady state ATF data analysis, it is crucial to have cold windmilling data, so as to eliminate any heat soakage influences on the values studied. Cold Steady state data is required for comparison with the steady state component maps. A general study of ATF test data allowed the author to gain an understanding of the varying engine performance of a range of flight and operating conditions.

By study of the ATF data the unique windmilling operating curve (or working line) could be found with increasing speed as a function of increasing flight Mach number, however, this would vary depending upon power offtake and any heat soakage effects.

On Engine A the design bypass ratio is below one, and the fan root specific work is higher than the fan bypass specific work. Therefore the fan root specific work and pressure ratio were compared for all engines. It was found that with all engines at windmilling, the fan outer always acts a turbine and the root always acts as a stirrer, where there is an increase of entropy from the temperature rise created ($PR<1$ and $TR>1$). The stirring effect of the fan root is probably due to the disturbance from the large shift in bypass ratio diverting most of the flow to the bypass duct.

The bypass ratio (BPR) was analysed through the range of windmill conditions and the comparison of these values with the groundstart and assisted windmill relight BPR's. At windmilling, BPR ratios can be around 100 in engine C and low as 3 in engine A, to as low as 0.1 in starter assists. In starter assists the BPR is so low due to core rotation from the starter motor inducing the flow through the core. BPR becomes much lower in groundstarts as the LPT receives little useful work thus the fan does not initially rotate lagging far behind the HP spool acceleration, therefore the fan bypass flow is practically zero.

For the mixer studies in chapter 7, the mixer entry and exit conditions were required. For engine A most of this data was directly available, except the cold duct static pressure. Instead the fan exit data could be used directly, or more accurately, the pressure could be determined by an iterative process using the continuity of mass flow as the match could be used. Therefore considering the duct flow adiabatic and simplified as frictionless, the cold duct mixer entry static pressure could be calculated from the cold mixer duct area. For all high bypass engines little data was recorded for the fan exit, thus making engine data analysis impossible for all engines other than engine A.

To assist deriving a starter characteristic, from the assisted start and groundstart ATF data, (as required in chapter 3), starting torque data was assessed. The calculations to determine the starter motor torque (the acceleration torque) are shown in Eq 4, 5 and 6.

$$\tau_{rotor} = -\tau_{compressor} - \tau_{MECHANICAL\_LOSSES} + \tau_{turbine} \qquad \textbf{Eq. 4}$$

$$d\tau_{ACCELERATION} = I_p \cdot \frac{d\omega}{dt} = 2\pi I_p \cdot \frac{dN}{dt} \qquad \textbf{Eq. 5}$$

$$Starter\_motor\_torque = \tau_{rotor} + d\tau_{ACCELERATION} \qquad \textbf{Eq. 6}$$

Agrawal [1] describes rotor torque to be a summation of the torque required by the compressor and mechanical losses and offtake, and he considers the turbine to be producing power. However, it is the opinion of the author of this thesis that the turbine, during a groundstart dry crank from the starter motor, will likely be a drag as prior to combustor light-up enthalpy change will be negligible. The turning of the flow and high negative incidence angles to the rotor could also be stirring the flow contributing to a drag effect. Therefore considering these two points the turbine should not be fully discounted. As a result these two points made by the author complicate the ability to

calculate the rotor torque, as the only way to understand the work across the rotor is from the total temperature change across the stages, and in the turbine these temperatures are not available from the test data.

In the following chapters the main engine ATF data required and their use in the research are briefly discussed.

2.3.3.1. Engine A analysis

Engine steady state and transient data were required for model analysis in chapters 3 and 4, data was also required for CFD analysis in chapter 9.

2.3.3.2. Engine B Analysis

Engine steady state and transient data were required for model analysis.

2.3.3.3. Engine C Analysis

Only steady state windmilling engine data was required for CFD and cascade test rig analysis in chapter 9.

2.3.3.4. Engine D Analysis

The engine ATF data was not electronic therefore data was taken from charts and graphs. Data was required for CFD analysis in chapter 9.

3. Sub-idle simulation modelling

3.1. INTRODUCTION TO SUB-IDLE MODEL BACKGROUND

For a new engine an accurate predictive performance sub-idle model would allow more accurate design of the control system and control laws prior to the test bed. Whereas at present, approximations of the windmilling relight performance are used to derive a basic control schedule, which is then modified from engine testing. Thus a reliable sub-idle performance model could save cost and testing time.

This research utilised a Rolls-Royce sub-idle code called BD19 in its development stage, which had previously only been used to model 3-spool engines. The model's code is written in Fortran and is built on the system of RRAP component bricks and other routines and functions, using standard bricks as well as a few special bricks. Bricks are the code routines for components which provide ease of construction of an engine model and consistent passing of variables and calculations between routines. Two-spool models were constructed and developed for Engine A and B (all engine B data compiled by Leitges [38], with the exception of compressor and combustion characteristics, were used). The model for engine E, using the three-spool model, was used to learn how to run the code and the workings, from this code the necessary modifications and developments were accomplished to produce engine A and B engine models.

In the author's opinion, creating an accurate sub-idle performance model will always be difficult due the significance of the delta from a small error can have on the low operating pressures, temperature and massflows of sub-idle conditions. What can be achieved is a model which will perform reasonable working lines and parameter trends to within 10% error.

The BD19 engine model was assembled and run on a standalone (un-networked) SUN UNIX workstation computer based in the Rolls-Royce Performance UTC at Cranfield, which runs the ALICE system. The ALICE system is software that allows test data to be analysed and performance code simulations to be run. The workstation was updated to Solaris 12 also a code was included to allow creation of DVERSE on a Java script editor. The DVERSE allows the user to convert the code station data to the standard API engine station numbering. As a result of code changes and additions to the model the DVERSE was updated for the changes brick locations and station numbering.

3.2. LITERATURE REVIEW

3.2.1. ROLLS-ROYCE SUB-IDLE MODELLING

All sub-idle modelling to date has been either through earlier attempts at sub-idle steady state windmilling codes or the current transient development model as used within this research, called BD19. The above idle performance models within the sponsor's company can simulate windmilling steady state performance from a loss map available for this operation only, as discussed in [53]. Whereas the BD19 model can simulate from windmilling and starting conditions up to design point. Though the accuracy at design point, will be inaccurate compared to above-idle performance models as these have been stringently aligned with deltas and factors. Prior to this research thesis only simulations of three-spool engines were conducted with the BD19 unmixed models on engines E, F, G and some work with engine H. All prior BD19 simulations have used scaled maps of the original Engine F model's component maps, and these were developed/ extrapolated with the aid of windmilling test data and drawn by hand.

A report by Syed [56] explains the structure and running of the BD19 model, this was used as the main guide for the modelling in this research. The report also explains how matching on pressure is used to fully defined the more important low pressures at sub-

idle conditions and to avoid negative pressures resulting, particularly at the nozzle, which may result from using flow matching.

Modelling of engine E with the BD19 sub-idle model, was performed and reported by Monticelli [42] in which model results errors were between 3 to 10%. The scaling parameters for each component were defined by the relevant component disciplines, and much of the engine data remained the same, as it was from the same engine family. Simulations for Windmill relights, quick windmill relights and starter assists were run. These were performed by applying a time step lump sum fuel flow and allowing the model control limiters to control the acceleration of the model.

The starter assisted windmill relight simulations by [42], were begun after the starter motor acceleration and where the acceleration was flat prior to the light-up. To do this the starter pressure ratio was set (either from test data information or modified) to achieve the desired speed HP spool speed to start from as defined by the ATF data. Therefore a true starter assist was not actually performed, and the simulations lack any remaining acceleration torque from the starter motor on light-up.

The results of the simulations by [42] would seem to match up reasonably well with test data, with the exception of the IP spool working line and acceleration lagging the test data. The result of the IP error is likely to be a result of limitations imposed by scaling characteristics. Also the working line near idle seems typically to have a significant amount of error at certain windmill cases, this is sometime related to the IP error. A problem with the fuel schedule used, other than the starter motor simulation, was that the actual engine fuel schedule, applied in the test engine, is not defined as the model input data. Therefore it is difficult to fully examine the matching of the model with test data for validating the model.

A steady state model for engine B was assembled by Leitges [38] using the 3-spool BD19 model and entering dummy characteristics for the IP spool components. The dummy characteristics allowed continuity of flow but set speed and work to zero to avoid any pressure influence, therefore the components acted like a duct. This allowed the model to run steady state however, it could not run transiently. Component characteristics were extrapolated by spreadsheet tools developed by [53], which utilised graphical and some physics based calculations, with ATF test data were used to align the extrapolations. These tools were used and modified within this thesis for extrapolation of the characteristics. The model produced good results for windmilling steady state data, see Chapter 11.1.

An earlier steady state windmilling model of a military engine was developed by the sponsor, however, the code had significant problems running at any condition other than one altitude and flight mach number.

3.2.2. SUB-IDLE AND PERFORMANCE MODELLING

This chapter explores the open literature on sub-idle modelling and references general modelling techniques.

The simulation of the gas turbine is a complex calculation of solving many unknowns by inputting guesses and checking the errors between matching quantities and reducing this errors to defined tolerances. To solve the large number of unknowns, matrices are used and the resulting residuals are used together with the most common solver approach of using the Newton Raphson Solver as described in [46]. This is a gradient solver and many techniques have been derived particularly by the sponsor to make the iteration more robust, quicker and also other approaches to solving the unknowns if the first round of iterations cannot find a solution.

For a gas turbine simulation model to simulate particular engine operations, certain solution capabilities will be required. As highlighted by Fawke [15], for large fuel step changes over a short time a intercomponent volumes method is required to simulate the actual response time or the gas dynamics of the flow path gases. Otherwise if a purely iterative method is used the detail of the engine acceleration up and away from the constant speed curve trajectory will not be defined by the model. Secondary effects such as heat soakage, are also required to be modelled in large transients.

Engine models can be either of a mathematical dynamic type where the component performance is calculated or a mathematical model relying on component characteristics. De-You [11] attempted a dynamic model, whereby the compressor performance down to sub-idle starting conditions by means of stage stacking performance techniques. Their results seemed to align to the experimental data well, with errors between 2-6%. Another approach to the mathematical model was by Agrawal [1], who used the similarity laws to calculate the off-design conditions. The model was applied to starting simulation, however, admits this is only a preliminary tool to understand the general starting conditions and not the details of each engine design.

Work by Lim [39] and Choi [9] uses a mathematical approach with some reference to aerofoil loss and other loss parameters to calculate the compressor and turbine performance based on the resulting blade angles at these far off design conditions. The results seem very successful, though how the actual flow angles occurring at windmilling are known is not discussed. Flow matching is used, making use of the mass flow continuity, therefore prediction of fast transients and issues of negative pressures in windmilling relight may be a problem. The methods in this approach show promise and the author of this thesis used this research to point the way for developments made in chapter 9.3.3.4.

Most engine models use characteristics, which allow all losses to be included or factored onto the characteristic. The problems with maps is discussed in other chapters, however, Reigler [51] provides a good insight into the problems with component maps, their generation and application within a model. He outlines the wide range of effects from geometry, changing geometry such as VIGV's and second order effects relating to Reynolds number, flow distortion effects on pressure and temperature, and variable blade inlet flows angles depending on aircraft flight condition or manoeuvre.

A very complete and useful steady state windmilling modelling and configuration analysis, was produced by Braig et all [6] In which the turbojet and turbofan configurations were investigated and importantly the effect of mixer. Part of the work simply confirms that in a high bypass mixed engine the bypass pressure drop will be small in comparison with core flow, thus a mixed engine will have a higher pressure at the LPT exit and that the resulting higher bypass ratio will produce higher NL speeds. Also it is noted that the core is affected by the back pressure imposed by the mixer and lower core flows, combustor pressure and temperature. The work does not study any transient simulations, and therefore does not study light-up effect of the mixer addition or any influence on pullaway performance.

The commercially available performance program Gasturb [36] is not intended as a sub-idle tool, however, it has the capability to run transiently and to run down to low speed settings. It uses component characteristics extrapolated towards zero speed, using the linked tools of smooth C and Smooth T. The author of this thesis could not use these characteristics, as he found the smooth C tool was based on conventional parameters (PR, Eta_{ISEN} and WrT/P). This limited two things, the degree to which one could achieve pressure ratios below one, and the resulting efficiencies would have a discontinuity jump from highly negative to highly positive values of Isentropic efficiency. The Author of this thesis actually attempted using this code for sub-idle

modelling and found the same difficulties. This explains some of the reasoning for using linearized parameters, discussed in chapter 4.3.1.

To summarise, there seems a small quantity of research carried out on steady state windmilling, and little if any successful work on transient windmill relights. There is little work where comparison to test data is used to check the accuracy of the models.

3.3. SUB-IDLE MODEL RESEARCH METHODOLOGY

3.3.1. ENGINE MODEL CODING AND CHANGE TO TWO-SPOOL ENGINE.

The BD19 Sub-idle model, consists of a engine code which links all RRAP bricks and calculations with code station numbers. The matching and guesses are defined within the engine code to the relevant parameter and station number. Engine data, control parameters, the graphical numbers for component characteristics, and brick data are defined in an Engine file. The flight and engine conditions are described in a Flight Environment file along with schedules for fuel flow and any control limiters required.

Iterative solver within BD19 is damped Quasi-Newton method and uses numerical differencing to calculate the partial derivatives for the variables. The initialisation conditions used in this model are those at ISA SLS idle point. The guesses are a culmination of spool torques, work coefficient compressor values, spool speeds, Betas, velocities (for OGV and ESS loss predictions) and pressures for control bleeds. Additionally there is the handle parameter which is defined separately.

The values for the minimum and maximum range of the matching variables should be set not to the component map limits, but to the limits of expected solver iteration extrapolation. A typical example is the compressor beta lines that may extend towards

or just past the surge line, however, the iterative solver in the initial stages of the iterative loop may need to extend beyond these values until the error is minimised.

The model matches on torque spool balance and pressures, as opposed to the typical non-dimensional mass flow in other performance models. Pressure matching is used to minimise the case where if the flow matching was used a negative pressure at the nozzle could be achieved at windmilling. Which would invalidate the pressure momentum of flow passing through the engine. This case would not occur in above idle performance, where the nozzle exit total pressures and velocities will be higher than the ambient and assist in producing thrust.

Much of the code changes to a 2-spool engine and other changes to the coding for engine configurations, were completed within the sponsor company at Bristol with the development and engine A performance teams.

Conversion to a two-spool engine model was a rather simple process, however, the changes required a great deal of learning and understanding of the engine code along with RRAP programming methodology, which was found to be a much greater challenge. It was decided to apply a switch, to allow a simple change between a two-spool and three-spool engine configuration using the same code. The switch named IIPC removes the IP spool coding and transfers LPC root exit conditions to the HPC inlet and HPT exit data directly to the LPT inlet. All then required is a change in the engine model of setting IP related matching errors to zero, which implies turning off IP matching. The model also required other changes such as the representation of the control bleed valve switching was set to speed, rather than a defined pressure ratio. Further switches to the model were associated with application of a mixer, as discussed in chapters 3.3.2 and 3.3.3.

3.3.2. ADDITION OF A MIXER

The sub-idle model did not include (provide for) a mixer in its code structure. It was decided by the author that the mixing could not be neglected as in past modelling of high BPR engines, as in engine A the low BPR configuration mixing coupling effect of bypass and core stream may be very influential. The mixing theory is discussed in chapter 7, the change to the code is discussed here.

A change to the code brick structure for modelling first engine A, was formed by the author, and only after found this was similar to the structure used in the sponsor's above-idle transient model. However, the difference is the above-idle model uses a thrust calculation of individual cold and hot duct summed and compared to the mixer calculated thrust. At sub-idle conditions the thrust is either negligible or negative as the engine is a drag. The mixer was defined by brick 62 for engine A and brick 60 for engine B. In Figure 5. the arrangement applied for Engine A is described, notably the matches (which are pressures) are highlighted by the red circle.

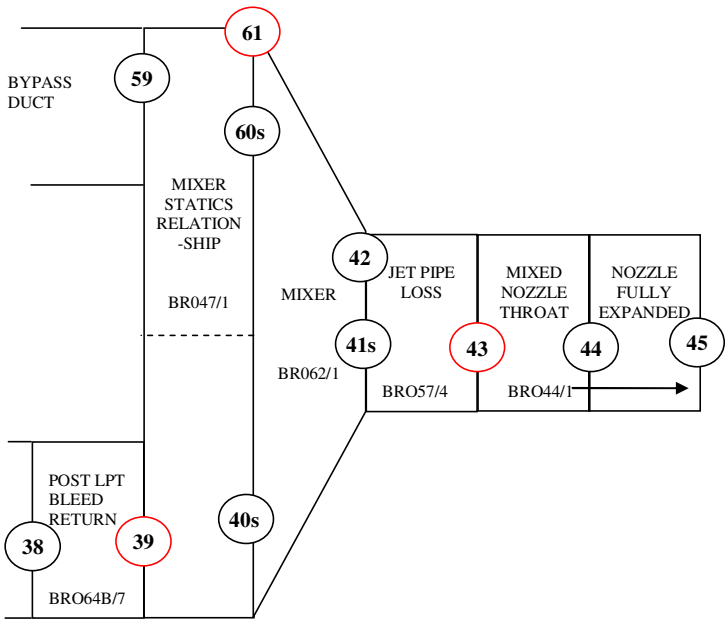

Figure 5. Brick modification for addition of a mixer to BD19 model structure.

As shown by Figure 5. brick 47 (BR047) was utilised in the addition of the mixer, as within this brick a function was available to enter a characteristics and relate the Static Mixer Pressure Ratio (SMPR Eq.7) between two ducts. Within this brick, it was selected that the bypass (cold) duct total pressure was iterated upon until the defined SMPR between the hot and cold ducts was achieved. This would produce a new total pressure value for the cold duct entry to the mixer. The use of only one nozzle results in a spare matching quantity and thus an imbalance of the matches and guesses variables. The new total pressure at 61 used the redundant matching quantity, thus balancing the number of matches and guesses.

$$SMPR = \frac{\textbf{Cold duct Static Pressure}}{\textbf{Hot Duct Static Pressure}} \qquad \textbf{Eq. 7}$$

In engine B it was expected that due to the larger BPR and nozzle areas at the mixer, not all of the cold stream will mix with the core stream especially as they are not forced to do so in a long pipe like in Engine A. Therefore brick 60 was employed to allow a % of the cold stream mixing with the core stream to be specified on a map as a function of HP spool speed or more applicable, the BPR.

3.3.3. FURTHER ADDITIONS TO THE MODEL

The existing model, after conversion from a three-spool to two-spool engine, required modifications to perform the studies required as per the subject areas and progressive decisions throughout the research. The second main modification to the model was addition of a mixer, discussed in chapter 3.3.2. Other modifications were required such to calculate the parameters required for the mixer modelling analysis and changes to the representation of the bleed calculation. These changes required the matching engine code station number in and out to be changed accordingly.

To make the code more flexible, switches were applied to allow the model to be run in two or three-spool mode or to be mixed or unmixed in two-spool mode, with variations on the defining parameters at entry to the mixer as discussed in chapter 7.3.3

As the Bristol combustion equation is the inverse of the Derby equation a switch was also added to allow a change between each representation for engine A and B.

The different integer switches are listed below;

IIPC :	*0 = two-spool mode,*	*1 = three-spool mode.*
IMIX1 :	*0 = mixed exhausts*	*1 = unmixed exhausts.*
IMIX2 :	*0 = Brick 62 mixing,*	*1 = Brick 60 mixing.*
IMIX3 :	*0 = Flight Mach,*	*1 = Cold Mach.*
IMIX4 :	*0 = BPR,*	*1 = MBPR.*
CCOMB :	*0 = Bristol combustion loading,*	*1 = Derby loading.*

3.4. ENGINE DATA

3.4.1. DATA AVAILABILITY

The model has an engine file in which the specific engine data for the engine being modelled is entered. Within this, engine design data, design point, (HP spool speed, shaft inertias, fuel flow etc), and data not normally required for above idle modelling is required to be entered. Information for starter motors, gearbox losses, hydraulic pump performance, IDG, and in some cases control bleed valve data, which is not included in above-idle simulation models, is required for this model. This presented a challenge to obtaining this data, particularly with engine A, as data availability was much less than other engines, suffering from an old engine and information on offtake components in the hands of a third party (in this case the airframe manufacturer, who is the customer).

Interestingly, enough ATF engine data was recorded for engine A that the hydraulic pumps design point (with gear ratios provided by the design group) could be derived.

Component characteristics from all main components were required, and were available in the following parameters,

COMPRESSORS ; $N/\sqrt{T}$, $\frac{\Delta H}{T}$, η_{ISEN}, $\frac{W\sqrt{T}}{P}$, β

TURBINES ; $N/\sqrt{T}$, $\frac{\Delta H}{T}$, η_{ISEN}, $\frac{W\sqrt{T}}{P}$

COMBUSTOR ; η_{COMB}, θ, FAR

Areas at stations for the OGV, ESS, Turbine NGV and bleed valve discharge were required, these were either obtained by using Eq 9, or obtained from drawings.

$$Q = \frac{W\sqrt{T}}{AP} \Rightarrow A = \frac{W\sqrt{T}}{QP} \qquad \textbf{Eq. 8}$$

(using Q = 0.333 (Mn ~ 0.6) and Engine A BDD (MTO, SLS, ISA condition).

Losses in ducts are defined by the equation 9 below, however assessing this loss factor found a difference of 2/3rds for the bypass duct in engine A, from design to off-design, rather than the factor being a constant.

$$K = \frac{W\sqrt{T}}{P} \Big/ \sqrt{\frac{\Delta P}{P}} \qquad \textbf{Eq. 9}$$

The gearbox losses are not known for Engine A, all other engines an approximate value at design is available, however the reliability of this is not certain. A request to the gearbox manufacturer through the sponsors request system, yielded little answer, with

the manufacturer unsure of what the losses are at design, let alone at off-design. The typical appraisal of gearbox losses by using an efficiency is not applicable within the sub-idle model, as a torque drag as a function of rotor speed is required. From this line of inquiry another question arose in this work, whether the losses decreased relating to the speed frictional losses or actually increased due to the increased loads on the gears and bearings tending towards static loads and not the central position as would be at design. This would be an interesting study either theoretically or by taking an actual gearbox and testing the torque drag at design and windmilling conditions.

Idle data was required, as discussed in chapter 3.5, this was run on the sponsors above idle model. It provides data that would not be measured in test data, in-particular temperatures and pressures between turbines.

3.5. IDLE DATA

Both design point and idle point data are required for constructing the specific engine data to run the model. The later is the more important for the sub-idle model as it is this which is used as the initialisation variables for the iterative solver. In this situation was where one of the greatest difficulties occurred, the ability of the above idle transient model to produce accurate idle conditions is poor. However, a model produces conditions at every station data required, whereas engine data is not available or capable of being measured at every station. Therefore the author considered these differences when extrapolating and validating simulation results.

The problems discussed above, are not an issue with the above idle models coding ability, more of the reliability of the component maps down at idle used in the model, as discussed in chapter 4.

4. Component map extrapolation

4.1. INTRODUCTION

Component characteristics are typically derived from the tested scaled rig, which is factored and scaled to line up with the component performance within the whole engine. Then the lower speed curves are usually extrapolated to idle.

In standard engine design, there are no measurements of engine components, such as compressors and turbines, in the low speed range, and measurement of these would be expensive, thus the original above-idle characteristics are required to be extrapolated into the sub-idle range.

The opinion of the author of this thesis on extrapolation of characteristic's, is that it is an acceptable approach if some alignment is used. In this thesis cold windmilling data is used to align the extrapolations of characteristics into the sub-idle region along with some theoretical physics based calculations. Without any alignment data the approach would not be valid, as what may seem reasonable extrapolations would be inherently weak as even small errors in characteristics at sub-idle conditions would produce large model simulation errors. The extrapolation approach used within this thesis uses guessed end points, thus is akin to interpolation approach, except interpolation would use a fully defined termination. Interpolation approach was developed and achieved later in the research and is described in chapter 9.3.2.

Within this research graphical, mathematical and physics based techniques are used to extrapolate the characteristic, whose alignment is assisted by the use of windmilling ATF engine data.

Previous Rolls-Royce simulations in the BD19 sub-idle code, used a scaled variants of the original extrapolated maps for engine E. As the engines within this research are far different from the previous engines, in terms of engine design and configuration parameters, each component characteristic required individual extrapolation into the sub-idle and windmilling operational region.

Little is understood of the sensitivities of a sub-idle engine simulation to the map profile at the sub-idle region, therefore this too is analysed within this chapter and chapter 0.

4.2. LITERATURE REVIEW

The process of extrapolation is to estimate a value of a variable outside a known range, from values within a known range, in the assumption that the estimated values follows logically from the known values. The following sub-chapters describe the extrapolation approaches and techniques from open literature.

4.2.1. COMPRESSOR EXTRAPOLATION

A typical approach for compiling component characteristics for gas turbines is discussed by Kurzke [33] where the following three conventional parameters WrT/P, N/rT and ΔH/T are explained as to define the Mach numbers through the engine. However, also the report confirms that at low Reynolds number, as apparent at windmilling, although here described is the low speed conditions, has the effect of increasing blade losses. It is discussed that when the compressor speed lines are vertical as would be at high speeds and choked flow, using N/rT does not allow all values of efficiencies to be represented. To rectify this issue the common practice of applying a Beta grid is described, and how to apply this to the compressor map and coverage of the surge line.

With reference to extrapolation, [33] describes the use of the commercially available tool 'Smooth C' and 'Smooth T' for extrapolating and comparison of the speed curves in different forms and how this aids extrapolation. The manuals for these two programs are references [34] and [35], and describe the parameters utilised for the map, which although can be presented in many other derived parameters, they utilise the non-linearised parameters of pressure ratio, Isentropic efficiency and WrT/P, with respect to N/rT and Beta. However, the paper also describes how extrapolating with these parameters or even $\Delta H/T$, will result in isentropic efficiency changing from $+\infty$ to $-\infty$ when traversing across the effective specific work of zero, as shown in Figure 6. . Therefore any characteristic produced by these methods would not be suitable for a sub-idle model, as the light-up trajectories pass through values of zero work.

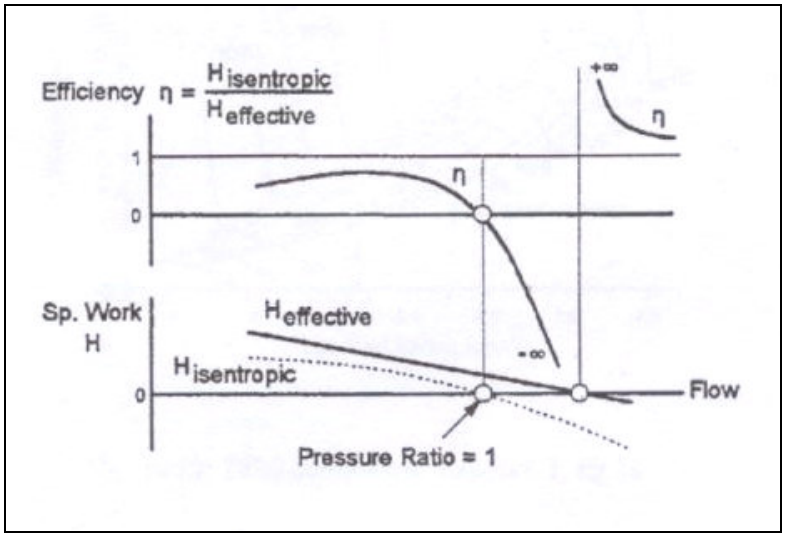

Figure 6. Effect on Efficiency at zero speed using conventional parameters [33].

One of the strongest functions for the extrapolation of a compressor parameter is shown by [33] to be that of non-dimensional mass flow versus speed and the extrapolation of the Beta lines, as shown in Figure 7. If we consider the zero speed curve the value of WrT/P at $\beta=0$ will be greater than zero, and its size will depend on how far below PR<1 is defined.

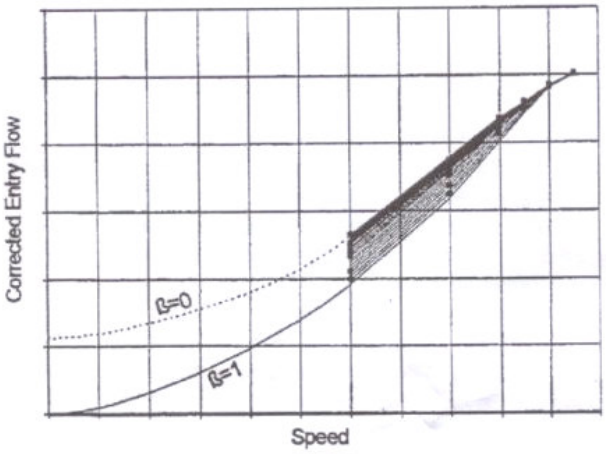

Figure 7. Extrapolation of non-dimensional flow [33].

The Gasturb simulation package and the conventional parameters for component characteristics were used by Gaudet [17], who found the same limiting problems of using these parameters where simulations running below pressure ratio of 1 the model failed. The simple extrapolation technique, [17] created using similarity laws seems a very good/ quick approach to creating characteristics at off-design speeds, but with the limitations mentioned above.

A retrospective analysis was performed by Hatch [22], whereby the data produced by windmilling tests was used to produce sub-idle characteristics in the windmilling region. This work shows that the phenomenon of windmilling and the representation in an engine model is just not limited to a gas turbine engine but also to a turbo-rocket for light-up from a windmilling condition at the end of the rocket launch phase. To determine the maximum flow the approach used is to assume the last stage is choked thereby estimating the maximum mass flow. The report describes the absolute magnitude of the efficiency and the work is questionable due to the low pressure and temperature drops. To achieve the pressure ratio the design pressure ratio was simply

factored by K= -1 as shown below in Eq. 10, where the subscript numbering relate 1 and 2 to the inlet and outlet respectively of the compressor.

$$\left(\frac{P_2}{P_1}\right)_w - 1 = k\left[\left(\frac{P_3}{P_1}\right)_d - 1\right] \qquad \textbf{Eq. 10}$$

Investigations into the various forms of characteristic representations and their advantages are discussed by Jones [28]. Also this paper describes the issues of discontinuity of efficiency going into the windmill regime. Importantly the paper describes the intuitive situation that pressure ratio and speed representation would be collinear at sub-idle conditions as both the speed and PR become flat, not producing a unique point. It is suggested that the Beta lines will assist this, though the author of this thesis would also suggest that the beta lines could also become very collinear with both speed and PR at very low speeds near the surge line (see engine A HPC characteristic in Figure 13.).

The performance simulation diagram shown in [28] uses the handle of Speed and a change to the TET. This would seem good for a steady state model, however, the author of this thesis would suggest the fuel flow (WFE) as the handle for a both steady state and transient windmilling model. Specifying fuel flow allows the engine component performance to balance to the set flight conditions applied to the engine, rather than accommodating a fixed HPC speed. For a transient simulation the fuel flow specifies the steady state windmilling condition (zero fuel flow) to the Light-up Fuel Flow (LUFF) for engine transient acceleration up to idle.

Another paper by Jones [27] references the technique employed by Choi [9], who used the relationships of lift coefficient and drag coefficient, which relate respectively to the enthalpy rise across the stage and the proportional to the square of the lift coefficient. A summation of the drag coefficients for the profile drag , the annulus wall and secondary flow losses was implemented. However, [9] obtained the profile drag loss from a loss curve of the design conditions aerofoil, depending upon the incidence.

The author of this thesis suggests that the incidence will be highly negative for windmill conditions, and little data is available at these highly negative conditions. If we were to consider that the drag coefficient for a higher negative incidence can be determined by simple extrapolation of a loss characteristic, the loss obtained will nevertheless have a significant error from the low Reynolds number experienced at windmilling conditions. The effect of Reynolds number on the loss coefficient values is described and diagrammatically shown by Massey [40], see Figure 8. below.

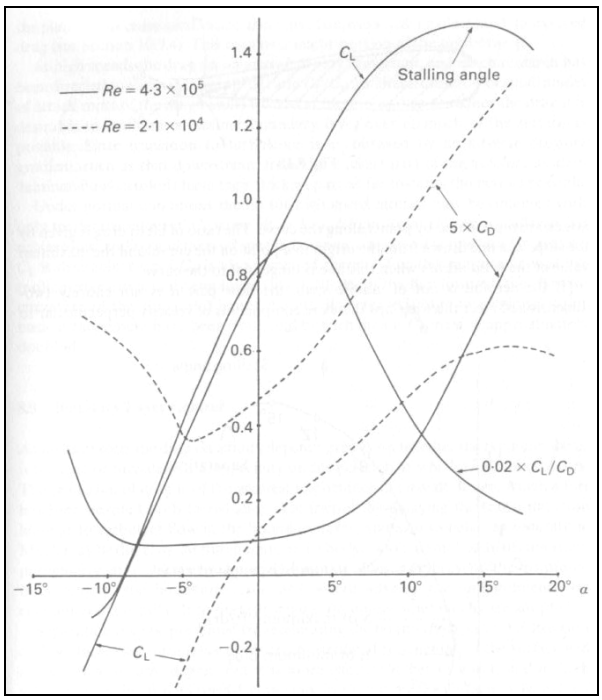

Figure 8. Reynolds number effect on lift and drag coefficients for an aerofoil [40].

As a result of the Reynolds number effect the accuracy of any prediction method using a loss characteristic has to be questioned, especially as there seems to be no loss characteristics available for the conditions experienced at windmilling. Additionally a loss characteristics for an aerofoil, does not typically account for 3D flow and blading effects on the losses. The author of this thesis produces generic compressor blade loss curves for locked rotor conditions, (see chapter 9.3.3.4 and results in chapter 11.4.2.1).

If this approach by [9] was to be used, the total pressure loss would be defined by the following equation,

$$\Delta P_c = 0.5\rho V_1^2 \frac{C_D}{s/c} \frac{\cos^2 \beta_1}{\cos^2 \beta_m} \qquad \textbf{Eq. 11}$$

relating the blade dimensions, angles and inlet flow momentum. From this the ideal Isentropic pressure loss can be represented by Eq 12.

$$\Delta P_{c\,Isentropic} = 0.5\rho V_1^2 \frac{\tan^2 \beta_1 + \tan^2 \beta_2}{1 + \tan \beta_1} \qquad \textbf{Eq. 12}$$

This presents a unique way of defining the Isentropic Efficiency, as shown below;

$$\eta_{stage} = 1 - \left(\frac{\Delta P}{\Delta P_{isentropic}} \right) \qquad \textbf{Eq. 13}$$

The above approach by [9] provides a stage by stage technique, whereby a stage stacking process can be performed to present the performance for the component at a given off-design speed.

An approach by De-You [11] used stage stacking the characteristics, by approximating the stage polynomials, and then extrapolating these polynomials. There are limitations of this method only being accurate to within the range of known data, rather than the sub-idle region required.

4.2.2. TURBINE EXTRAPOLATION

There are few examples in the open literature of turbine extrapolation techniques as attention is given to the more problematic compressor. A stage by stage approach was chosen by Jones [29] to represent the turbine maps. However, he notes the errors within this technique of reliance on empirical loss coefficients which are not aligned for the sub-idle operating conditions, such as low Reynolds number and unchoked flows. He recommends a zero speed curve using torque for extrapolation and this would improve the repeatability.

For the representation of turbines [33] describes that Betas can again be used, and explains flow may or may not be expressed as a function of the N/rT. The work or pressure ratio is usually plotted versus flow and the respective speed curves are added. The author of this thesis would suggest that it is also indicative, that with a turbine, the problem experienced with compressors of large changes in efficiencies of ∞ should not occur as the turbine is always acting in expansion mode.

It is proposed by [9] that the pressure loss in a turbine may be represented by the energy losses in both the rotor and stator from turning the flow with coefficients (k_s and k_r) obtained by the 'Soderberg correlation', and also the loss from off-design incidence can be represented. The losses for stator (Ls), rotor energy loss (Lr), and incidence loss (Li) are defined below, Equations 14 to 16. An issue with these correlations is the involvement of the profile loss is based around design conditions for design point assessment, instead of the high negative incidences at windmilling to locked rotor.

$$L_s = k_s\left(\frac{C_{in}^2 + C_{out}^2}{2gCp}\right) \qquad \textbf{Eq. 14}$$

$$L_r = k_r\left(\frac{V_{in}^2 + V_{out}^2}{2gCp}\right) \qquad \textbf{Eq. 15}$$

$$L_i = \frac{C_{in}^2}{2gCp}\left(1 - \cos^n\left(i - i_{opt}\right)\right); \qquad \text{where} \quad i_{opt} = -4^o \qquad \text{Eq. 16}$$

n = 2 (positive incidence)

n = 3 (negative incidence)

These formulas then require equating to a delta pressure, therefore the following calculation for the stator and the rotor is performed in Eq. 17.

$$\Delta P_T = \frac{\rho L_i Cp}{144} + \frac{\rho L_r Cp}{144} + \frac{\rho L_s Cp}{144} \qquad \text{Eq. 17}$$

As described by Dixon [12], the Soderberg correlation can define the stage efficiency by employing parameters of specific enthalpy and losses at design point, it is also useful to note the Reynolds number can be corrected.

To summarise, the extrapolation approaches are limited in their reliance on empirical coefficients and the error in these methods may be significant. A zero speed approach to extrapolation would be far less erroneous and improve extrapolation repeatability, this is attempted in chapter 9.

4.3. EXTRAPOLATION METHOD

4.3.1. SUB-IDLE MODEL APPROACH TO COMPONENT REPRESENTATION

A compressor map representing the component behaviour at the far off-design conditions of sub-idle operation, needs to capture the blade profile, annulus and secondary losses, and the effects of reduced Reynolds number on these losses. Graphical techniques using test data to align the extrapolations would include the losses, however, physics based derivation of extrapolated regions require accurate empirical coefficients to apply the losses. Typically loss coefficients are not devised for such flows and Reynolds number at off-design, and are instead created for the design point conditions with only a slight variance.

The main approach used for the creation of maps to be used in the engine models, implements the pressure, work and flow coefficient parameters as used by Rolls-Royce in the previous BD19 models, see equations 18 through to 21. The latter two of these equations are typically used in both turbine and compressor design. These parameters create a linearization of the conventional characteristic parameters of work and pressure ratio due to the speed term in the denominator.

Psi = $$\frac{\Delta H}{U^2} \propto \frac{\Delta H}{N^2} = \frac{\Delta H}{T} \div \left(\frac{N}{\sqrt{T}} \right)^2$$ **, the work coefficient** **Eq. 18**

For compressors;

$_{ISEN}$Psi = $$\frac{\eta \Delta H}{U^2} \propto \frac{\eta \Delta H}{N^2} = \frac{\eta \Delta H}{T} \div \left(\frac{N}{\sqrt{T}} \right)^2$$ **, the pressure coefficient.** **Eq. 19**

For turbines;

Psi_{ISEN} = $\frac{\Delta H}{U^2\eta} \propto \frac{\Delta H}{N^2\eta} = \frac{\Delta H}{T\eta} \div \left(\frac{N}{\sqrt{T}}\right)^2$ **, the pressure coefficient** **Eq. 20**

Phi = $\frac{Va}{U} \propto \frac{WT}{NP} = \frac{W\sqrt{T}}{P} \div \frac{N}{\sqrt{T}}$ **, the flow coefficient** **Eq. 21**

In a compressor using of non-linearised parameters such PR or ΔH/T and WrT/P, when the pressure ratio passes from 1 to < 1 (therefore in a stirrer or turbine mode in windmilling), the isentropic efficiency will become negative. Assuming the compressor is in a stirrer mode, of increasing entropy with the temperature ratio above one, it can be seen that if a pressure ratio just below one is applied in Eq.22, the -1 term in the numerator will make the numerator small and the efficiency negative. The efficiency can switch back to a positive efficiency when the compressor temperature ratio decreases (temperature ratio is less than one) and the compressor behaves as a turbine with a specific enthalpy drop (to achieve this, the compressor pressure ratio would fall further below the stirrer pressure ratio).

$$\eta_{Isen} = \frac{\left(\frac{P_{out}}{P_{in}}\right)^{\frac{\gamma-1}{\gamma}} - 1}{\frac{T_{out}}{T_{in}} - 1} \qquad \textbf{Eq. 22}$$

Extrapolation of linearised parameters avoids the discontinuity of efficiency with conventional parameters, as extrapolated curves of Isen_Psi as a function of Psi allows Isentropic efficiency to be selected from the graphs, simply by dividing Isen_Psi by the Psi calculated by the model. Thus avoids having to determine the Isentropic efficiency from ratios of pressure and temperature as used in other methods.

Using spreadsheet tools by Leitges [38], mathematical and graphical techniques were used for the extrapolation technique with some physical definitions for termination of some characteristics. These tools were modified by the author of this thesis, to provide compressor non-zero flow towards zero speed, the beta extrapolation was smoothed to avoid model iteration jump errors, and the extrapolation curve equations were modified (particularly for engine A).

The following chapters discuss the extrapolation methods and approaches implemented with the spreadsheet tools, to define the characteristics for implementation in the sub-idle models.

4.3.2. DATA REQUIRED FOR EXTRAPOLATION OF COMPONENT CHARACTERISTICS

The first step is to convert the above idle characteristics into the coefficients described by equations 18 through to 21.

The approach in the extrapolation of the compressor characteristic is to use ATF cold windmilling test data to align the extrapolation from the existing idle region of the map. The ATF engine data can be used define the parameters of pressure ratio, non-dimensional mass flow and work, at low speeds, and the linearised parameters can be defined via the ΔT and PR. The use of cold windmilling data is important to ensure that no heat soakage effects are included which can have significant impact on the windmilling values calculated, such as the temperatures across the compressors.

Additionally some understanding of quantity of power offtake is required to ascertain the compressor work. Ideally ATF runs with zero power offtake would be more suitable for defining the true compressor performance. However, in most tests and engine test-bed time, this is not practical.

4.3.3. INITIAL EXTRAPOLATION STUDIES

Initial attempts at extrapolation of characteristics used the commercial code Smooth C and Smooth T. Although this program provided some great comparisons of the effects on the parameters in certain plots, the program was found to be not suitable for extrapolating characteristics into the extreme sub-idle conditions.

The software predicts a lower speed curve from previous values, which can then be graphically modified. The problem with this extrapolation tool is when pressure ratios below one are attempted, by spreading the beta grid to low pressure ratios, the efficiency term is derived from the work and pressure ratio extrapolations. Thus discontinuities of $-\infty$ and then $+\infty$ appear in the efficiency plots, which as a result could not be used in a simulation code. Another problem with the tool is that the beta spread below pressure ratio of one is very limited to around only 0.99.

The code does have some benefits for representation of characteristics above pressure ratio one, as the program allows visualisation of many other parameters such as torque. The program however, does not provide repeatable techniques, as with mainly graphic based definitions the code relies heavily on the users experience and interpretation of what is a good characteristic.

4.3.4. COMPRESSOR EXTRAPOLATION

The compressor characteristic was one of the most difficult to extrapolate into the sub-idle region, as three phases of operation are apparent, compressor, stirrer and turbine (shown in Figure 10.). Steady state cold windmilling data was available, and idle data from the performance model and test data, however, no data is available between these two regions of operation. The ATF data can be used to align the extrapolation in a variety of map representations, shown in figures 10, 11 and 13.

The pressure ratio in the turbine mode of windmilling is still calculated in the same way as it is in compressor mode (using Eq 22), thus at negative pressure ratios, negative isentropic efficiencies will result.

Three maps of each coefficient as a function of Beta and N/rT are produced. Thus a point on one map relates the same beta, non-dimensional speed on another coefficient parameter map.

$$Psi = f(Beta, N/\sqrt{T}),\ Isen\_Psi = f(Beta, N/\sqrt{T}),\ Phi = f(Beta, N/\sqrt{T}$$

Both the non-dimensional speed (N/rT) and Beta lines require extrapolating. However, in extrapolating the speed, the beta lines are used to define the limits of the coefficient parameter.

The following chapters describe the extrapolation process for each component characteristic parameter and how these relate to one another. The approaches used are discussed and their description assisted by logic flow diagrams. These extrapolations were then modified and improved by running the model in an adaptive approach as discussed in chapter 0.

4.3.4.1. Extrapolation of Psi and Isen_Psi,

The extrapolation process is complicated and is best described by the logic flow chart in Figure 9. depicting the extrapolation of Psi. The following paragraphs discussion describes the process. Extrapolation for Isen_Psi follows the same routine, although the selected values differ slightly as shall be discussed at the end of this sub-chapter.

To initiate the extrapolation a minimum speed somewhere in the region of 1 to 5% N/rT needs to be selected and then the Psi or Isen_Psi range for this speeds min and max beta lines. A curve equation using the gradient between the coefficient parameters of the previous two speeds uses constants defined by the end limit to extrapolate the coefficient values, at each speed defined, between the original map lowest speed and the minimum extrapolation defined speed. The author found for engine A that a linear equation suited the lowest speed curves to that of the quadratic equation used for engine B. The problem with the quadratic is that close to zero speed the gradient of the curve becomes zero promoting that the work changes little through the lowest speed curves. However, due to the effect of N/rT^2 in the coefficient term and also that this is the x-axis parameter, then the resulting specific work may not fall fast enough for the particular engine towards zero speed.

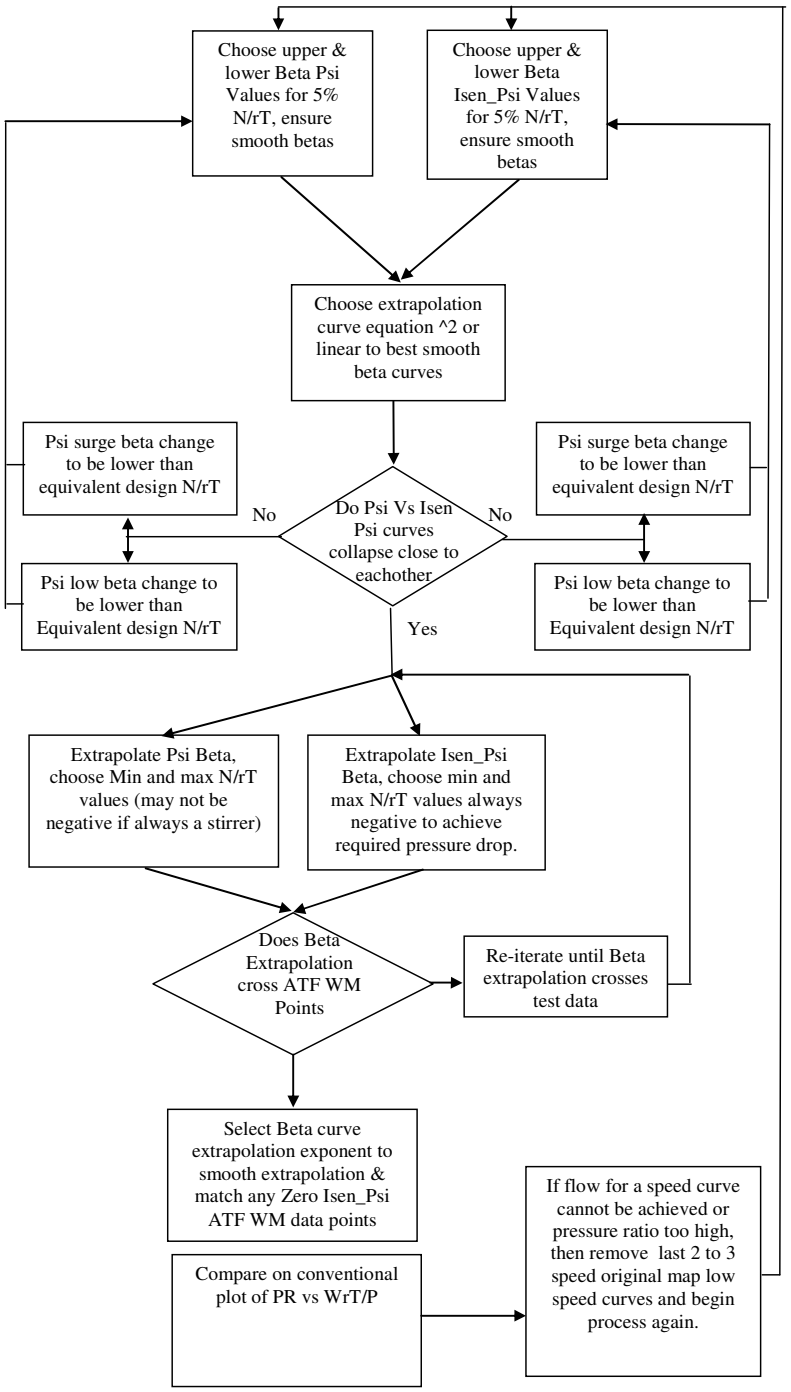

Figure 9. Logic Flow diagram of extrapolation process for Psi (same process can be used to obtain Isen_Psi).

The Beta lines can then be extrapolated into the windmilling region of the compressor. As the difference between the beta lines is linear, a plot of Psi as a function of Beta would create sharp transition from the existing beta grid to new, therefore a dummy equation defines the beta spread, to smooth the beta extrapolation. The beta extrapolation works in the same process as the Psi extrapolation, however, now the limits are the min and max non-dimensional speeds of the entire extrapolated coefficient parameter.

Now the Psi and Isen_Psi extrapolations require alignment which firstly relies on plotting all of the above idle and extrapolated speed lines with the extrapolated beta lines on axis of Isen_Psi versus Psi. The effect is that all of the main body of each speed curve should fall onto each other, and if they do not, the process in the above two paragraphs has to be repeated. The beta lines should extrapolate out linearly from the compressor mode through the stirrer mode and into the turbine mode, as shown in Figure 10.

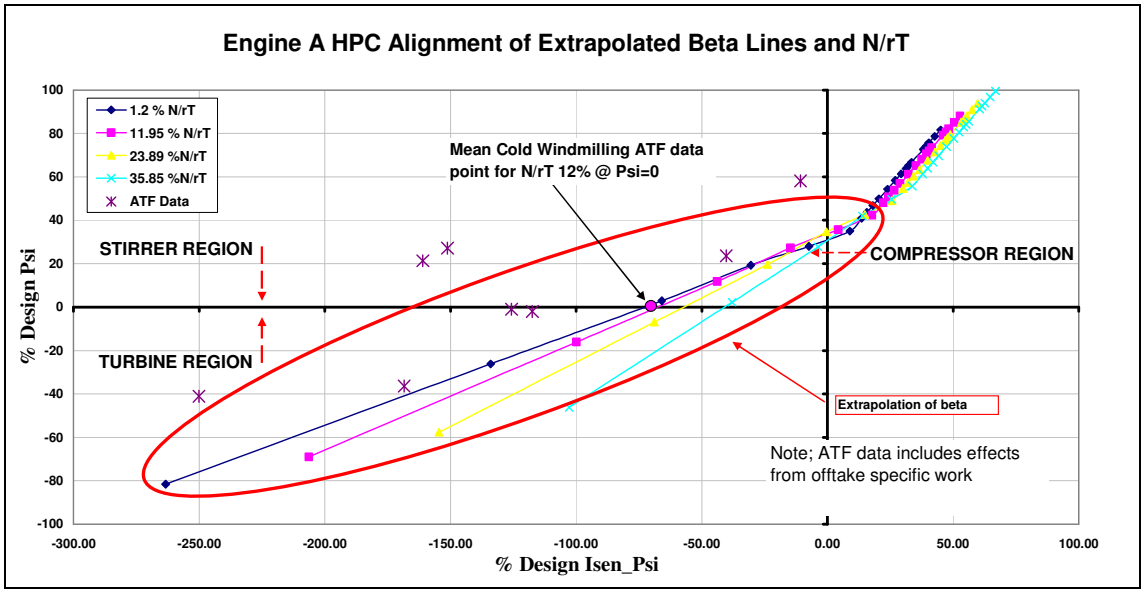

Figure 10. Alignment of Isen_Psi vs Psi extrapolation to ATF test data.

In the turbine region, the lower speed curves may spread out to match the spread of test data. For correct application, the lower speed should always be higher towards the stirrer region as a locked rotor would create a larger stirring effect than a windmilling rotor in which the blade incidences are less, as described in chapter 9.

This process can be very iterative, and small changes make significant differences to component performance, particularly the sensitivity of the work coefficient on the smaller engine A. It is also important to understand that changing the parameter range on the minimum speed curve will also change the respective range achievable in Phi extrapolation, as discussed below.

4.3.4.2. Extrapolation of Phi.

The author discovered that the techniques for extrapolation of non-dimensional mass flow within the extrapolation tool were incorrect. The principle for flow representation was to consider WrT/P zero at zero N/rT (or the minimum defined N/rT), however, this is not true as even a zero speed curve would have a range of flow conditions possible, each for a given flight Mach number and altitude. Engine B maps were initially created on this principle, and the author of this thesis found that when running transient simulations the lack of WrT/P range which in turns limits PR for a given N/rT, limited the acceleration potential and model would not accelerate.

If we now consider there to be a range of flow instead of zero, for the minimum speed, there is another problem of the influencing effect by the denominator of N/rT tending to zero, thus the Phi values become extremely exponential to achieve some value of WrT/P as shown in Figure 11. a) To overcome this problem, instead of extrapolating Phi (WT/NP), WrT/P was extrapolated first, creating a range of flow for the lowest extrapolated speed using the smoothed easy represented by equation of curves of the beta grid, as shown in Figure 11. b).

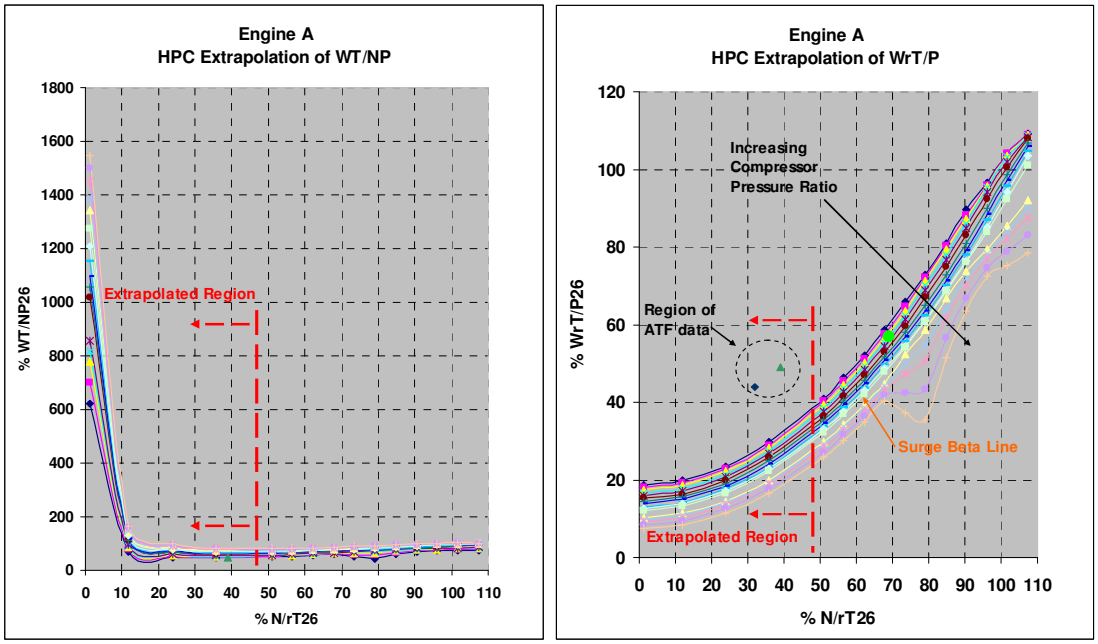

Figure 11. a) Phi Extrapolation. b) WrT/P extrapolation solution.

Once the WrT/P extrapolation is complete conversion to Phi is completed. This is a much more satisfactory technique, as it is impossible to find a suitable curve equation to represent extrapolation in terms of the Phi parameter.

With the culmination of the Psi and Isen_Psi to derive pressure ratio, the alignment of the WrT/P against PR can be represented on the conventional representation of the compressor characteristic as shown in Figure 13. If the flow does not match for a particular speed, it may be that the flow was defined incorrectly or the efficiency thus the Isen_Phi and Psi extrapolations are incorrect.

The explanation of the extrapolation process to obtain Phi is described in the logic flow chart of Figure 12.

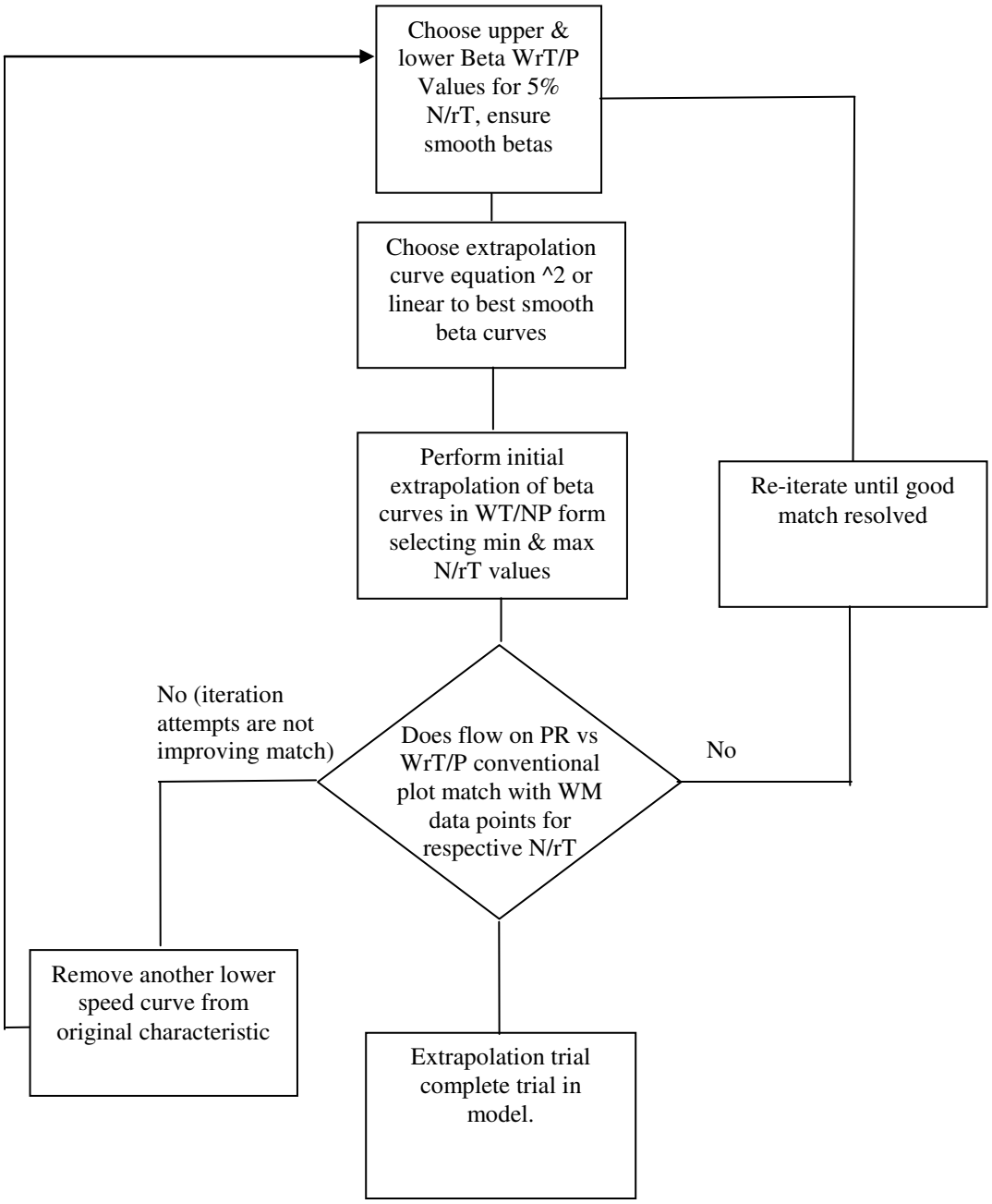

Figure 12. Logic flow diagram for extrapolation procedure for WrT/P, thus WT/NP.

Figure 13. presents the resulting extrapolated HPC characteristic, and also identifies the lack of definition at low speeds, particularly the 1% N/rT curve which has no pressure ratio definition. The surge line gradient for engine A becomes very flat at around 36%N/rT, reducing the pressure ratio (P30Q26). The non-dimensional mass flow (WRTP26) is that at the inlet of the compressor.

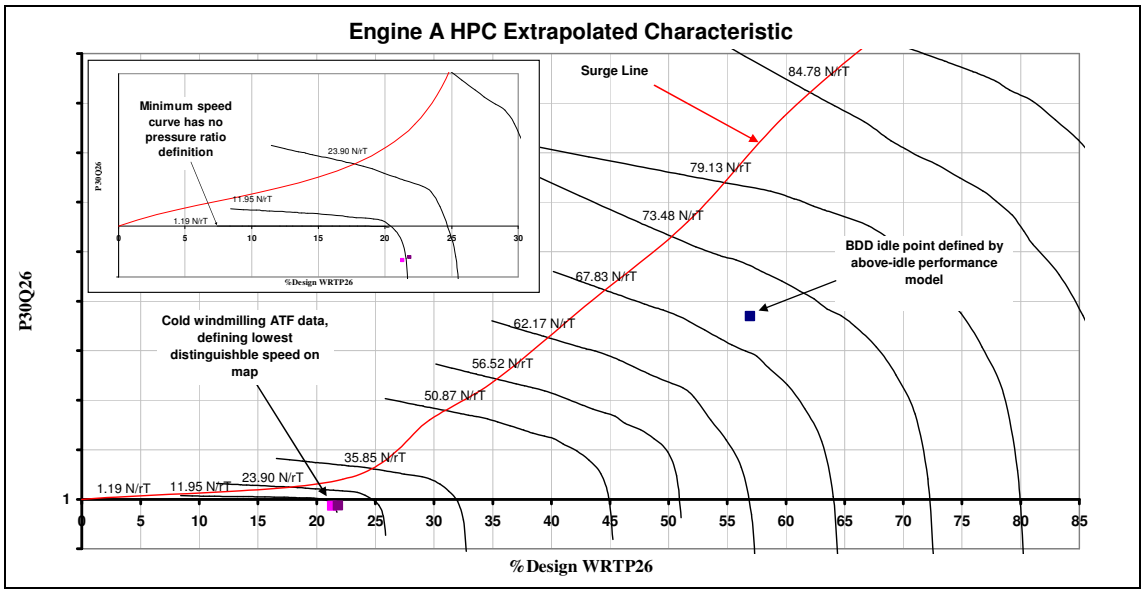

Figure 13. Extrapolated HPC characteristic presented in conventional parameters.

Points of cold windmilling ATF engine test are shown in figure 13. and these were used to align the most difficult low speed curves close to 10%N/rT. Also shown in the idle point taken from the sponsors above idle performance model.

4.3.5. FAN EXTRAPOLATION

4.3.5.1. Total fan map

The fan map is typically represented by a split fan map and has been produced by a defined change in bypass ratio, from design to idle. However, in the vast range of far off-design conditions of sub-idle modelling, the bypass ratio is not a constant function of speed. Instead the bypass ratio is less affected by speed and more by the operating condition, as discussed in chapter 2.3.3.

The Fan Outlet Guide Vane (OGV) can be defined as a separate loss based on extrapolated curves from the design modelling, or as with engine A, the OGV losses are included within the fan characteristic. This separation of approaches makes the comparison of component characteristics difficult.

The modelling of the fan in the BD19 sub-idle model, uses a total fan characteristic. A total fan map should exist from original testing of fan. However, this is typically difficult to find as the fan characteristic for the typical design process is immediately split into the root and tip characteristics. As a result of no total characteristic being available for either engine A or B, these had to be constructed from the split maps.

The following equations 23 and 24 were formed to combine the above idle root and tip characteristics as a function of the BPR (where BPR is used to create a fraction and the total above idle fan characteristic formed may be extrapolated into the sub-idle region). The BPR for the design and idle operating points, taken from the above idle model ISA SLS simulations, were used to define a simple linear relationship between of BPR versus non-dimensional speed. Thus for each speed line on the map the respective beta points for PR and Isentropic Efficiency would be proportioned by the corresponding value of BPR. The non-dimensional flow for the characteristics were already defined as total flow.

$$TotalFanPR = \frac{BPR}{BPR+1} xPR_{Tip} + \frac{1}{BPR+1} xPR_{Root} \qquad \textbf{Eq. 23}$$

$$TotalFanIsenEta = \frac{BPR}{BPR+1} xIsenEta_{Tip} + \frac{1}{BPR+1} xIsenEta_{Root} \qquad \textbf{Eq. 24}$$

Alternatively the Specific Work could be used instead of pressure ratio in the above equation 23. One should be careful not to get confused and use the BPR as a multiplier on its own, as the Specific Work for the fan will actually be the average ΔT across the whole fan, not a summation of the root ΔT and the tip ΔT. In fact the author initially requested a total fan map to be assembled by the sponsor's partners'. However, it would seem they had summed the specific work of the root and tip, producing a fan that required twice as much work at design, than the split fan work, just highlighting mistakes easily can be made.

When extrapolating Beta and after much development, a more satisfactory representation was found by representing Psi as a linear extrapolation and Psi-Isen as a curved extrapolation. This achieved a more suitable curved extrapolation on the Psi_Isen versus Psi plot, see figure 26.

In the later stages of the research the author of this thesis came to the conclusion that within BD19 there is a problem with the calculation of the LP spool power balance, when using the total fan characteristic. The total fan work and mass flow are used to determine the LP compressor power, and the root work is ignored. However, from the total fan work, the ΔT (an average of the total fan and not just the ΔT for the bypass) and Isentropic efficiency are determined to calculate, not the total fan PR, but the

bypass PR. The fan bypass pressure ratio and temperature ratio will not be correct, however, these values will vary due to the influence of BPR. This problem will be more pronounced for low BPR engines as the work from root to tip are very similar. In fact at windmilling, the root stirring work could negate any windmilling work produced in the bypass. Therefore the error from this problem is insignificant on large bypass ratio engines, however, on low bypass ratio engines it is significant, where in engine A the design fan root work is larger than the bypass.

The author would recommend further study into making changes such as separately summing the root and bypass powers once the BPR total fan split has been calculated. Therefore only bypass Psi and Isen_Psi parameters would be defined against a total WT/NP characteristic. The fan would no longer represent changes in the pressure ratio and work from large swings in BPR, however, this may not be a problem on low BPR engines.

Also for ground starting the effective required work from an LPT for a large bypass ratio engine is likely to be higher than a low BPR engine, even with a typically lower fan pressure ratio. However, the opposite would be true in windmilling, where the high BPR engines fan would be producing much more work in turbine mode than a smaller multi-stage fan, thus the turbine would be required to do less work.

4.3.5.2. Root fan map

A root characteristic for Psi and Isen_Psi is required to determine the pressure and temperature changes through the fan root, to provide entry conditions to the downstream ESS. In previous models a constant value of Psi was entered in the model data and single curve for Isen_Psi was a function of Beta for all non-dimensional speeds. In the low BPR design of Engine A the root work and pressure loss (Psi and Isen_Psi

respectively) were significant as at design the root work is higher than the bypass. Therefore complete root characteristics were created for Engine A.

The spread of the fan root map must end in the same values of Psi as the total map, even if the Isen_Psi values do not. This is to maintain a consistent extrapolation approach.

Upon aligning the root compressor to the ATF windmilling data, it was apparent in windmilling conditions the behaviour was always that of a stirrer.

4.3.5.3. Summary of compressor extrapolation

The compressor characteristics are extrapolated based on mathematical curves and graphical comparisons with ATF test data. This process is very user intensive and requires user knowledge although it is hoped the chapters discussions, assist future work.

The author discovered there are many approaches to defining the beta line limits, past surge would indicate a negative flow on the minimum speed curve. Also the surge line slope effect's how to represent the beta grid, with the limited equations for the extrapolation. To follow the surge line, say in engine A (see Figure 13.),would require changing the extrapolation curve equations for the last three low speeds to suit the surge line shape of flat pressure ratio but still changing flow.

An improvement to the extrapolation technique was to extrapolate the above idle characteristic beta curves into windmilling range, prior to extrapolation of the speed curves. This negated any further need to extrapolate the new low speed curves Beta, although this technique removed the flexibility of providing more WrT/P for lower speed conditions.

It is the shape of the speed curves on Figure 13. which are difficult to represent as there is no data other than the windmilling data. Although the initial transient acceleration up the constant speed curve during a windmill relight may be used to aid the definition of this curve, reservation must be given to the data due to its the transient nature.

To avoid forcing the model to run along a constant relationship of ΔT to PR, Isen_Psi is spread at the end of the beta extrapolation. As for each windmilling condition there is not a unique speed, due to the interaction of power offtake and this spreading should also aid the matching of the model.

The extrapolation process could be significantly improved by the approaches discussed in chapter 9, whereby a zero speed curve would define the lower limit data to extend the characteristic to and help define the speed curve shape at low non-dimensional speeds.

4.3.6. TURBINE EXTRAPOLATION

Turbines are unlikely to have the problems of discontinuity of variables as experienced in compressors as the turbine always behaves as a turbine. However, the turbine may behave as a stirrer during the dry-crank of a groundstart. The enthalpy change across the turbine is a function of the flow angles which are similar to the blade angles at windmilling conditions. The gas path air ratio of specific heats and specific heat during cold windmilling will be the same as that passing through the compressor.

The turbine maps are much simpler than the compressor maps, instead of Beta, the parameters are all a function of Psi and also N/rT a shown below, and once converted to the linearised coefficients the following two characteristics are formed, as shown below.

$$Phi = f(Psi, N/\sqrt{T})$$

$$Psi\_Isen = f(Psi, N/\sqrt{T})$$

To extrapolate Turbine maps, the author along with [38] found the lower at speeds around 5% and below the flow could be considered incompressible and as a result, as highlighted by engine E BD19 characteristics of Psi versus Phi, this speed line is practically linear (shown by region 3 in Figure 14.). From this linear curve for the lowest speed, the intermediate speed curves could be extrapolated as shown by region 4 in Figure 14.

Using the turbine blade angles an incompressible momentum calculation is used to calculate the inlet axial velocity. Assuming continuity of mass and iterating upon initial exit conditions with assuming incompressible conditions, the exit conditions can be found to define the Psi, and Phi for design WrT/P and zero WrT/P. Thus define an incompressible curve for a small speed, which produces practically a straight line.

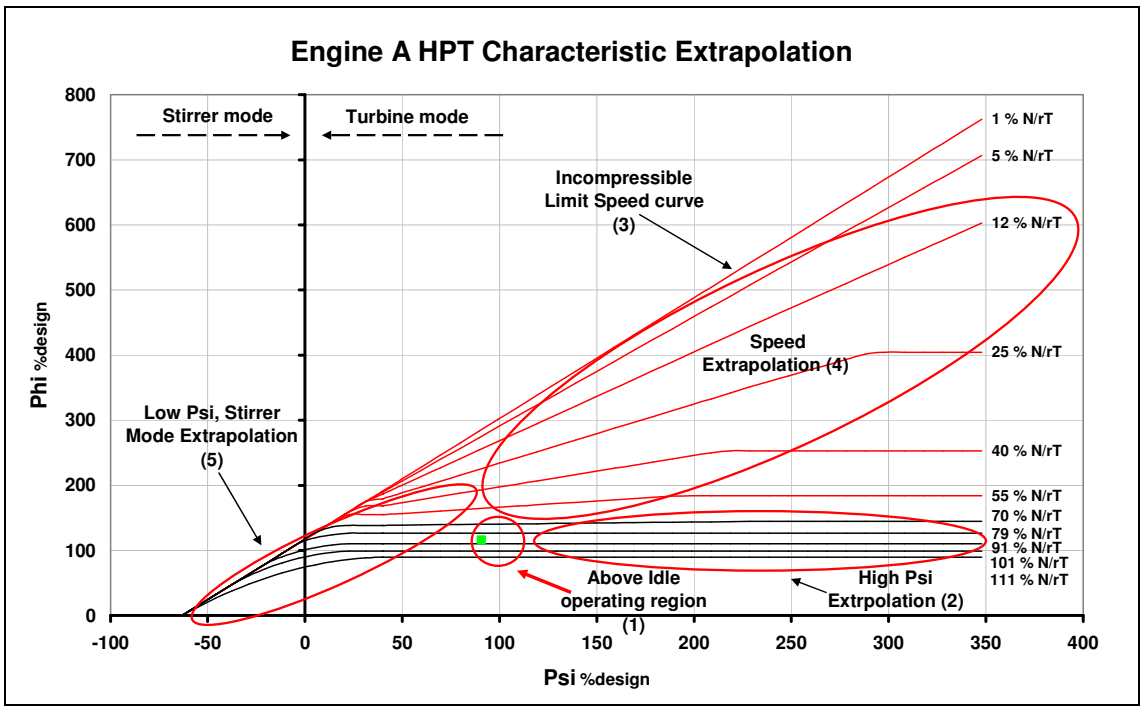

Figure 14. HPT extrapolated characteristic, defining extrapolation regions.

The higher Psi extrapolation is required for light-up accelerations in the low speed range, therefore to complete the extrapolation region (1) is extrapolated to region (2) based on the turbine choked design WrT/P. From regions (1), (2) and (3), the low speed curves in region (4) can be extrapolated. This then only leaves region (5), required to define important windmill and groundstart region. To achieve smooth curves here, some of the data from the original above idle characteristic has to be replaced by the extrapolation functions. For calculation of incompressible limit, see Leitges [38].

Prior to the calculated method described above, was an attempt to define the incompressible limit line by approximated ATF data rather than the use of the turbine blade angles to calculate the curve. The model windmilling and acceleration light-ups matched well at flight Mach numbers below 0.6. Derivation of the incompressible limit curve by using the calculations based on the blade angles, produced simulations where at all flight mach numbers the windmilling speeds matched well.

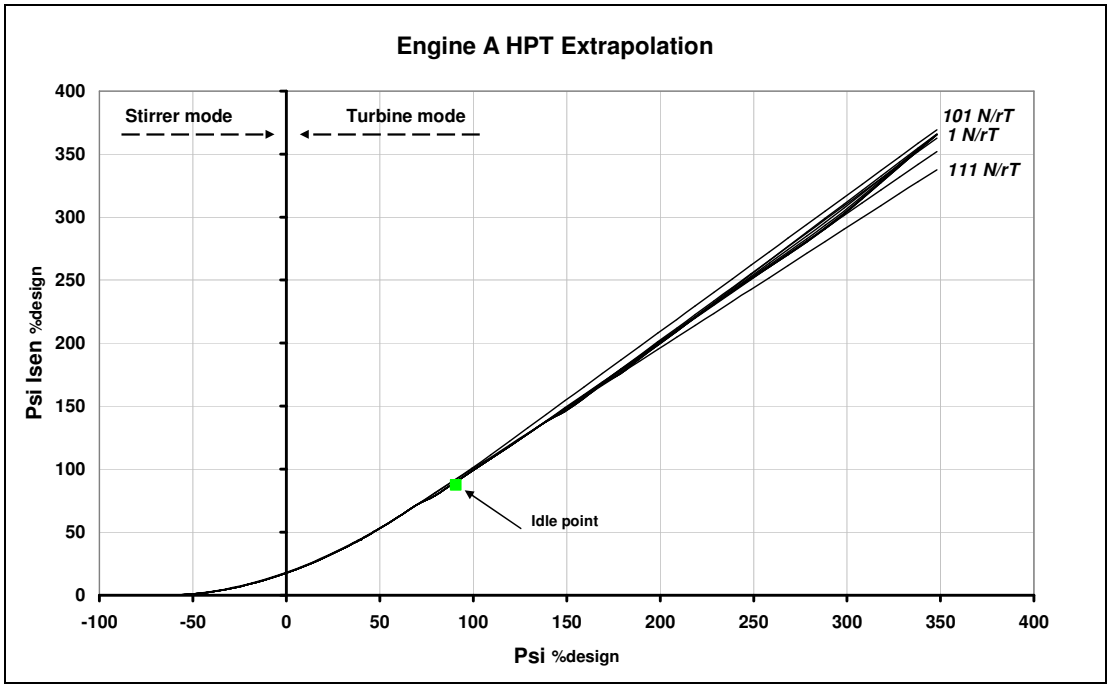

Figure 15. HPT extrapolated characteristic of Psi and Psi_Isen relationship.

To obtain Psi_Isen, the above relationship where the non-dimensional speeds generally fall on top of one another is applied, as shown in Figure 15. . The speed curves tend to spread out at high Psi values and even more so for the LPT. Psi_Isen is extrapolated using a polynomial equation to zero and the minimum Psi value determined by the incompressible limit curve in Figure 14.

4.3.7. COMBUSTION CHARACTERISTIC EXTRAPOLATION

The combustor characteristic typically does not extend to low light-up efficiencies required at windmilling, however, test data is typically available to with some confidence extrapolate the characteristics. In this research work it was found no test data was available for engines A and B. Engine B only had a single curve representing a range of AFR's, therefore another similar engine combustor characteristic was scaled.

Definition of the combustor characteristic is by the loading parameter, combustor efficiency and typically AFR or FAR, as defined below, where W31 is the combustor air inlet mass flow.

$$FAR = \frac{Fuel}{W31} \quad \text{Eq. 25} \qquad \text{Therefore AFR} = \frac{1}{Fuel/W31} \quad \text{Eq. 26}$$

If AFR or FAR is used for light up simulations, there will be large swings of values from zero fuel flow and with high air flows to high fuel with low airflows. AFR was found to be producing inconsistencies and jumps in the model results, it was therefore decided to convert to the combustor inlet non-dimensional mass flow WrT/P30. Typical approach within the sponsor is to assume a constant value of AFR or 40 and enter a range of WrT/P30 curves (where 30 refers to station 30, the HPC compressor exit).

Due to the large changes in operation required by the model from windmilling to assisted starts, the author decided to analyse the relationship of AFR to WrT/P30 for a

range windmilling light-up conditions along with design and idle points. The results for engine A are shown below in Figure 16.

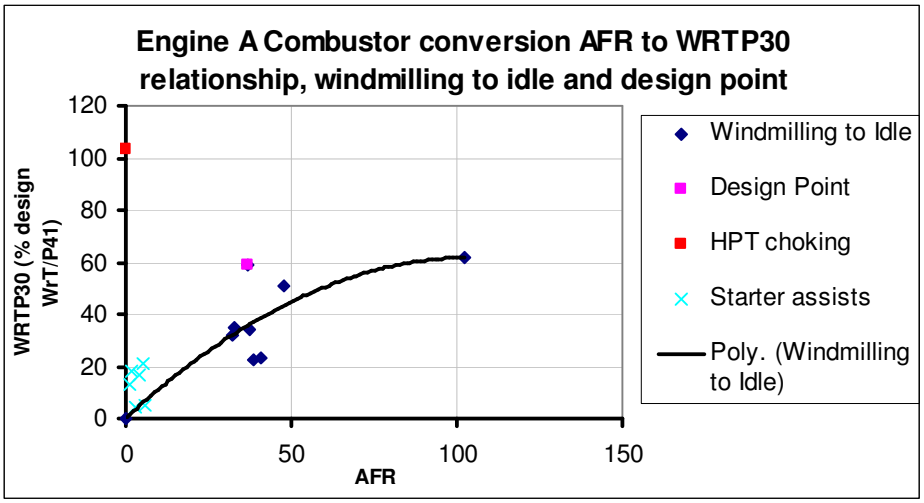

Figure 16. Derivation of relationship between combustor AFR and WrT/P30

As can be seen from Figure 16. using a value of AFR 40 would not be suitable for all sub-idle operating conditions. Therefore a trendline was used to produce a quadratic relationship to convert the combustion characteristic AFR values to WrT/P30 (where the compressor exit non-dimensional mass flow at station 30 is a percentage of the HPT design choking flow at station 41). As pressure loss is a function of WrT/P, this presents a better relationship with combustor operation prior to light-up than AFR, as also includes altitude effect on the pressure. However, the limitation of this solution for performance simulation modelling, is that the combustor characteristic no longer has a direct definition related to the fuel flow.

Using WrT/P does not solve the extrapolation of the characteristic, but it does assist, therefore the sound assumption that the combustion efficiency will be zero at steady state (unlit) windmiling conditions was used. Therefore using the windmilling ATF data a relationship for the spread of curves of WrT/P30 along the combustion loading axis, for zero combustor efficiency, would create an end limit for the extrapolation of

the combustor WrT/P curves. In the author's opinion this was satisfactory as the curves of WrT/P also terminate with close to a vertical gradient.

The relationship found is shown in Figure 17. in which a strong function was found between the two parameters. A trend line was produced with the limit on WrT/P30 being that of the HPT choking non-dimensional massflow. Assuming the pressure loss is minimal the steady state windmilling value of WrT/P30 would be practically equal to WrT/P40 at entry to the HPT, prior to light-up.

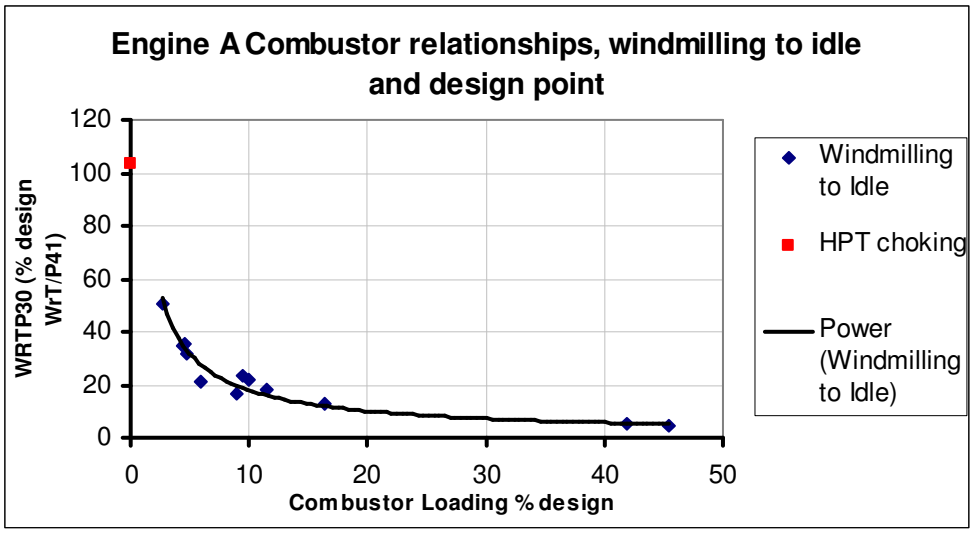

Figure 17. Derivation of relationship between combustor Loading and WrT/P30.

With the spread of WrT/P30 determined, a sensible equation for the extrapolating the curve was selected and the combustion map extrapolated as shown in Figure 18. If there is enough confidence in the engine turbomachinery characteristics, the sub-idle model could be run to find the windmilling Loading and WrT/P30 thus defining the end limits. The issue with this approach is that any model error will be multiplied, as this will then be used to compose the combustion characteristic.

$$\theta = \frac{Vol\_FACTOR x P31^{1.8} x 2.71828^{T31/300}}{VOL_{COMB} x W31} \qquad \text{Eq. 27}$$

The combustion volume forms part of the combustion loading parameter, defined in equation 27 (for engine A) and described in chapter 8. As such, any changes to the volume would effect the relationships obtained between combustion loading and WrT/P30. Therefore to study the effects from the design and previous engine Mk combustion volumes, two sets of combustion volume characteristics were derived.

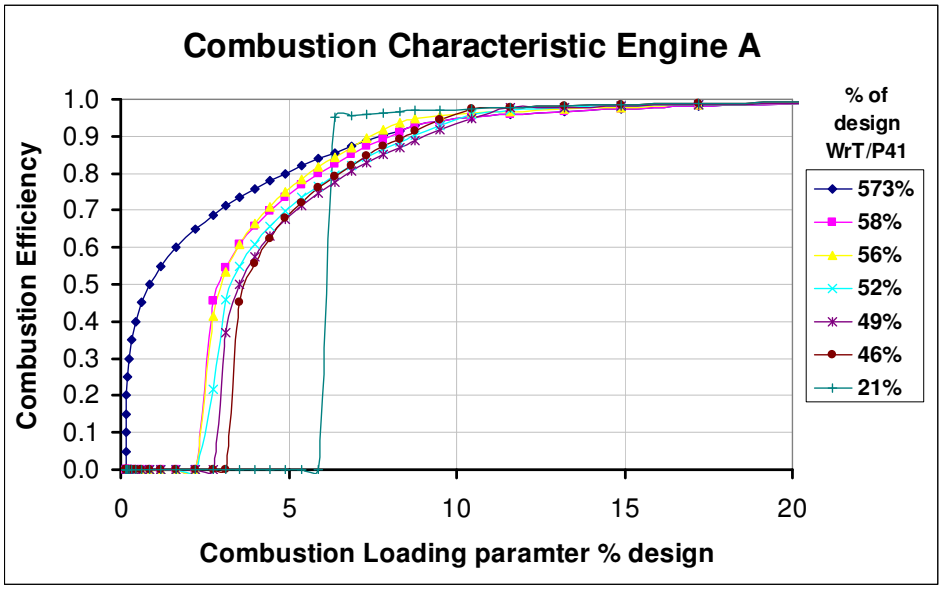

Figure 18. Extrapolated combustion characteristic, curves of WrT/P30.

As Figure 18. highlights a cross-over of the lines of WrT/P from the higher combustion efficiencies through around 90-80%. This is the relationship of WrT/P with loading (as for engine A) influencing the termination of the characteristic. Another characteristic was attempted by a relationship of the windmilling (prior to LUFF) WrT/P versus AFR, however, the characteristic did not perform well in the model, as it is a conversion of the AFR in the lit range which is required.

The sub-idle model required a combustion characteristic to run transient light-ups, in which the extrapolated region of the characteristic efficiencies will be used to obtain the efficiency. This could be modified by the inefficiency factor, which was also used to improve the map iteratively.

5. Adaptive running of sub-idle model simulations

5.1.1. INTRODUCTION

To produce accurate model representation over a range of sub-idle conditions and transient simulations, an adaptive approach was required. The approach consisted of modifying the component maps and factors to align the model to the ATF engine data. This is described in this separate chapter to combine the knowledge and analyses of the previous two chapters 3 and 4, required to understand the approaches used and defined by this chapter.

- For windmilling and quick relights the component maps and a combustion inefficiency factor were modified, to derive suitable characteristics, representing both windmilling and transient trajectories on component maps of the engine.

- In assisted relights the component maps were fixed, however, the accessory starter turbine characteristic was modified and when at LUFF speed the combustion inefficiency factor was then modified to correct the acceleration rate produced by the energy input of the combustor.

- The adaptive process was also used for understanding of how to define the conditions entering the mixer and the effects the mixer imposes on the steady state windmilling speeds, as discussed in chapter 7.

Running steady state adaptive simulations conditions requires that a first characteristic extrapolation attempt is made from idle to windmilling speeds. However, once the windmilling condition is well matched, it was found that the region for transient operation was not a good representation to produce accurate transient simulations. Thus transient simulations would also be required in the adaptive approach.

Adopting this approach of adaptive modelling of course has its problems. One of these is the complication the mixer imposes on the adaptive process and the reliability of the component characteristics derived. The mixer effects are not fully understood, especially the validity of the static pressure difference between the hot and cold ducts on Engine A. However, in the sub-idle model a map is entered imposing a static pressure difference between these ducts. If the mixer map is wrong it couples the fan and core errors via the LPT and thus the adaptive definition of both the core component and fan maps can be erroneous.

During the adaptive simulation it was found that flow chooses speed on compressors and turbines just accommodate, this is discussed further in chapter 11.1.1.3.

The results of the characteristics produced by these adaptive approaches is shown in chapter 11.1.

5.1.2. INITIALISING OF MODEL SIMULATION PARAMETERS

Prior to any simulation the engine data is entered, it is required to specify the particular design parameters of the engine.

Although the sub-idle model contains a control schedule, it is rudimentary, using only fuel schedule limiters based mainly on WFE/P30 for engine C. Therefore the control system would allow the model to accelerate based on a time input and determine the models fuel flow dependant upon the speed.

Spool speed such as the HP should not be used as a handle in windmilling simulations, as it does not allow the components to operate with respect to the flight conditions imposed upon the engine.

The control system within the model allows the model fuel flow input and engine acceleration to run up to and between limiters. A much more accurate comparison of model results with engine test data is required by this research, thus the actual fuel flow used in the test data is used as the handle throughout a transient manoeuvre. In this sense we are therefore studying the dynamic response of the model. Also this approach allows further studies with the combustion.

To begin the simulation the flight conditions of the model need to be set, such as the delta on ambient air temperature, fuel temperature, flight Mach number and altitude as well as when the pumps are turned on. Typical operational limits of the model were found to be below flight Mach numbers of 0.3. Below this, one could say the ram air momentum does not provide enough momentum energy for turning the fan, and HPC and the speeds are almost zero so that the work is zero.

The initialisation conditions were that of the idle point as described in chapter 3.5. Therefore to run simulations at windmilling or from a specific windmilling condition, the model has to be run down from the idle condition. This could be achieved in steady state steps of decreasing the WFE, and thus resulting in defining a steady state working line, or the deceleration could be achieved transiently, decelerating the fuel (this is useful when trying to include heat soakage affects in a windmilling condition). Both methods were used, however, it was found that the steady state deceleration to save time and reduce simulation size.

5.1.3. STEADY STATE ADAPTIVE SIMULATIONS APPROACH

5.1.3.1. Compressor and Turbine Characteristic Derivation

With the flight conditions set and fuel reduced to zero from the initial idle conditions, the model reaches steady state windmilling mode. The model spool speeds versus time predictions are the first parameters to be assessed against the windmilling ATF engine data, errors of under 5% were considered acceptable. Next the engine working lines on the compressor characteristics maps of PR and WrT/P were compared. As the model matching was based on pressure, it was deemed that although inherently linked, pressure ratio accuracy was more important than non-dimensional mass flow. This decision had to be taken as it seemed, from attempts at modifying the characteristic, both parameters of PR and WrT/P could not be matched. While pressure ratio error was typically below 3%, the non-dimensional mass flow could easily have 10% error. (Although some of this error could be calculation of test data flow values). This adaptive process is defined in Figure 19.

Obviously the combustor requires no checks as the fuel schedule is zero, however, the windmilling loading parameter may be useful.

It was found that at steady state conditions the model Matching Quantity (MQ) tolerances could be set to the small values of 0.0002. If the MQ tolerances are set higher then the model errors are likely to be higher.

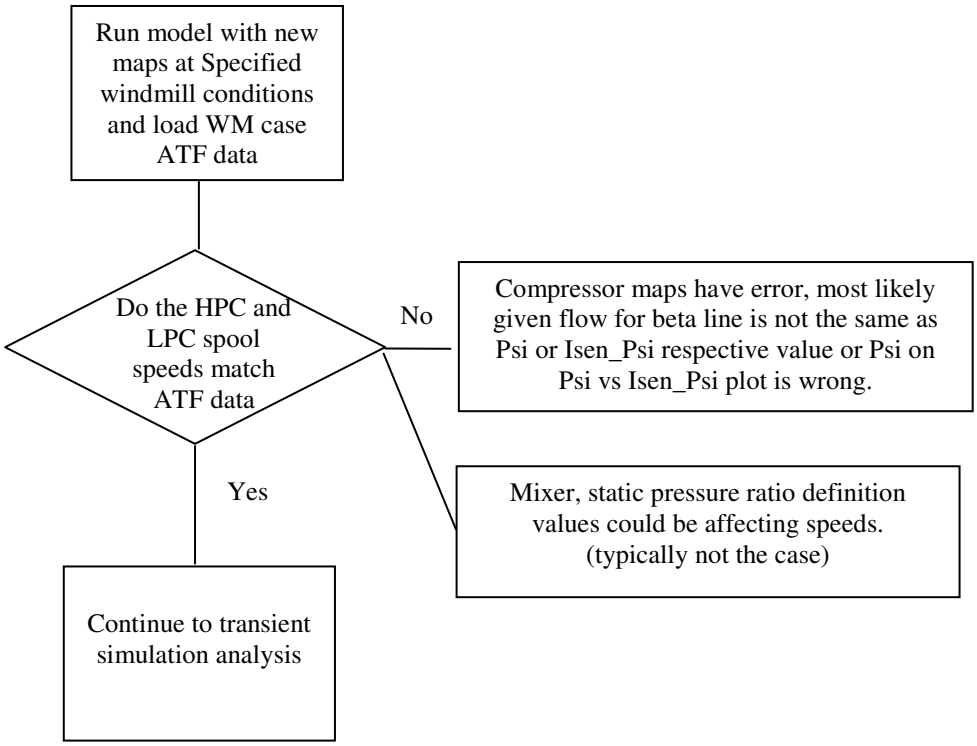

Figure 19. Steady state Windmilling evaluation and adaptation of characteristics.

After a few iterations of the extrapolations, a final set of component characteristics were ready for transient analysis.

5.1.3.2. Selection of mixer representation and values

Adaptive modelling was also used to investigate the significance of SMPR in Mixing (relating to the Exhaust Mixing modelling research work within chapter 7.3) and whether a characteristic was required or not. To do this, the switch on mixing was used to allow the model to either calculate the static pressures into the mixer from the individual stream flow conditions, or the static pressure of the cold duct was defined by a pressure ratio selected from a characteristic derived from test data relating the hot duct static pressure, as described in chapter 7.3. From this analysis the effects of the two

approaches could be studied and the best suited chosen. Other studies were also performed as shown below;

- SMPR characteristic
- SMPR derived from individual stream flow conditions
- SMPR set to 1
- Unmixed

Windmilling steady state runs for a range on conditions were considered for this run to identify these conditions.

5.1.4. TRANSIENT ADAPTIVE SIMULATIONS APPROACH

The same steady state MQ tolerances cannot be used for simulation of highly transient engine operation, such as windmill relights. This was found due to the large changes in shaft torques that initiate at light-up, produce large imbalances for the solver to minimise, and the accuracy defined by tolerances of 0.0002 cannot be achieved. This was found the case on both large and small two spool simulations for engines A and B.

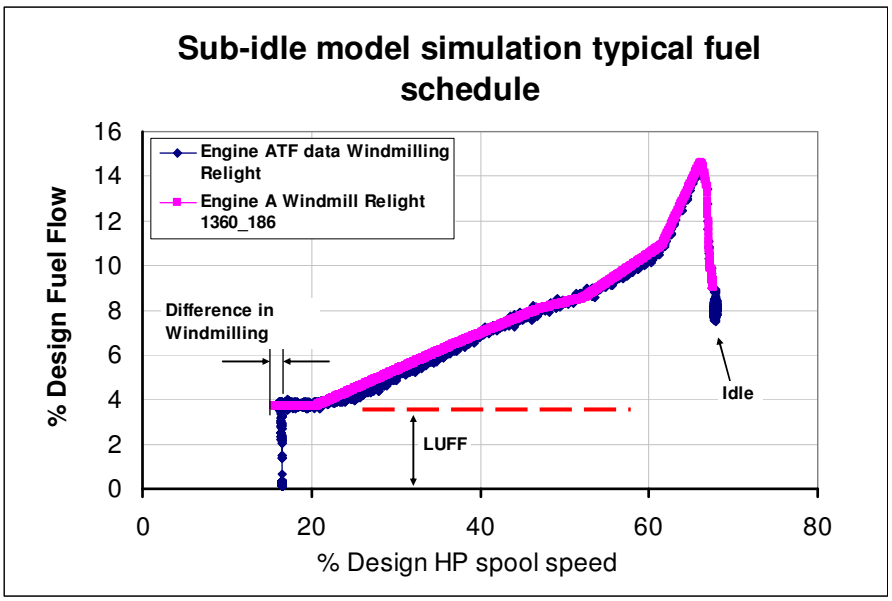

Figure 20. Typical Windmilling Light-Up Fuel Flow (LUFF) schedule and error on model windmilling speed and ATF data.

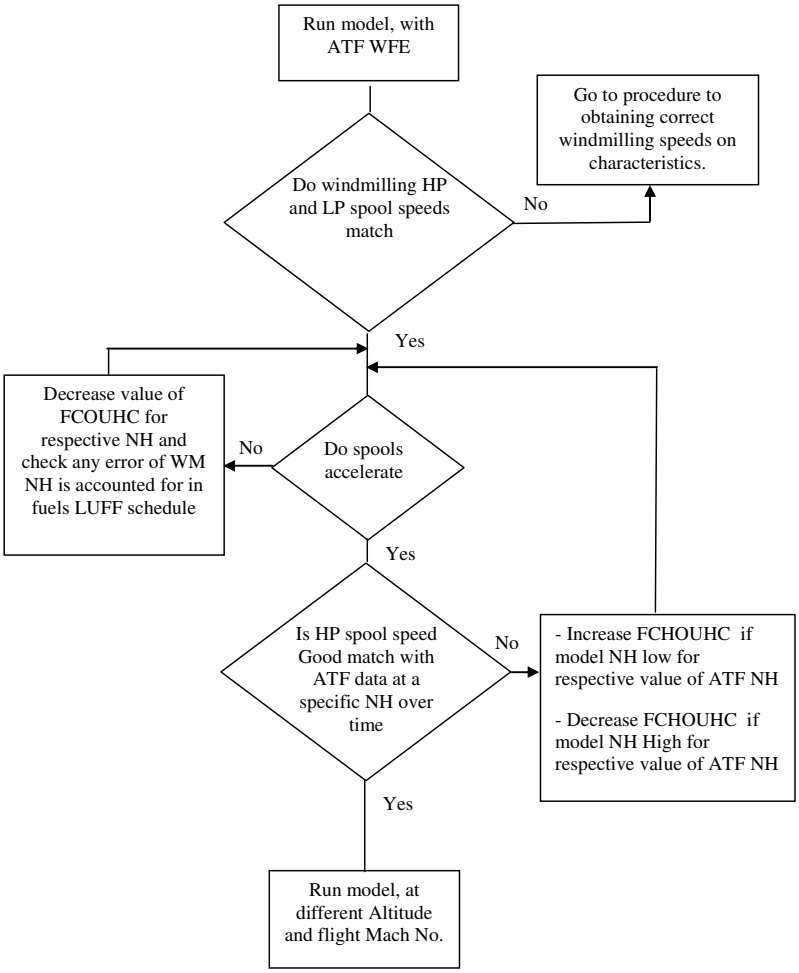

Figure 21. Transient windmilling relight evaluation and adaptive process of creating aligned characteristics.

Difficulty in transient modelling is that the model error on HP windmilling speed to that of the test data, will cause the fuel schedule to start early or late, as depicted in Figure 20. Typically the LUFF was applied in a time of 0.4 seconds, any smaller and again the sudden acceleration would cause model failure in the MQ tolerances. To improve the transient windmilling light-up region and particularly the shape of the compressor speed curves, the adaptive process defined by Figure 21. was performed with the sub-idle model.

Through the studies it was found that the matching tolerances had to be reduced to accommodate the significant changes during the light-up phase, where pressures change rapidly and particularly the HP shaft torque. Once this process was complete the model could be satisfied to run at many other conditions and provide confident results.

Quick windmill relights were useful as they show whether or not the model spool momentum response to the sharp deceleration from a fuel cut, with that of the test data.

5.1.5. STARTER ASSIST ADAPTIVE SIMULATIONS APPROACH

This research produced the first starter assisted windmill relight transient simulations attempted with the BD19 sub-idle model. Engine A's limited data meant no characteristic for the starter was available for this research's engine model. For other engines the starter characteristic was available. Therefore an approach was required to define engine A's starter characteristic.

As discussed in chapter 3.2.1 the sub-idle model previously had never fully been used to simulate starter assists, whereby the acceleration of the engine from the starter was performed.

One approach would be to analyse the test data through calculations of the acceleration torques of the engine, that take place in the engine at start-up as depicted in Figure 22. and the difficulties and the calculations are discussed in chapter 2.3.2. The other approach and that also used, was to make the assumption that through the adaptive simulations of improving the characteristics, that these characteristics and thus model will be approximately aero-thermodynamically correct. The model could therefore be used to back-out the starter characteristic by adjusting the characteristic torque values to align the acceleration of the model to that of test data. The handle will still be fuel flow,

set to zero, and the actual scheduling of the starter will be by using the ATF starter pressure ratio against speed entered into the model, (as long as the schedule has an increasing gradient of torque where the windmilling spools speed intersects then as the model switches to transient mode it will accelerate).

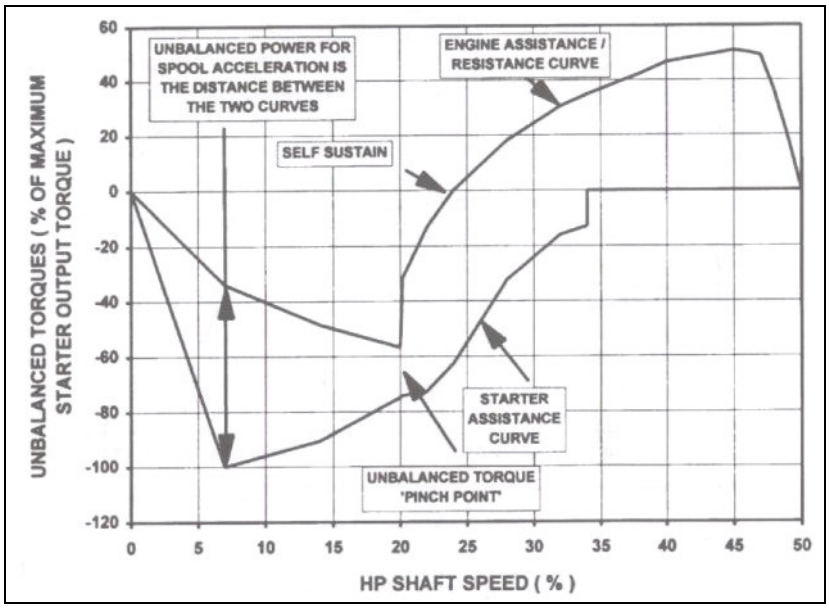

Figure 22. Engine starting torques, of starter motor and engine resistance [59].

As in previous adaptive processes, the rotor speed versus time is compared and the starter torque values modified until the engine spool speeds align with ATF data spool speeds. Two main prerequisites are required, the simulation should be a starter assist case where the flight Mach number is significant to avoid windmilling spool speeds close to zero and that a good definition of starter inlet pressure is available in the ATF data.

It was found the torque changes were so small that the matching tolerance tightness had to be increased (to 0.0002) to accommodate otherwise errors would be larger than the torque step change of the engine.

6. Comparison of engine sub-idle characteristics

6.1. INTRODUCTION

Although a small research area within this thesis the work can be quite useful for knowledge in applying the techniques in previous chapters, as there is little experience of what the sub-idle characteristic should look like.

6.2. COMPARISON OF COMPRESSORS

To understand the component map extrapolation variation from engine to engine ATF test data was compared, this was particularly important for the HP compressor as it is very sensitive to the work and pressure loss coefficient.

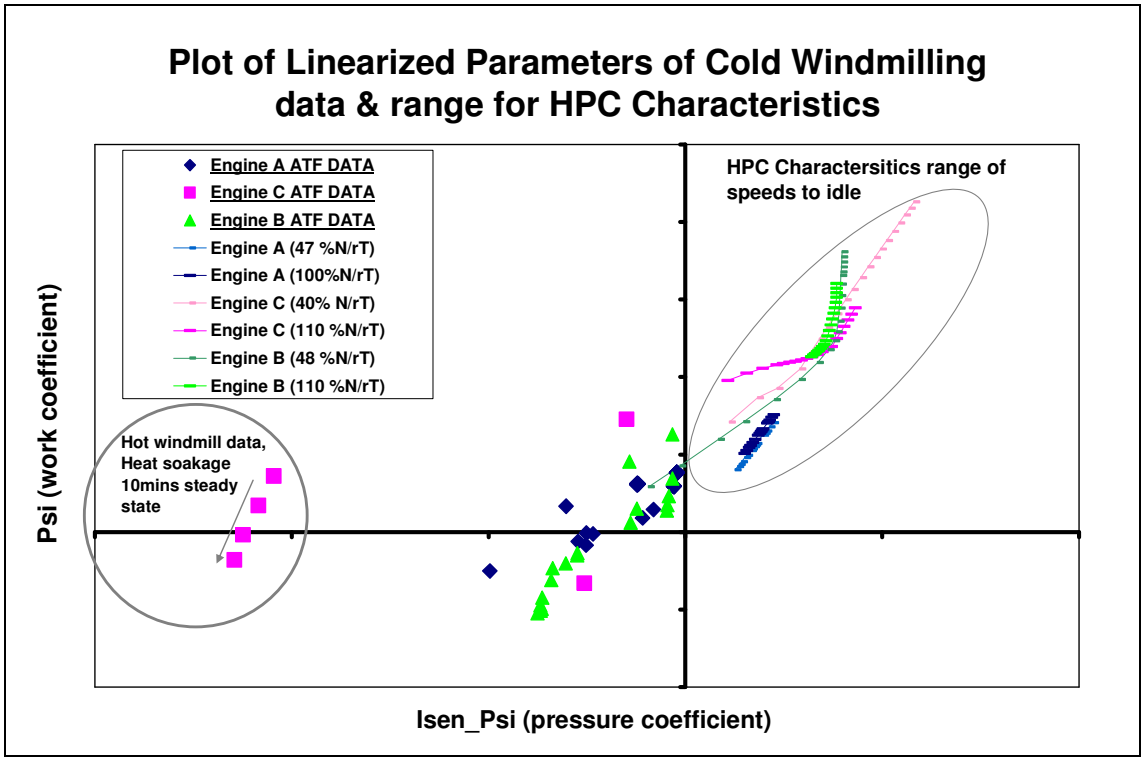

Figure 23. Comparison of compressor Psi vs Isen Psi from range of above-idle component characteristics to Cold windmilling ATF data for range of engines.

As shown in figure Figure 23. the windmilling ATF engine data from a range of engine types had been compared, along with the maximum and minimum component characteristic curves of N/rT. It can be observed that all test data tends to fall onto one trend, however, the error range is in fact very large comparatively to these sub-idle conditions. The smaller design parameters of engine A can be seen relative to the other engines. Also defined in Figure 23. is the influence of heat soakage and the cooling effect on the values, thus highlights the dependency of ATF data defined linear parameters accuracy on temperature measurement.

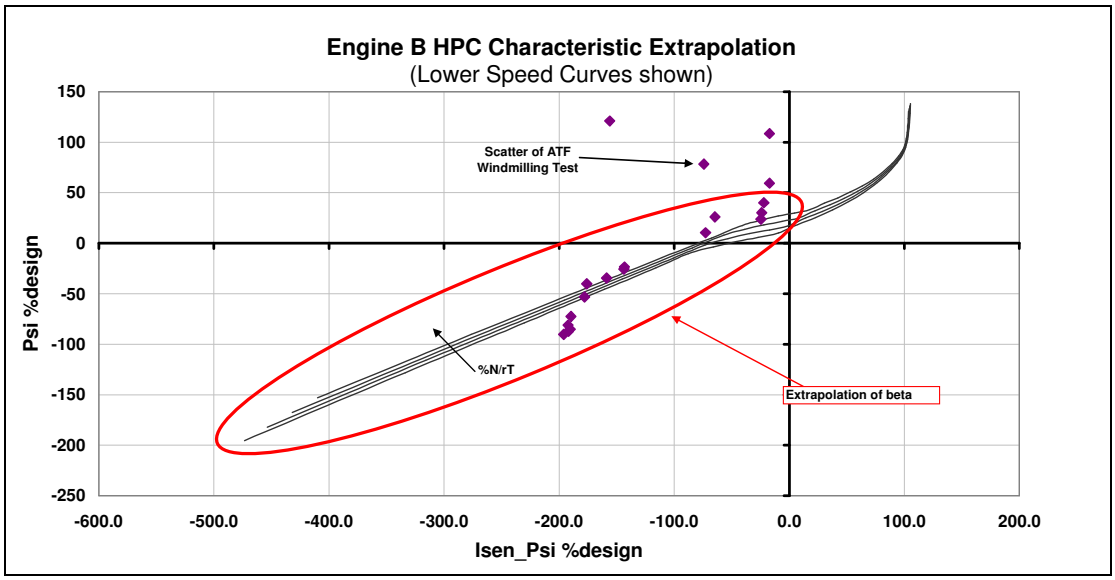

Figure 24. Engine B Beta Extrapolation to windmilling operating region.

Figure 24. defines how the ATF data is used to align the Beta extrapolation in terms of Psi and Isen_Psi.

In comparing Engine A and Engine B HPC characteristics (figures 10, 13 and 24, 25 respectively), Engine B HPC has twice a many compressor stages than engine A's, which produces speed curves with more pronounced choking profile (fish-hooked like curves) toward zero speed and therefore less range in WrT/P in each curve of N/rT. Whereas engine A, with its inherent lower design pressure ratio (relating to number of compressor stages), the losses are much less and a much larger mass flow can pass

through the compressor for a given low speed N/rT curve. As an example, Engine B's HPC characteristics 10%N/rT curves chokes at only 10% of design WrT/P, compared to Engine A's 10%N/rT curve, which chokes at over 20% of design WrT/P.

The speed curves are extended to below pressure ratio of one to provide smooth extrapolation of lower speed curves. Also toward lower speeds, windmilling operation will be in this region as the density mismatch between stages becomes more pronounced in which the later stages are highly choked and negative pressure coefficients will be dominating, compared to the first stages which will tend to move toward stall (this can be understood further by analysis of velocity triangles and the incidence on the blade).

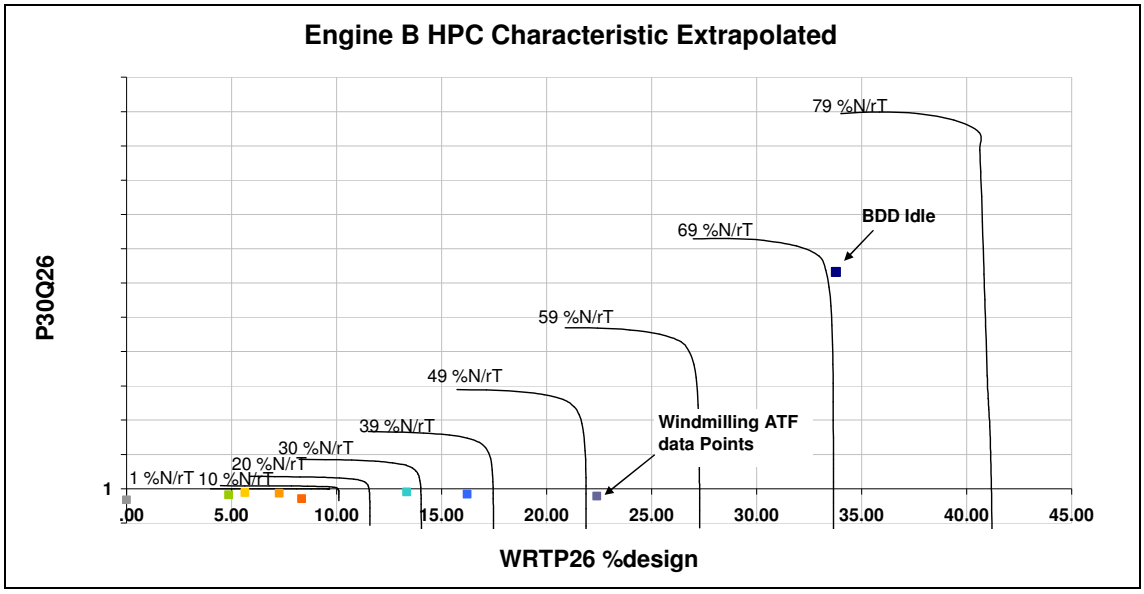

Figure 25. Engine B HPC Extrapolated conventional characteristic.

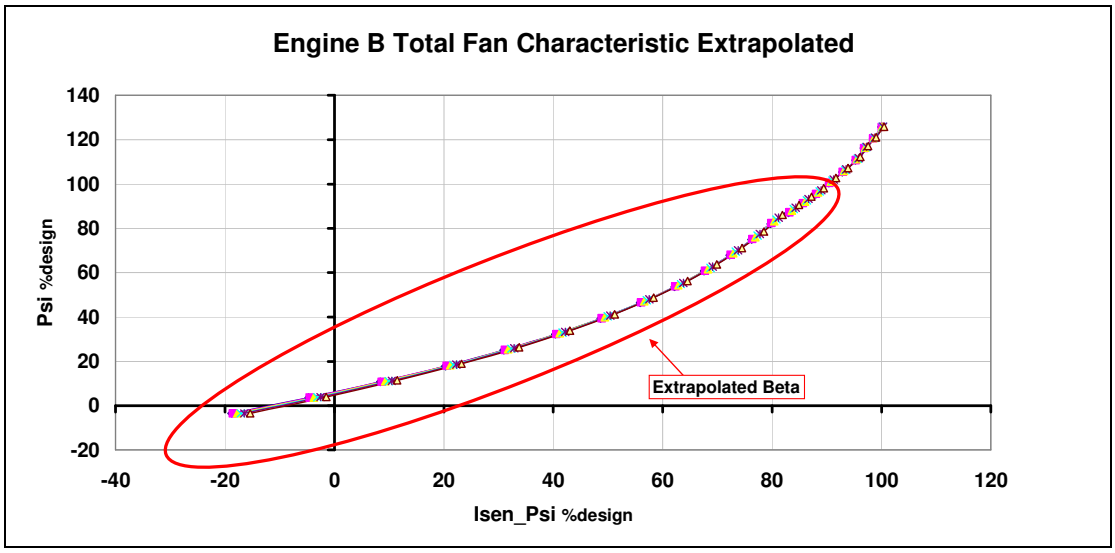

Figure 26. Engine B Extrapolation of Beta in windmilling operating region.

The result of the smoothed curve definition for Isen_Psi extrapolation of Beta is shown in Figure 26. for the total fan. This presents an improvement in the extrapolation to line up with the existing characteristic.

6.3. COMPARISON OF TURBINES

On a two spool engine the LP spool lags the HP spool in acceleration, and upon light-up, the LP spool is initially almost stationary. Most of the energy from light-up is used within the HPT, resulting in increased mass flow through the LPT compared to a small change in ΔT and pressure drop, therefore Phi (WT/NP) becomes very high at low speeds. Therefore the LPT is extrapolated to equivalently much higher values (as shown in Figure 27.) than compared to the HPT Characteristic (see Figure 14.).

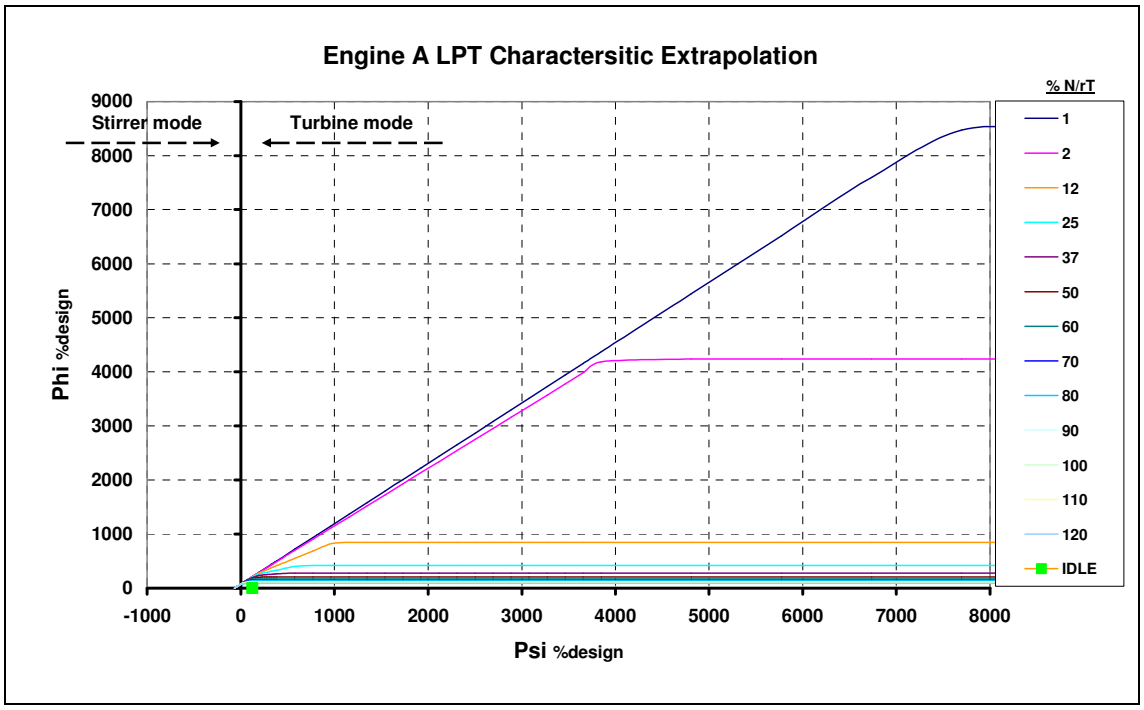

Figure 27. Engine A LPT Extrapolation of Psi versus Phi.

6.4. COMPARISON OF COMBUSTORS

Combustors from different engine types are not easily comparable unless the same basic combustor design (geometric shape) is used only scaled by the dimension, typically the volume. Loading can be used to compare combustors design, as shown in the results in chapter 11.3.

7. THE EXHAUST MIXER AT SUB-IDLE CONDITIONS

7.1. INTRODUCTION

The sub-idle simulation within this research is focused on Engines A and B which both have mixed exhaust configurations. Previous sub-idle simulations using BD19 have all been unmixed engines with the exception of Engine F, with was actually modelled as unmixed.

There are practically no research into off-design engine mixing, therefore this research approached this area with the aim of changing the model to allow mixing of the exhausts, investigate off-design mixing processes and how best to but simply represent the mixing process at off-design within a performance model.

Investigations and findings from this research can be used for later more in-depth studies into off-design mixing, however, with the emphasis more towards representation within a performance model.

7.2. LITERATURE REVIEW

7.2.1. MIXING FOR DESIGN POINT

Mixing of gas turbine exhausts, as Walsh [59] discusses, is required for a range of reasons from mission to design, such as mixing prior to nozzle reheat or where mixing can achieve a small benefit in SFC and specific thrust improvement. From the study of the literature it would seem that with respect to windmilling, the influence of the mixer is a result of the design point selection and no allowance for the windmilling performance is taken into account. Kerrebrock [31] adds that pressure loss from the mixing process may be outweighed by the engine performance benefit, in particular

engine designs with a low fan pressure ratio and bypass ratios above 2. Below this bypass ratio the benefits are much reduced. Military engine exhausts are mixed usually to enable afterburning and reduction in exhaust heat signature.

All standard literature on gas turbine theory pertaining to mixers, such as [59], [54], [41], [16] and [31], lends the statement that in every case the mixer static pressure ratio is one. As Mattingly [41] discusses, this assumption would lead to the total pressure ratio also being almost at unity, also the bypass ratio and fan pressure ratio are highly limited by this configuration.

Mattingly [41] discusses the steady state off-design behaviour of a mixer in a turbofan engine and presents results explaining the changes in parameters with decreasing fan spool speed. The bypass ratio increases with decreasing fan speed, resulting in significantly increased bypass Mach numbers, much higher than the core Mach number. The core Mach numbers decrease slowly and the pressure ratio across the low power Turbine increases slightly.

As with the design point, the analysis for off-design performance still relies upon dimensional and station data, for the mixing of two streams the typical arrangement on a engine and station numbering would be as shown in Figure 28.

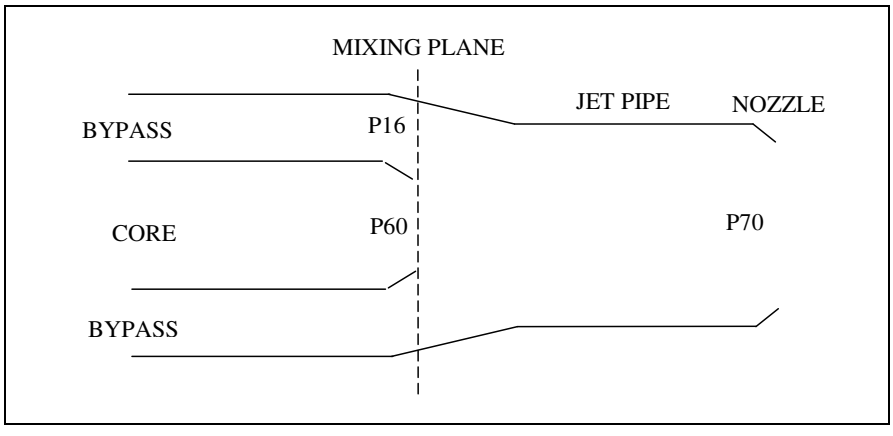

Figure 28. Diagram of mixing two streams an engine station numbering.

7.2.2. MIXING THEORY

Typically the literature pertains to the mixer and its selection of design parameters and sizing for the design point condition. In which a simple mixing calculation is performed on the momentum balance and enthalpy balance, these in turn calculate a pressure loss for mixing. Sara [54] discusses that a static pressure ratio maintaining an equal static pressure between the core and bypass ducts is to minimise swirl. With considering mass flow continuity and some iteration, the simple mixing process and calculations of the enthalpy and momentum balance can simply define the outlet mixed conditions, these are shown respectively in equations below;

$$m_c c_{pc} T_{016} + m_h c_{ph} T_{06} = m c_{pm} T_{07} \qquad \textbf{Eq. 28}$$

$$\left(m_c C_c + p_{16} A_{16}\right) + \left(m_h C_h + p_6 A_6\right) = m_7 C_7 + p_7 A_7 \qquad \textbf{Eq. 29}$$

The ratio of total to static pressures determine the mixing. The temperatures only determine the densities, as described by Kerrebrock [31], who also explains how mixing is an irreversible process causing an entropy increase. The viscous losses from mixing maybe offset by implementation of a lobed mixer. Mixing is typically complete in a downstream duct, at a distance of the outer diameter [31].

At a design bypass ratio the core flow must have enough stagnation pressure for the static pressure of the core and bypass to match.

Ejector pump theory describes the situation where the static pressure at the mixing plane, between the core and outer chutes remains equal with the availability of an infinite source. Where the velocity in the pumped stream can be achieved for the desired velocity and pressure, to maintain a balance of the pressure forces, thus equal static pressure at the mixing plane. This ejector pump principle is explained by Gullila

[19] in reference to the mixing in test beds of the nozzle flows, inducing secondary flow from the surrounding chamber into the de-tuner and the resulting mixing taking place.

Further description of an ejector mixing is shown in Figure 29. and Bradshaw [4] describes the mixing layer effects of shear layers between two separate flows velocity differences. From the shear flow analysis the velocity distribution of the mixing flows can be described at a distance x downstream.

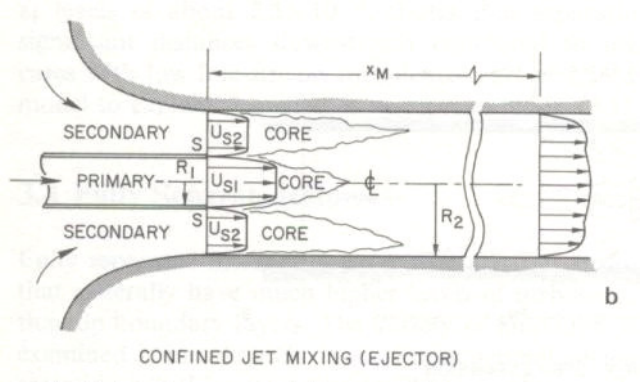

Figure 29. Confined jet mixing Bradshaw [4]

The research by Nixon [45] proposes a mathematical representation whereby vortices characterise the mixing. Most research is aimed at repeating vortices or flow patterns compared to a test bed results, and not offering a reliable predictive approach to defining the total pressure losses during mixing.

Comparison of two stream co-axial mixing theoretical calculations with test data was carried out by Peters [48]. Although the analysis was for high Mach number flows greater than 1, the approach for sub-subsonic flows was also applicable. The approach in this work was to account for turbulence in mixing and assess the effects of if whether the static pressure was indeed constant between the two ducts. To include turbulence into the calculation some empirical constants were required to define a turbulent mixing parameter. This parameter was defined by another, and extends down into the sub-sonic

Mach numbers. The findings of this work were that there was a significant static pressure difference between core and duct flows, reconciling the typical assumption in a theoretical model that the static pressures should always be equal.

7.2.3. OFF-DESIGN AND WINDMILLING MIXING

The Sponsor's above idle performance model for Engine A [53], considers the static pressure between the core and bypass does vary a small amount when the engine departs from design condition. Either the Mach number for the cold duct can be calculated and the static pressure calculated, or a graph can define the static pressure in the cold duct. Matching criteria is that the imperfectly mixed thrusts from the separate nozzles should match the mixed nozzle thrust.

One of the few studies examining sub-idle and windmilling mixer was by Zwede [61]. In which the mixer for engine B has been modelled in CFD by Rolls-Royce with also some work on Engine F. From studying this work the author of this thesis would suggest the behaviour of the two stream model is suitable for sub-idle modelling acting as an injector pump effect. Also the report provided the approximate mixing % cold duct flow values at windmilling for engine B.

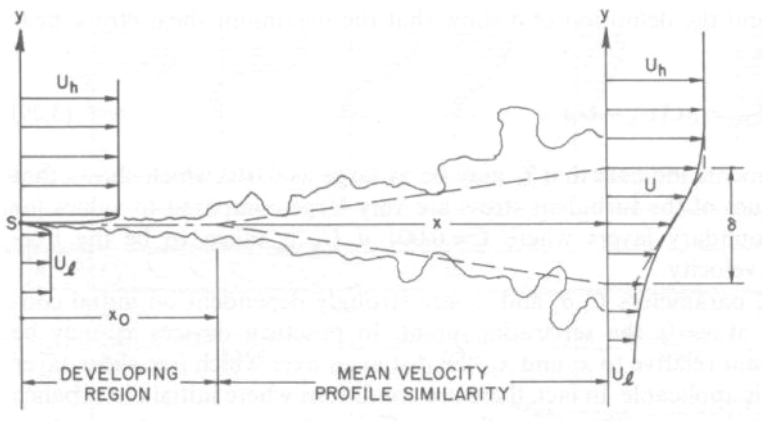

Figure 30. Shear layer development in mixing of coaxial flows [4].

Mixing of coaxial flows, where complex physical processes of shear layer (effect of the velocity gradient) vortices generated by boundary layers, and turbulent flow interaction, is discussed by [4]. Figure 30. presents the mixing of two coaxial flows with different velocities and shows how the mean velocity in the mixed zone is represented. The velocity gradient after shear layer mixing at a distance x can be defined by empirical formula defining the shear layer mixing momentum loss, this approach is defined by [4].

7.3. SUB-IDLE MIXING METHODS AND APPROACHES

7.3.1. TEST DATA ANALYSIS

To understand the methods required to represent the mixer at off-design conditions down to windmilling, as study of engine A test data was performed. From this study there was found a strong relationship between flight Mach number and increasing SMPR, as presented in Figure 31.

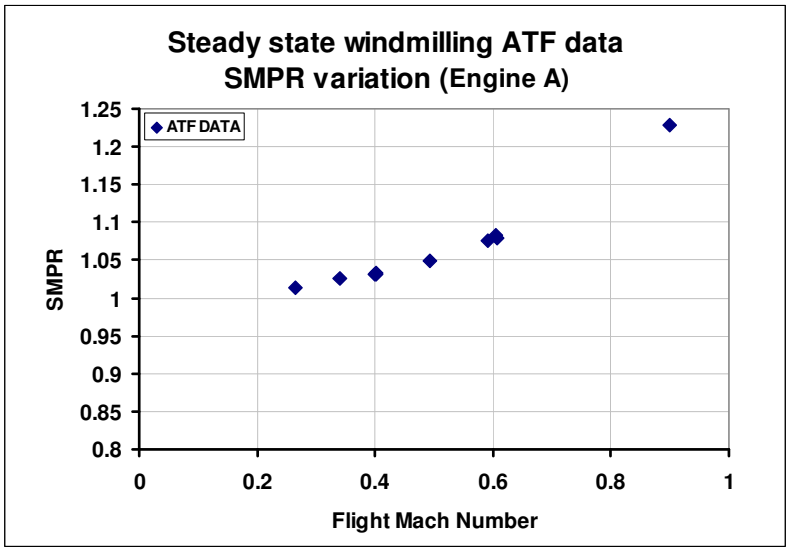

Figure 31. Analysis of engine A mixer static pressure ratios as a function of engine flight Mach number.

As the flight Mach number increases both the static pressures decrease at entry to the core and bypass duct, however, the core static pressure becomes higher than the bypass, as via the increase in BPR, the core has proportionally less flow and lower velocities than bypass duct. The core non-dimensional windmilling flow increases with flight Mach number and pressure losses increase from the higher velocities. As a result the static pressure also falls and as core losses are greater than the bypass, the static pressure at entry to the mixer is lower than the cold duct. There is also the effect of area increasing overall from HPC entry to the LPT exit which should increase static pressure, however, this is offset by the pressure losses.

In considering the above description of the pressure changes, it is important to note the mixing process downstream, will probably have an effect on the pressures upstream.

7.3.2. DISCUSSION OF WINDMILLING MIXING PROCESS AND CONDITIONS

As discussed in the previous chapters the problem with the typical mixer calculations is that these are for design point where SMPR = 1, at which even the total pressures are very close. The Opposite is true for the stream temperatures where at design these would significantly differ from the hot core flow to the colder bypass flow. At windmilling the temperatures of the two streams will be very similar and only begin to differ as the engine lights up.

The ratio of specific heats for both the cold and hot streams will approximately be the same at windmilling, and it was assumed to be 1.4 for general analysis. There is a Total loss through bypass duct from frictional losses but also static loss from change in area.

The velocity ratio (of bypass to core) for engine A is very high compared to higher bypass engines, as the magnitude of the velocity is influenced by the low bypass design area ratio (of bypass to core) of the cold nozzle to the hot nozzle area.

The flow was treated as fully developed flow, therefore there is no inviscid flow region, if such a blockage flow existed where the boundary layers do not mix, the higher velocity inviscid flow region created by the wall boundary layers would also result in a lower static pressure, than the average static pressure used. Also the boundary layer growth particularly on the outer bypass through to the mixed duct, could be significant.

A problem with the mixing calculation is the assumption the pressure forces are dominant and that mixer influence on pumping is only on pressure affects. In fact from high velocity ratios between the core and bypass streams could be more dominant. In which the high momentum is dominant and the mixing shear layer restrains the pressure force balance across the mixing plane.

Extremely important to remember is that at engine design conditions, the mixer has little influence on the upstream momentum of the core and bypass streams as the energy input from a lit engine with power provided from the turbines being so high and pressure differences large. However, at windmilling the energy within the spools is so low, that the mixing effect and pressure losses within the mixer, will have an influence on the back pressures upstream. This is because the pressure changes over particularly the compressors and turbines changes are similarly small. Therefore the mixer static pressure and momentum balance can thus significantly proportionally influence the speeds of the spools.

Initially the fan exit static pressures were used, as no measured data was available for the cold bypass mixer entry static pressure. Later the static pressure at the cold mixer

duct was recalculated by iteration, showing that the difference from that of the fan exit static pressure was less than 2.5%.

Separate calculations were performed outside the model to understand the robustness and results of the mixing equations (Eq. 28 and 29). ATF data was used to specify the windmilling conditions of each stream at entry to the mixer. The result of the mixing calculations then compared the error of the mixed Total pressure calculated with the ATF value. In addition the mixer loss using calculation by [50] as presented in 7.2.2 methods of shear loss was also applied in another set of results. The calculated momentum of the shear loss, to that of the bypass stream, is typically only around 5%. The results are shown in chapter 11.2.2.

To understand the changes and visualisation of the mixing process, a CFD 2D and 3D analysis was performed for engine A. This research was carried out by Julien Rasse [49] an MSc student supervised by Prof. Pilidis and the author of this thesis. In this analysis flight Mach numbers of 0.6 to 0.9 were simulated to understand the difference in mixing from low to high velocity flows at windmilling conditions and the effect of mixing in the long jet pipe. A study of the main results of this analysis are discussed in chapter 11.2.3.

Using the performance model to understand mixing at windmilling and the influence of SMPR, three simulations of the engine model were performed; One where a characteristic of the static pressures from ATF data is applied in the model (the representation of which is described in the following chapter). The second is where a SMPR value of 1 was set within the model. The third was where the model was set up to freely to calculate its own required static pressure, based on the component performance. The results are shown in chapter 11.2.1.

Remembering that at windmilling the bypass ratio is extremely high and a low area ratio in engine A, the resulting velocity differences between the core and bypass are thus very high causing large wakes and shear flows at mixing. This can also create large swirl and thus could be accountable for the difference in static pressure.

7.3.3. DEVISING MIXER REPRESENTATION FOR OFF-DESIGN

From the test data studies and explanations of the SMPR described in chapter 7.3.1, it could be suggested that the model will simply calculate the inlet conditions and thus reproduce the SMPR values at entry to the mixer. However, also discussed is that there are effects within the mixing process that could influence the pressures upstream.

Therefore it was decided to include a characteristic to represent and ensure the model produced these same SMPR values from windmilling. Also by applying these through the transient simulations, we impose any mixing effects that cannot be represented by the simple mixing calculations.

As discussed in chapter 3.3.2 along with the addition of the mixer to the BD19 code, a brick called brick 47 was added. With this brick a characteristic could be used to define the SMPR prior to mixing.

The evaluations of the test data, found that Static Mixer Pressure Ratio (SMPR) were a strong function of flight mach number and a slightly weaker function of BPR, shown by Eq. 30.

$$SMPR = f(flight\_Mach\_No, BPR) \qquad \textbf{Eq. 30}$$

Although these relationships were basic in terms of they related to engine flight conditions they were easy to apply as the parameters were defined or derived respectively within the model iteration scheme. Therefore a simple characteristic of

these parameters was used within the model, though to apply these, a way of relating these parameters was required.

Other relationships were coded into the model, were to allow the SMPR to be related to more immediate conditions at entry to the mixer. These involved the cold duct entry Mach number and the total pressure ratio (replacing the flight mach number) shown below in Eq. 31, and the BPR being replaced by the Mixer BPR as defined by Eq. 32.

$$SMPR = f(Mn\_cold, BPRmixer) \text{ or } f(PRtotal\_mixer, BPRmixer) \quad \text{Eq. 31}$$

$$MixerBPR = \frac{BPR}{1+f} \quad \text{, Where } f \text{ is the fuel air ratio.} \quad \text{Eq. 32}$$

In the derivation and calculation of the mixer characteristic static pressure ratio first required the bypass duct static pressure to be calculated, as this was not available in the ATF test data. This was calculated by an iterative procedure of guessing Mach number at the station and matching on mass flow derived as the bypass mass flow plus control bleed flow (control bleed flow was derived from bleed flow chic, using ATF data total pressure at station 30 to static pressure in bypass duct ratio). The resulting calculation of iteration and calculation for Mach number to determine the static pressure ratio in the bypass duct, was very susceptible to mass flow calculation error as described in chapter 2.3.2.

8. Combustion relight studies

8.1. INTRODUCTION

8.1.1. DEFINITION OF THE SUB-IDLE COMBUSTION PROBLEM

The ability of an engine to light at sub-idle windmilling and starting conditions is obviously very important, and the combustor design sizing is therefore based on providing sufficient volume and to decrease the flow velocity enough for propagation of the ignition flame and increase residence time.

Within the design process of sizing of the combustor, the combustion department become very dependant upon the performance group to provide the engine conditions at entry to the combustor, for the range of relight conditions. The performance department will use experience and scaled data from other engine relight conditions to approximate the entry conditions, and as such the combustor department make the combustor slightly bigger to allow for error in these proposed inlet conditions. The combustor design therefore includes a safety design factor on its sizing, which causes greater pressure loss, penalising design point performance and also a greater geometric space required by the combustor.

Many factors effect the combustor at windmilling conditions, ignition, stability limits, fuel temperature, heat soakage, fuel scheduling, and the inlet flow conditions depending upon the engine operating conditions and flight environment.

A fully aligned and predictive sub-idle performance model would have the ability to provide the windmilling conditions at entry to the combustor prior to light-up. With a preliminary predicted combustor characteristic and control system, the model would be able to devise the fueling, combustor inlet conditions, combustion efficiency and combustor volume, required for a given required acceleration schedule. This would be

the ultimate direction of developing the performance model and thus provide predictive combustor inlet data and predictive combustor performance within an engine, to the combustion team for their combustor design in a new engine.

8.1.2. AIMS AND OBJECTIVES

The aim of this area of research is to investigate the process of sub-idle combustion with respect to the information required for running a sub-idle performance model.

During the research and out of necessity methods were developed to extrapolate Combustor characteristics and thus there became an objective to provide a technique for this research work and future extrapolation of combustor characteristics.

A main research objective required by the sponsor was to derive or 'back-out' the combustion efficiencies from the sub-idle relight and starting simulations. By compiling the data obtained from the models, the combustion efficiencies at light-up can be analysed versus the engine conditions.

The objectives in the two preceding paragraphs are based on the premise, that the performance model characteristics and representation are thermodynamically and aerodynamically correct within the sub-idle region. However, the performance extrapolation technique is not perfected and each characteristic has its own inbuilt error. To reduce the complexity the error, only the model combustor inlet conditions to that of test data are considered with the backed-out combustion efficiency results.

Due to suggestions from the literature review it was decided to investigate the suitability of the current characteristic combustion loading definition at low pressure conditions experienced by a relighting engine combustor. The methodologies and analysis of the above objectives is covered in chapter 8.3.

8.2. LITERATURE REVIEW

The main literature on gas turbine combustion is by Lefebvre [37], who has in the past performed rig tests, compiled others research and developed equations to define combustor parameters at a range of operating conditions. These equations are typically empirically derived formulations, and one of the most notable of these is the combustion loading parameter, defined by equation 33.

$$\eta_{C,\theta} = f(\theta) = f\left(\frac{P_3^{1.75} A_{ref} D_{ref} \exp(T_3/300)}{\dot{m}_A}\right) \qquad \text{Eq. 33}$$

The loading parameter is a function of combustion efficiency and relates the inlet conditions and size of the combustor, allowing a comparison of typical combustor designs. As Lefebvre [37] describes, the experience with combustors can be used to compile a database combustor performance on the plot of loading versus combustor efficiency to allow selection of the combustor size as shown by the representation in Figure 32. for annular and tubular combustor designs .

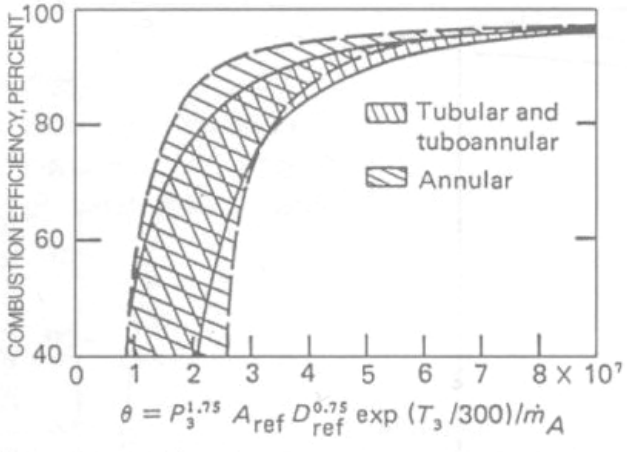

Figure 32. Design chart for conventional combustors [37]

The loading parameter defined by [37], shown in Eq. 33, is based on the combustion limiting process of heat release being the reaction rate, other limiting conditions in combustion are the mixing rate and the evaporation rate (shown in Eq 34). The evaporation rate of combustion is not limiting in normal combustor performance of gas turbines, however, [37] does mention that at low pressures and at light-up the evaporation rate may become limiting. These low pressures are the conditions experienced at windmilling light-up conditions. The possibility of evaporation becoming limiting is a function of many factors, one such is the atomiser performance.

$$\eta_{COMB\_EVAP} = \frac{8(k/Cp)_g \ln(1+B)(1+0.25\,\mathrm{Re}_D^{0.5})t_{res}}{\rho_f D^2} \qquad \textbf{Eq. 34}$$

The evaporation time differs for mono and poly dispersed sprays as presented by [37], in two respective equations. This calculated time can be affected by air temperature through the mass-transfer number. The evaporation time decreases with increased turbulence, increases with temperature and larger droplet sizes (droplet size is the SMD as defined in the following paragraph). The residence time t_{res} is affected by the combustions design volume and the recalculating flow design within the primary zone.

Under the low pressure conditions experienced at high altitudes, the combustor performance will be effected by reduction in fuel atomisation. Discussions with Harding [21], suggests that at windmilling at low pressure conditions, the atomisation can be such that the fuel flow enters the combustion chamber as a stream, using the analogy of a flow like that from a watering can. Atomised fuel droplet sizes are typically defined by the parameter Sauter Mean Diameter (SMD). The larger the SMD the larger the drop size and thus a fuel sheet would be a larger SMD. The larger the SMD the smaller the total fuel surface area for evaporation, and for any study of the combustor conditions at light-up an idea of the high SMD values around windmilling and sub-idle conditions would be useful. An investigation presenting typical SMD

values for sub-idle conditions are discussed by Caines [7], where values are typically 150 to 300 μm. Also in some cases the sheet of fuel at low pressures, can pass through the combustor and proceeds to hit the walls and puddles on the walls of the combustor and the sponsor has experience of this flow igniting, which can surge the engine.

To define the break-up of a jet of fuel a parameter called the Weber number defines the disruptive force of the air and the surface tension of the fuel.

The region of flight conditions in which the combustor can relight, is often termed as the ignition limits. Prior to engine testing a combustor ignition test at constant inlet pressure temperature and mass flow with wide range of AFR is carried out to defined the ignition limits. This ignition limit curve is the lower limit on the air mass flow versus FAR charts, within which ignition is possible, as shown by Figure 33. a). When the combustor is lit the range of FAR at which combustion is maintained needs to be described.

Tests are performed like that for ignition tests, although with the combustor lit, for a given air mass flow the fuel flow is decreased to determine the lean stability limit and fuel flow is increased to define the rich limits, as shown by Figure 33. b). Within these limits loops are region of stable burning for a given pressure. From the discussion within this paragraph an understanding of the relight process is obtained, and that fuel scheduling of either too much or too little fuel flow, can cause failure to light and ignition. Also failure in ignition and stability can be due to the operating flow conditions entering the combustor such as a high mass flow to the low constant inlet pressure.

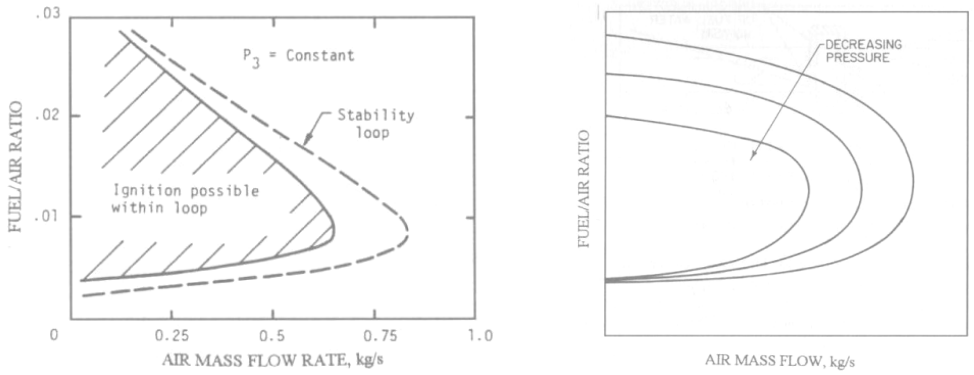

Figure 33. a) Combustor ignition loop. b) Combustor Stability loops. [37].

Previous research within the Performance UTC at Cranfield, studied the following areas of work, Kupcik [32] studied the air temperature effect on ignition, and found that the droplet size decreased with decreasing air temperature, which would benefit combustion. However, increased viscosity and Reynolds number along with the need to produce more temperature rise have an adverse effect on combustion.

Due to ATF test rigs providing warmer fuel temperatures than would actually occur at windmilling, Haghrooyan [20] studied the fuel temperature effect on ignition. By calculating the resulting fuel drop sizes, developing ignition loops, he found that high fuel temperatures would produce optimistic results for the ignition loop.

The successfulness of light-up relies on the heat of the initial kernel lasting long enough to propagate downstream, however, the heat soakage of the combustor liner could significantly affect this and was studied by Allan [2]. His studies found that the TET can drop as much as 10K on start-up due to the heat soakage within the combustor.

A report by Monticelli [42] in modelling of engine E with the sub-idle code BD19, experienced some difficulties relating to the combustor. To achieve successful quick-windmill relights the combustor heat soakage parameter had to be removed. The

combustion maps were extrapolated using test data and curves of WrT/P converting from the AFR representation by assuming a constant AFR of 40.

The sponsor's combustion department carried out a study, to provide data and a prediction method of understanding the relight flow conditions at entry to the combustor for future designs based on present engine data. Although the obvious problem with this approach is it is not applicable to new engine designs, it is a useful tool providing a capability for generic information. The report by Zedda [60], suggests that for a particular engine the BD19 sub-idle model will provide more improved engine specific flow data at entry to the combustor for a range of conditions.

The mixture strength ratio is the AFR or FAR, and [37] presents a diagram to present the effect on the loading curves as a function of combustor efficiency, see Figure 34. This description and the position of the curves is very useful for understanding how to extrapolate combustor characteristics to the sub-idle region of windmilling light up.

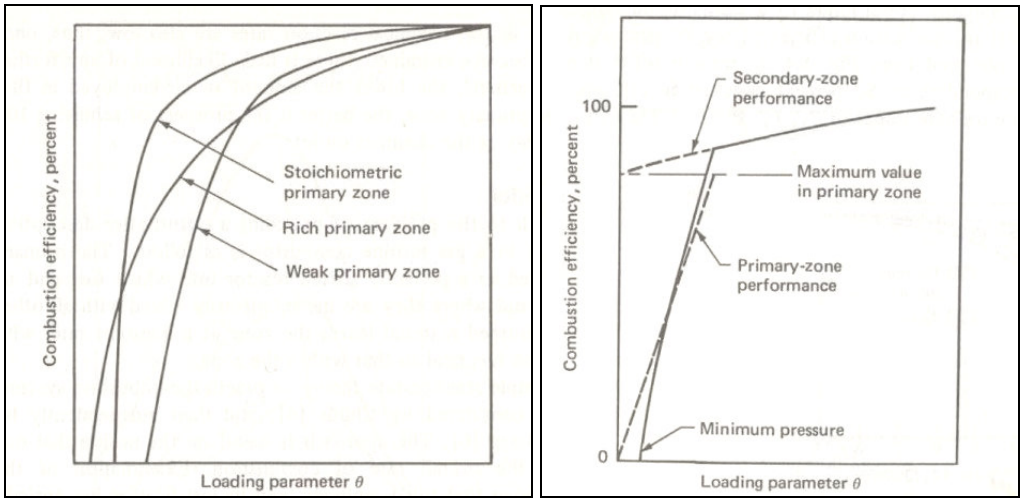

Figure 34. Effect of primary-zone mixture strength (AFR or FAR curves) [37].

As Figure 34. shows, the weak primary zone (high AFR) crosses the rich primary one (low AFR) curve as the combustion loading decreases. The stoichiometric primary

zone has much lower loading parameter at higher combustor efficiencies, though lower than the high low AFR condition.

At windmilling prior to light-up, there will be a extremely high AFR at entry to the combustor (very weak primary zone as the flow will be zero), then upon light-up the primary zone will have a rich mixture, thus in any simulation model there will be large changes on the combustor characteristic. Lefebvre goes on to describe that the primary zone combustion is dominant in determining lower combustor efficiencies below approximately 80%, and above this the secondary zone performance influences take effect, as shown in Figure 34.

8.3. METHODOLOGY AND ANALYSIS

8.3.1. COMBUSTION CHARACTERISTIC AND APPLICATION IN MODEL

A steady state combustion characteristic was required for the performance modelling, however, combustion data for engines A and B did not pass beyond idle conditions. Unlike other engines, combustor test data at windmilling or at least low power setting conditions, was either not available or the tests had not been carried out. The combustion tests for engine A had not been carried out as the engine was a later Mk, even though the combustor was redesigned. It therefore fell to this researcher to extrapolate the combustion characteristics (see chapter 4.3.7) for the performance model to run from. An approach to improve the extrapolation by defining an end limit was devised. Using previous extrapolated combustion characteristics which had test data available as a comparison, an equation of curve was developed for the extrapolated curves of WrT/P.

Extrapolation is inherently erroneous, therefore an adaptive process involving running the performance model and factoring the combustion efficiency was used, this is discussed further in chapter 8.3.4

8.3.2. ANALYSIS OF THE SUITABILITY OF COMBUSTION LOADING PARAMETER FOR PERFORMANCE SIMULATION OF RELIGHT

The typical combustion characteristic used in the modelling uses combustor loading versus combustor efficiency and a function of WrT/P or AFR. The definition used in Rolls-Royce only differs by that defined by Lefebvre [37] in that a volume for the combustor is used rather than flow area. The equation definition between Derby and Bristol sites differs only in terms of the order of the numerator and the denominator. The Derby loading equation is divided by 10^5 and should be noted when trying to compare the Bristol and Derby equations.

As indicated from the literature review, the evaporation rate efficiency may become limiting rather than reaction rate, at low pressures (very high altitudes).

To analyse the above statement, research was carried out by Narkiewicz [43], an MSc student supervised by Dr. Pachidis and the author of this thesis. Application of steady state combustion equations to the relight case was applied to determine other definitions for deriving combustion efficiency. These were calculated from model and ATF engine data, with sensitivity analysis of the effect of Reynolds number and other influencing parameters. Using the sub-idle model windmilling relight results, the model derived combustion efficiency (reaction rate based) was compared with an evaporation based calculated combustion efficiency. Also the Weber number was calculated to understand the droplet size in terms of how well the fuel is dispersed. This work was aimed at providing information and improvement to the basic definitions and characteristics used within the sub-idle model. The results are discussed in chapter 11.3.3.

8.3.3. TEST DATA ANALYSIS

Due to the low pressures and Reynolds numbers at windmilling conditions it would be reasonable to suggest the combustor pressure losses will be different to the design point values. The liner pressure loss term is neglected from the definition of the loading parameter on the assumption that it varies little between combustor designs. To check the combustor linear pressure loss, the following calculations are used to derive the values for engine A.

The pressure loss of a combustor is made up of the cold and hot losses, the hot losses are defined by [37] "the fundamental loss arising from the addition of heat to a high velocity stream". Therefore if we are trying to find the pressure loss at steady state windmilling, the hot loss can be ignored as the combustor is not lit. Therefore the total pressure loss across the combustor is just due to the cold loss from the diffusion and frictional losses, and reduces to the following;

$$\Delta P_{3-4} = \Delta P_{cold} \qquad \textbf{Eq. 35}$$

The overall pressure loss of the combustor is defined as;

$$\frac{\Delta P_{3-4}}{P_3} = \frac{\Delta P_{3-4}}{q_{ref}} \frac{R}{2} \left(\frac{W_3 \sqrt{T_3}}{A_{ref} P_3} \right)^2 \qquad \textbf{Eq. 36}$$

Where $\frac{\Delta P_{3-4}}{q_{ref}}$ **is the pressure loss factor.** **Eq. 37**

From the loading equation or if the combustion volume is known, the linear cross-sectional area A_{ref} can be found, alternatively a drawing could be used. Therefore from the fluid dynamic relationships as defined by Lefebvre [37], the following calculations determine the Pressure loss.

$$U_{ref} = \frac{W_3}{\rho_3 A_{ref}} \qquad \textbf{Eq. 38} \qquad \textbf{and ;} \qquad q_{ref} = \frac{\rho_3 U_{ref}^2}{2} \qquad \textbf{Eq. 39}$$

$$M_{ref} = \frac{U_{ref}}{(\gamma R T_3)^{0.5}} \qquad \textbf{Eq. 40}$$

Using the above calculations and the engine ATF data total pressures, at inlet and outlet to the combustor, the pressure loss factor (or loss coefficient) could be found. This is an important parameter as it removes the effects of the operating conditions and describes the combustor aerodynamic pressure loss, as described by [37]. Now the combustor liner pressure loss would be useful as if this does vary significantly from design then the significance of this in the derivation of the combustion efficiency could be important and should be included with the loading parameter definition as shown below in Eq. 41.

$$\eta_c = f\left(\frac{P_3^{1.75} A_{ref} D_{ref}^{0.75} \exp(T_3/b)}{W_A}\right)\left(\frac{\Delta P_L}{q_{ref}}\right)^{0.5m} \qquad \textbf{Eq. 41}$$

Therefore to define the liner pressure loss the relationship of the pressure loss factor and the diffuser pressure loss has to be used.

$$\frac{\Delta P_L}{q_{ref}} = \frac{\Delta P_{3-4}}{q_{ref}} - \frac{\Delta P_{diff}}{q_{ref}} \qquad \textbf{Eq. 42}$$

$$\Delta P_{diff} = \bar{q}\,\lambda\left(1 - \frac{1}{AR^2}\right) \qquad \textbf{Eq. 43}$$

If we assume the area ratio to be the change from the outlet HPC area to the annular area. The typical value for λ is suggested by [37] is 0.45. The mean total to static pressure change across the combustor is defined below, for incompressible flow as;

$$\bar{q} = \bar{P} - \bar{p} \qquad \textbf{Eq. 44}$$

The results of this analysis can be found in chapter 11.3.2.

8.3.4. MODEL DATA ANALYSIS

Work by the author of this thesis obtained the combustion efficiencies backed-out from the sub-idle engine model. The approach for running the model and obtaining these efficiencies is discussed in chapter 5.1.4. As the model results will contain errors, the combustion efficiency would be affected as a result. Therefore to reduce the number of parameters to consider only the errors for P30 W30 and T30 were compared to the results obtained as these are the parameters are a function of the combustion efficiency, as defined by the combustion loading equation.

From these results trends of light-up trajectories and light-up efficiency values could be used to form opinions and useful reference for designing combustion chambers. As the volume of the combustor is the design variable for sizing the combustor and is a strong function of the residence time, a sensitivity analysis on varying this volume was performed.

Heat soakage during transients take place within the engine components, and the combustor is no exception. The sub-idle model uses design point heat transfer coefficients, though these may be affected by the Reynolds number and thus affecting the Nusselt number. The heat soakage equations are basic, forming only a lumped sum calculation. However, the analysis of the magnitude of heat soakage effects within the combustor versus the other engine components, was thought to be a useful analysis for later study proposals. Therefore the heat soakage temperature differences are studied within the modelling results, in chapter 11.1.1.4.

9. Locked rotor studies

9.1. INTRODUCTION

9.1.1. PRESENT LIMITATIONS CREATING A NEED FOR THIS RESEARCH

As discussed in earlier chapters, extrapolation of component characteristics into the sub-idle region is required for a sub-idle performance model which uses characteristics. Extrapolation is an estimation process from known data as described in chapter 4.1, and within the work of the thesis ATF cold windmilling data was used in assistance to align the extrapolations and reduce error where possible. Without engine test data alignment of the extrapolated characteristics used within the sub-idle model described in chapter 3, the model results would have large error. Therefore this approach's reliance on ATF test data means it is not a predictive technique.

Another impetus for this research area came from the need to simulate groundstarting. However, the sub-idle model cannot start from zero rotational N/rT speeds as it uses parameters of specific work. If there is no rotation then the tangential distance is zero so work done is zero, from Eq. 45. Also from the thermodynamic aspects, without any work put in or extracted, such as that at zero speed, then there is zero total temperature change (ΔT), Eq. 46.

$$\textit{Workdone} = \textit{force} \times \textit{tangential distance} \qquad \textbf{Eq. 45}$$

$$\textit{Specific Work} = Cp\Delta T / T \qquad \textbf{Eq. 46}$$

This discussion highlights two clear overall objectives, to produce a predictive technique to produce component characteristics, the second to define a zero speed curve with suitable parameters to enable groundstart simulations.

The definition 'locked rotor' is a another term for zero spool speed, whereby zero spool speed has been caused by either mechanical failure or whereby the power offtake is much higher than he momentum available in a windmilling engine spool and thus producing zero spool speed.

9.1.2. THE AIMS AND OBJECTIVES

If a method could be devised whereby the termination point for each parameter extrapolation could be defined, the extrapolation process would actually become an Interpolation process as shown in Figure 35. This approach is the aim and focus of this chapter's research area. To achieve this aim, the following objectives were carried out.

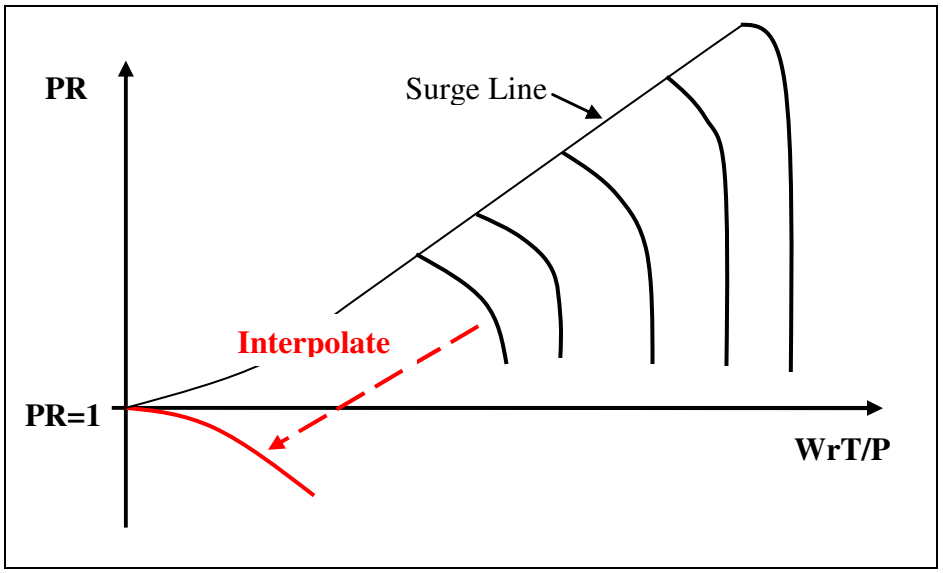

Figure 35. Interpolation of compressor characteristic in conventional parameters.

Torque was the selected parameter to define the zero speed curve and the aim was to define this torque and the pressure losses at zero speed, via 3 approaches; theoretical methods (discussed in chapter 9.3.1), CFD studies (discussed in chapter 9.3.3), and to design a test rig that can later validate the CFD results (discussed in chapter 9.3.4). As

discussed in the literature review the loss coefficients for an aerofoil seem not to have been studied at the far off-design conditions of windmilling and locked rotor. Therefore, from the results of the CFD modelling these shall be defined. What would be useful is a generic approach to calculating the locked rotor curve for any compressor using the loss coefficients developed.

On definition of the zero speed torque, it was required to define how to apply this parameter within a component characteristic and the changes required within a performance model with any benefits, and this is discussed in chapter 9.3.2.2

Definition of a zero speed curve is also required for the objective of providing the ability to simulate groundstarts. The possible case of negative speed, whereby the engine is reverse windmilling from a tailwind is not considered within any of this research.

9.1.3. THE BENEFITS

With a definition of the zero speed curve, the performance department would have the ability to not just reduce sub-idle component representation error, but more importantly, provide a predictive ability/technique for expansion of the component characteristics into the sub-idle region. Thereby providing the ability to run predictive engine sub-idle performance simulations. This would be an important step for a new engine where no ATF engine data is available to align extrapolated characteristics. Also early in the design process performance data could be made available to other departments, such as the combustor department.

A performance modelling benefit can be claimed if the full advantage of utilising torque is realised. If torque matching is performed, and no conversion to power balancing, then the possible problematic situation of multi-match points within a sub-idle

windmilling simulation will be greatly reduced, if not removed. There can be only one speed for a defined value of torque or shaft momentum, as shown in Figure 36.

The issue of multi-match points is well described by Braig [6] and is shown in Figure 36. below. Figure 36. explains how when at a certain flight mach number in windmilling, the HP spool (considering this is the power offtake spool) momentum produced from the flow through the engine, only has sufficient momentum energy to provide for the power offtake load. Thus the solution can provide two possible spool speeds on the power parabola. The simulation model runs from previous points, so at high flight Mach numbers where the maximum of the parabola is far from the power offtake limit, the large differences in speed would be ignored by the stepping iteration. However, when at low flight mach numbers this multi-matching of two possible speeds is possible, and the momentum and power offtake available within the spool is much less, creating a lower power curve parabola. From which the possible solutions for speed are so close to the power curve parabola's maximum and each other, that the iteration steps could jump from one to the other, producing an inaccurate windmilling speed, or unstable model result.

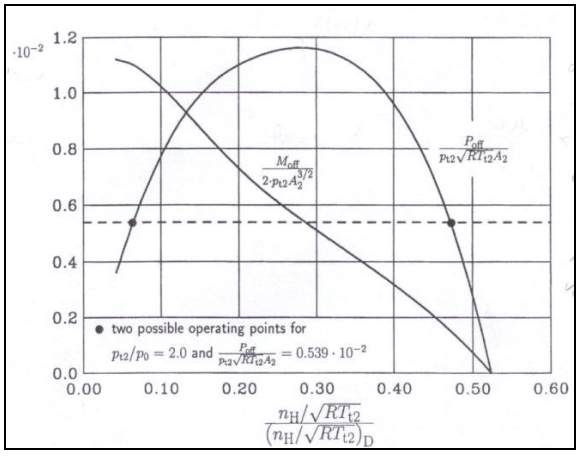

Figure 36. Multi-match power offtake shaft power balance issue balance, for a given flight Mach number [6].

The starter motor is represented by a torque characteristic, which is then converted to power in the BD19 model, which would be avoided in a torque balance calculation. Pump and IDG powers can easily be converted to Torque, dividing by the operating rotational speed.

9.2. LITERATURE REVIEW

There is little literature on this subject partly as this is a concept that has only been deemed useful from findings within the research of the sub-idle modelling at Cranfield UTC in Performance. Particular areas of previous locked rotor studies and design methods for cascade and cascade rig design, are required for this research and discussed herein.

9.2.1. DEFINITIONS OF TORQUE AND CASCADE LOSSES

The issue of using parameters of work in terms of $\Delta H/U^2$ is explained in [33], where the work done at zero speed is zero. Two interesting points are explained for the zero speed curve, that the mass flow can be positive or negative around the surge line and that at PR =1 and zero flow, the efficiency will be the highest as the losses are the least.

It is suggested by [28] that a specific torque and modified pressure loss can represent the zero speed curve, as shown below in Eq. 47 and Eq. 48, where P_{out}' is the ideal pressure.

$$\tau_{spec} = \frac{-\Delta H / \gamma.R.T_{in}}{N.\pi.d / \sqrt{\gamma.R.T_{in}}} \qquad \textbf{Eq. 47}$$

$$P_{Loss}{}^{*} = \frac{(P_{out}{}' - P_{out}).\left(1 + \frac{\gamma-1}{2}.M_{in}^{2}\right)^{\gamma/\gamma-1}}{P_{in}.M_{in}^{2}.\gamma} \qquad \textbf{Eq. 48}$$

Another representation of torque is suggested by [36] whereby both the specific work and the non-dimensional mass flow are combined to produce torque with reference to the inlet pressure, Eq.49. Equation Eq. 49 presented below, is in a quasi-dimensionless form, however, the author of this thesis would suggest that the Q formula description for mass flow where the area is included (Eq. 50)and using the mean rotor diameter, would provide a fully dimensionless form. Instead of using the flow area approach [59] suggests that the m^3 term should be expressed by three diameters, producing Eq. 51.

$$\frac{Torque}{P_{in}} = \frac{W\sqrt{T_{in}}}{P_{in}} \cdot \frac{\Delta H\sqrt{T_{in}}}{T_{in}N} \quad \textbf{(quasi-dimensional)} \qquad \textbf{Eq. 49}$$

$$Q = \frac{W_{in} \cdot \sqrt{R.T_{in}}}{A_{in}.P_{out} \cdot \sqrt{\gamma}} \qquad \textbf{Eq. 50}$$

$$\frac{Torque}{P_{in}} = \frac{W_{in} \cdot \sqrt{R.T_{in}}}{A_{in}.P_{out} \cdot \sqrt{\gamma}} \cdot \frac{\Delta H\sqrt{T_{in}}}{T_{in}N} \cdot \frac{1}{dia_{mean}} \quad \textbf{(fully non-dimensional)} \quad \textbf{Eq. 51}$$

There are many good sources of cascade analysis and the conversion of cascade results to derive the pressure loss and efficiency, Saravanamuttoo [54], Gostelow [18] and Hawthorne [18]. These all consider that the axial velocity at entry is equal to exit axial velocity. Now this would be the ideal case for design analysis of obtaining the dynamic loss of the blade without the affects of accelerated flow across the cascade being included. In reality in most rig designs [18] explains there can be an average velocity ratio of up to 1.1, due to the accelerated flow from boundary layers at the end blades of the cascade row, where the sidewalls have no boundary layer suction.

Again [54] and [18] derive the Lift and Drag and the related coefficients, by treating a the momentum change across a control surface where the flow is considered steady,

incompressible, reversible and applies Bernoulli's. The approach requires the pressure loss to have been measured for the blade row, and the flows and incidence angles are around the design conditions. To derive the efficiency, which is the ratio of the actual pressure rise to the theoretical pressure rise, [54] explains that with cascade analysis it is the pressure rise required (in windmilling this is a loss) rather than the temperature rise as required in compressor stage analysis. He goes on to explain that for a 50% reaction rotor, the rotor blade efficiency can be considered equal to the stage efficiency as the total temperature change across the stator will be very small and can be neglected, and for any other % reaction the mean of the two's efficiencies can derive the stage efficiency, see Eq. 52.

$$\eta_b = 1 - \frac{\bar{w} / 0.5\rho V_1^2}{\Delta p_{th} / 0.5\rho V_1^2} \qquad \textbf{Eq. 52}$$

Where the theoretical static pressure rise and the total pressure loss is given by the following equations respectively;

$$\Delta p_{th} = 0.5\rho V_a^2 \left(\tan^2 \alpha_1 - \tan^2 \alpha_2\right) \qquad \textbf{Eq. 53}$$

$$\bar{w} = P_{o1} - P_{o2} \qquad \textbf{Eq. 54}$$

Hawthorne [18] provides more data than most with charts defining the Drag and Lift coefficients to highly negative blade inlet incidences. However, this work is related to design flow conditions with varying the blade angle to create a range of incidences. Also the analysis, as typical with all such studies, considers the axial velocity at inlet and outlet to be the same. Due to these considerations in the method for design cascade analysis, the author was hesitant whether the same information such as the drag coefficient could be applied to any flow conditions. The thought was that these could

not be applied to windmilling conditions with any confidence, particularly when at windmilling conditions the Reynolds number drops considerably and axial velocity ratio across the blade is increasing from inlet to outlet.

9.2.2. LOCKED ROTOR WINDMILLING STUDIES

It was noted by Walker [58] that previous studies found that the under windmilling conditions the front few stages of a compressor produce a pressure rise and the last stages produce a pressure drop. This observation could argue that at some windmilling conditions the compressor pressure ratio can be greater than unity. This becomes very useful when considering the CFD work in chapter 9.3.3 and see if the above analogy is true.

A comparison of windmilling to locked rotor internal drags was studied with a turbojet engine, by Vincent [57]. Within this report it describes the locked rotor drag as being less than the windmilling internal engine drag. The author of this thesis would recommend caution when considering this reports results. In a bypass engine the flow can divert through the bypass duct when the core is rotor is locked, however in a turbojet all the flow passes through the engine. One would actually expect in a bypass engine the locked rotor drag to be higher, and what the report fails to mention is that in the locked rotor mode there is more spillage flow at the engine inlet. This would seem true as the comparison of drag versus flight Mach number only looks at the engine loss overall, what the report fails to identify is that the non-dimensional massflow at locked rotor is one third of that, for an equivalent flight Mach number at windmilling (at 0.9 flight Mach number). What this report does point out is that windmilling drags can be greater than locked rotor with turbojets as all of the flow has to pass through the locked rotor.

As part of the prior EngD research by Jones [2], a MSc researcher Chambard [8] carried out 2D CFD locked rotor analysis of Engine D HPC. To achieve the effects in the change in the annulus area the compressor blades were thickened, producing and inaccurate definition of the spacing. All of the seven stages were simulated in a steady analysis, and on comparison with experimental results the pressure drop was higher than the experimental data, though it seemed the predicted general shape of the pressure loss curve was similar. The CFD simulations found the separation conditions difficult to manage and entered a cyclic mode not allowing the residuals to meet the defined limit. This work recommended further transient CFD studies, however, it did not mention 3D CFD or test rig analysis.

9.3. LOCKED ROTOR RESEARCH METHODS

9.3.1. THEORETICAL APPROACH AND CALCULATIONS

The first of the three objectives was to produce a theoretical calculation method to produce the torque and the pressure losses within a stage, and eventually a whole compressor. This approach can then be used to define the zero speed torque in terms of whatever the characteristic torque parameter is chosen, as discussed in chapter 9.3.2.2. Albeit a theoretical calculation would be limited in its representation of the complex flows actually taking place, the results would provide information for preliminary designs at which point in time the complex geometry of the component will not be fully realised.

As discussed in the preceding chapter, the parameter of specific work cannot be used to define the zero speed, as it also would be zero, whereas if the parameter of torque was used, it involves no speed terms and only considers the energy from vectors of forces, as shown in Eq. 55.

Torque = force x radial distance, **Eq. 55**

(this is an implied force over a radial distance)

However, Torque can also be expressed in terms of rotation with reference to power, as shown by Eq. 56.

Power = Torque x rads/s **Eq. 56**

Work to produce a basic theoretical calculation from first principles was derived with Bittan [3] an MSc Researcher at Cranfield Uiversity, supervised by Prof. Pilidis and the author of this thesis. The approach utilised expressions for cascade analysis, wherein

the flows are considered incompressible flow, which is very suited to the incompressible flow conditions from windmilling to locked rotor conditions. The following equation Eq. 57, was derived for torque within a rotor.

$$Torque_{rotor} = \frac{n.W^2[\tan(\alpha_2) - \tan(\alpha_1)]S}{\rho\pi^2(R_{tip} + R_{hub})^2} \qquad \textbf{Eq. 57}$$

Later within the research the theoretical calculation was scrutinised further as the need became apparent to attempt a simple prediction of the pressure drop across a compressor blade and the outlet conditions.

With the increased knowledge during the research of windmilling component behaviour, it was realised the original calculation had two main limitations. Firstly the calculation considered the velocity *Va* to be constant across the blade. This would be true for a cascade blade for measuring design point performance. However, a windmilling blade has a pressure drop and decreasing flow area, from the reducing annulus from inlet to outlet, thus both effects produce an increase in velocity. An approach was required to calculate the exit velocity, and was achieved as follows. Secondly the equation only considered the change of momentum across the blade from inlet to outlet considering the blade angles, it did not consider incoming flow angle to the mean blade angle onto the suction surface at windmilling conditions, and the resulting momentum forces that would result (a flat plate analogy, as described in chapter 9.3.1.1.

At locked rotor conditions the total temperature difference will be zero as there is zero external energy extracted or added to the system. Interestingly this situation of zero total temperature difference helps to obtain the outlet conditions, for of course a locked

rotor only. Thus the equations for stagnation temperature at inlet and outlet reduce to equation Eq. 58 and Eq. 59.

$$T_{o_{in}} = T_{o_{out}} \qquad \textbf{Eq. 58}$$

Therefore;

$$t_{in} + 0.5\rho_{in}V_{in}^2 = t_{out} + 0.5\rho_{out}V_{out}^2 \qquad \textbf{Eq. 59}$$

If we consider at locked rotor conditions, like in the stator, in the rotor blade there also is no total specific enthalpy change when the flow is relative to the blade angles. Thus as Saravanamutoo [54] indicates for turbines, from the steady energy equation, the static enthalpy can be deduced from blade angles and transposed by trigonometry back to relate to axial velocity at inlet. The same approach was used here, and the substitution and rearrangement of the formulas carried out in the research, to obtain blade exit axial velocity and exit static temperature is shown in the following equations.

For equal axial velocities inlet to outlet the equation would be;

$$C_p\left(t_{in} - t_{out}\right) = 0.5V_a^2\left(\tan^2\beta_{out} - \tan^2\beta_{in}\right) \qquad \textbf{Eq. 60}$$

Rearranged for different axial velocities;

$$2C_p\left(t_{in} - t_{out}\right) = V_{out}^2\left(1 + \tan^2\beta_{out}\right) - V_{in}^2\left(1 + \tan^2\beta_{in}\right) \qquad \textbf{Eq. 61}$$

By substitution of the following rearrangement of Eq. 62, as shown below, and substituting into Eq. 61. Then arrive at a rearranged formula of Eq. 63.

$$t_{out} = t_{in} + 0.5\rho_{in}V_{in}^2 - 0.5\rho_{out}V_{out}^2 \qquad \textbf{Eq. 62}$$

$$V_{out\_axial} = \sqrt{\frac{-V_{in\_axial}^2 \tan^2 \beta_{in}}{\tan^2 \beta_{out}}} \qquad \textbf{Eq. 63}$$

The exit static temperature is simply found by using above result into Eq. 61. With the axial velocity and static temperature at exit now defined for a typical locked rotor, the calculation of the torques and pressure losses can be concluded from Eq. 64.

$$F_{y\_blade} = S\rho Va\left(Ca_1 \tan\beta_1 - Ca_2 \tan\beta_2\right).\left(R_{tip} - R_{root}\right) \qquad \textbf{Eq. 64}$$

The torque could be expressed as shown in Eq. 65 below, however, the definition of force is per unit length, therefore the torque over the length of the blade is actually defined by the Eq. 66.

$$\tau_{blade} = F_{blade}.R_{mean} \qquad \textbf{Eq. 65}$$

$$\tau_{blade} = F_{blade}.\left(R_{tip} - R_{root}\right) \qquad \textbf{Eq. 66}$$

Now a simple attempt to achieve an approximate theoretical calculation of the pressure loss would be to simply take the static pressure drop from the resulting drag

By resolving the reactions of the fluid to the changes in momentum, imposed by the turning across the blade through the blade angles drag force can be deduced as, shown in Eq. 67.

$$D = \frac{F_{y\_blade}}{\sin(90 - \alpha_{mean})} \qquad \textbf{Eq. 67}$$

$$S\Delta p = D.\cos\alpha_{mean} \qquad \textbf{Eq. 68}$$

The static pressure at exit is now able to be determined, then using velocity out determined from Eq. 63, and from continuity of mass flow we find density, then we find static temperature and then Mach number allow the total pressure ratio to be defined.

However, the approach above is a very simple derivation which will have large errors in drag as it does not include the wake losses. There are lift and drag coefficients determined experimentally to fully define the lift and drag forces. As discussed in chapter 4.2.1 and Figure 8. However, there are no values at the high incidences and low Reynolds numbers at windmilling.

Research into implementing locked rotor loss coefficients was developed from CFD results in chapter 11.4.2, as a function of flow incidence to the blade. From which the derived loss coefficients were applied in the following equations to define the drag and lift forces and the pressure losses. The torque for the rotors was then derived from the forces.

A form of stage stacking whereby the exit conditions of one calculated stage are applied to the inlet of the next stage was used to create a whole compressor locked rotor characteristic. The method used the theoretical method above, however the pressures were derived by the following calculations.

The lift and drag forces are defined by equations Eq. 69 and Eq. 70, using the loss coefficients derived by CFD, and the blade incidence. The first rotor (without any IGV) receives flow axially, so the incidence is the blade angle itself. For the next blade such as the stator, as the flow is incompressible it is assumed the flow leaves the blade at the exit angle of the blade, therefore this upstream angle and the blade inlet angle derive the incidence and so on.

$$D = 0.5\rho C_D U_o^2 A \qquad \textbf{Eq. 69}$$

$$L = 0.5\rho C_L U_o^2 A \qquad \textbf{Eq. 70}$$

The total pressure loss is determined by Eq. 71, using the pressure loss coefficient from the derived CFD values.

$$\varpi = \frac{P_{in} - P_{out}}{0.5\rho V_m{}^2} \qquad \textbf{Eq. 71}$$

The static pressure loss is then determined by Eq. 72.

$$\Delta p = 0.5\rho V_a^2 (Ca_{in} \tan\beta_{in} - Ca_{out} \tan\beta_{out}) - \varpi \qquad \textbf{Eq. 72}$$

9.3.1.1. Compressor locked rotor definition

The compressor at locked rotor and also windmilling conditions is working in an operating condition it was not specifically designed for, whereby it is expanding the gas path flow. The compressor is designed for an adverse pressure gradient and although this now does not exist in the locked rotor condition, the annulus geometry is still decreasing axially as for its original intention to maintain a constant Va.

This chapter is the ideal place to describe the actual flow angles and understand the forces on rotor and stator blades at locked rotor and windmilling condition and the author found there was no public literature that sufficiently described these effects.

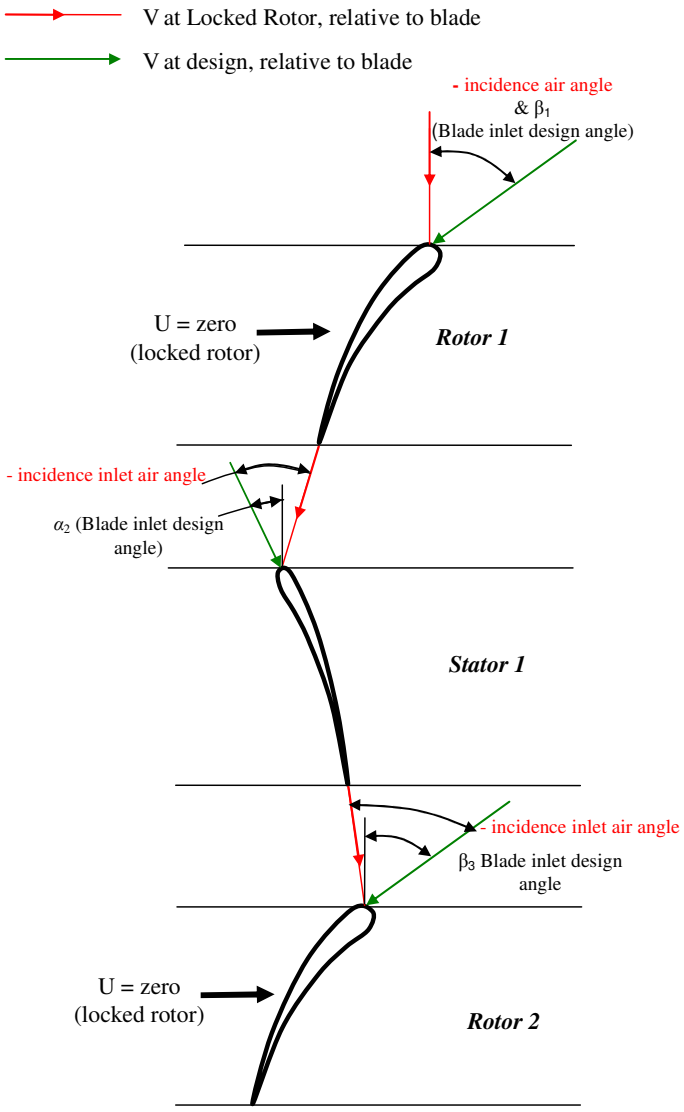

Figure 37. Compressor Locked Rotor flow angles [1].

What is evident from a drawing of the air angles at locked rotor conditions, is that the stator is most likely to experience the highest negative incidence angle for incoming air

[1] Blade angle terminology uses same as described in Saravanamuttoo [54].

from an upstream rotor. In addition to the stator exit blade angle shown in Figure 37. the angle could be negative, actually reducing the negative incidence angle of the air on Rotor 2, for example.

The highest momentum change will not be across the rotor, from the change of momentum of the air from blade inlet to exit angle. Instead the highest momentum forces will come from the incidence of the air to the blade design angle, thus the two angles for inlet and exit respectively are the inlet air angle and the inlet blade angle. This can be defined by an analogy of a flat plat to an oncoming flow, where the blade mean angle or inlet angle defines the flat plate angle to the flow. The flat plate representation of windmilling flow forces onto inlet of blade is represented in Figure 37.

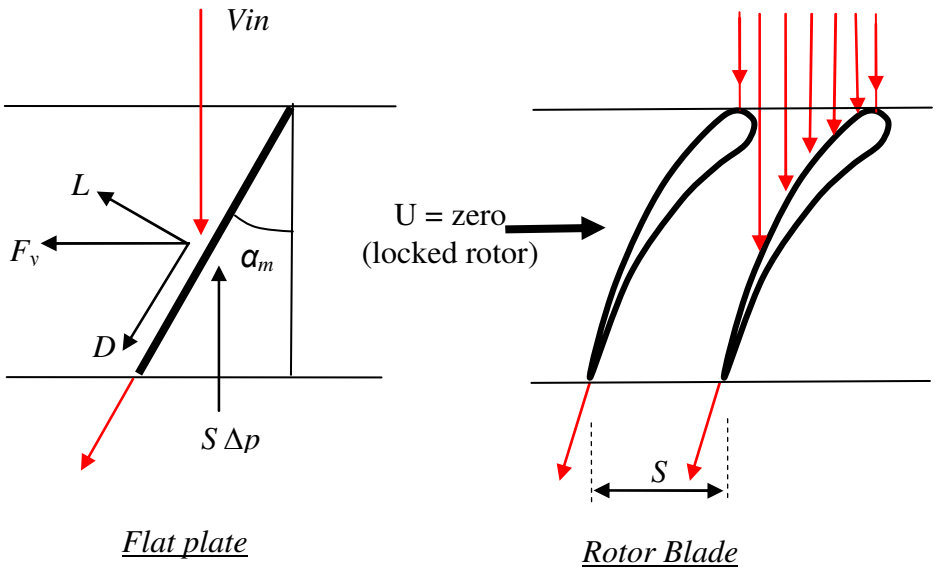

Figure 38. Compressor flat plate analogy.

The mean angle, shown below Eq. 73. It was decided instead that the inlet angle be chosen as it is to the inlet region of the blade which experiences most of the inlet flow momentum. This changes Eq. 64 to Eq. 74 as shown below. In the first rotor stage with

no IGV, the flow would typically enter the blade with an air inlet angle of zero and the accordingly highly negative incidence angle. The confidence in the flow entering axially would be improved by the presence of a swan neck at entry assisting straightening of the flow, the sense of which was agreed by the sponsor.

$$\alpha_m = (\beta_2 + \beta_1)/2 \qquad \textbf{Eq. 73}$$

$$F_{blade} = S\rho Va(Ca_1 \tan\alpha_1 - Ca_2 \tan\beta_1).(R_{tip} - R_{root}) \qquad \textbf{Eq. 74}$$

The above force can then be used to define rotor torque by Eq. 66.

Actual blade profiling may have little effect on any results, it is the angles which are most influential. Some stators have negative exit angles proving a lot of turning within the blade.

9.3.1.2. Turbine Locked rotor definition

The turbine in locked rotor conditions will always be behaving as a turbine as the blade angles are designed to expand the flow, as required in windmilling conditions also. As can be observed from Figure 39. the turbine angles even at the far off-design conditions of locked rotor, deviate little from the design air angles. In fact the flows follow closely to the blade angles. Therefore analysis of the momentum change across the turbine should be very suitable defined in chapter 9.3.1 theoretical method

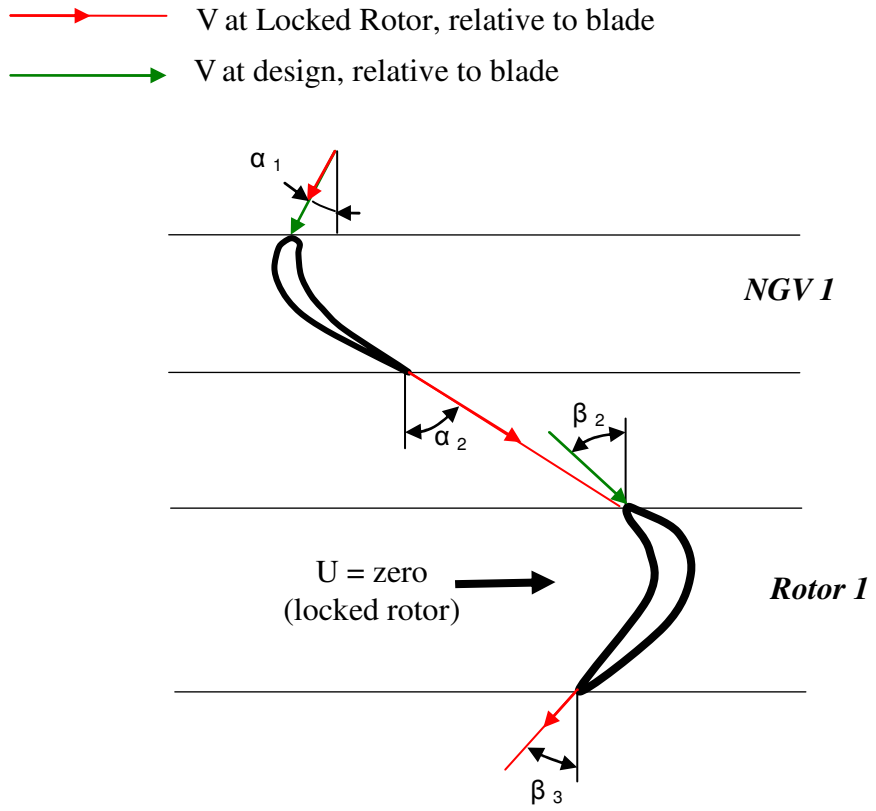

Figure 39. Turbine Locked Rotor Flow angles[2].

The turbines Torque, to within some degree of accuracy, can simply be calculated from the momentum change across the blade using the blade angles, utilising Eq. 64. A first approach simple analysis of the pressure loss may be determined by ignoring the profile loss from the incidence variation, the annulus, secondary flow and tip losses also.

Therefore from Eq. 62 and 63 the static temperature and exit velocities have been defined, knowing the exit area use the continuity of mass flow to define density and

[2] Blade angle terminology uses same as described in Saravanamuttoo [54]

then static pressure are exit. The Mach number can also be defined at exit, thus allowing calculation of the total pressure at exit.

As the calculation can easily be validated against the extrapolation of the linearised parameters and the turbine is behaving in its design condition of expanding flow, the theoretical approach discussed here could, as a first approximation, be used to define the zero speed curve for torque characteristic interpolation/extrapolation.

9.3.1.3. Application of Theoretical torque approach

The first application of the theoretical method defined by [3] in Eq. 57. was on the compressor of engine D. The blade geometry was obtained from the compressor overall design specification, which the author sourced from the sponsors files. The results are presented in chapter 11.4.3.1

Application of the more thorough approach as defined in this thesis was applied to the compressors for engine A and C. Generic compressor blade geometric data were provided by the sponsor and, the results were then aligned against the CFD analysis, as discussed in chapter 9.3.3.4. Results are shown in chapter 11.4.3.2.

A complete theoretical method of using the derived CFD generic blade loss coefficients, using a stage stacking technique to generate the whole compressor locked rotor speed curve was implemented. The results are shown in chapter 11.4.3.3.

9.3.2. INTERPOLATION OF CHARACTERISTICS UTILIZING ZERO SPEED CURVE.

9.3.2.1. Introduction

Extrapolation of compressor characteristics, or any characteristic for that matter, is not an approach that produces the greatest confidence in the results by referring to the sole the nature of the term 'extrapolation'. Also as discussed in chapter 9.1, using cold windmilling test data to align the extrapolation has only limited benefits and does not provide repeatable methods, particularly when there is a new engine and no test data yet available, how will there be any confidence in the extrapolation. Therefore methods for repeatable and reliable prediction of component extrapolations is required, thus the avenue of this area of research.

At an early stage the desire was to convert the current extrapolated characteristics into torque and attempt to derive an equivalent zero speed curve definition. This was later realised as not possible, as from study of the characteristics using the linearised parameters showed the influence of speed, as speed tends to zero, produces very small range of values. The actual values of pressures are small at windmilling, however, approximating these would be very inaccurate an even a small error, would produce a large model error. It was therefore decided to use reasonable values produced from the CFD results for the first assembly of the torque characteristics zero speed values.

9.3.2.2. Parameters to define torque for use in a performance model

The specific torque representation by [28] , as shown by Eq. 47 could be used to define the torque and thus the zero speed Specific Torque. However, this parameter was considered problematic when considering the zero speed curve definition. The numerator and the denominator within the calculation both approach zero and although this may result in a finite value still present at zero speed, it was considered the torque

values would be very small compared to the rest of the characteristic. Another problem could arise in model stability, where the tolerances of the matching equate the enthalpy rise to be zero before the rotor speed has also achieved zero.

As a result of the above discussions, the actual torque derived in the following representation in Eq. 75 was chosen to be implemented, which combines WrT/P ΔH/T and N/rT.

$$\frac{Torque}{P_{in}} = \frac{W}{P_{in}} \cdot \frac{\Delta H \cdot 60}{2N\pi} \quad \text{units are;} \quad \frac{Nm}{Kpa} \qquad \text{Eq. 75}$$

The definition described above in Eq. 75 is basically a power calculation with reference to the inlet pressure. Therefore the equation provides a definition of actual torque that can be represented by both the standard above-idle characteristics and the locked rotor representations. Thus enabling the zero speed curve to be directly implemented into the component characteristic.

The pressure loss is required, particularly at zero speed, as using the torque parameter, the temperature difference will be zero, and therefore the total temperature ratio will be unity. With these points in mind the isentropic efficiency will simply be a direct function of the pressure ratio. It would seem this to be a viable approach, though the transition from zero speed to the next iteration defined speed, may mean that the temperature increase may be so small as to not be significant in the iteration step size.

Parameters used in this approach are; Torque/Pin, PR, both versus N/rT, WrT/P and Beta lines. The isentropic efficiency is required, the torque can be divided by WrT/P and multiplied by N/rT to find the ΔH/T, which defines ΔT to be used with PR in Eq. 22.

9.3.2.3. Approach to Extrapolation/ Interpolation

The result from the second of the three objectives had two possible directions, one direction was to use the zero speed data and allow interpolation but then convert parameters back into linearised parameters while choosing a minimum speed of 5%N/rT to avoid zero work complications. The issues resulting of this approach, of flat speed curves with a limited no useful range, are discussed in chapter 3. The second direction was to produce new parameters of torque for each of the component characteristics, and utilise in the sub-idle model. The difficulty faced in this approach was using a definition for the zero speed curve (with any additionally defined low speed curves) which could also be used to convert the original above idle characteristic to this new form. The advantage of this second direction would be the ability to attempt to run the sub-idle performance model for groundstarts from zero speed.

In addition this should improve the extrapolated characteristic as the curve of the lower speed curves will be better defined rather than relying on the curve shape of the idle speeds.

Once converted to torque the existing characteristic is inserted into the same extrapolation tool as used for the linearised parameters. However, the 5% speed is now replaced with a zero speed value and the data for each beta is not defined as a linear spread between the high and low beta values, instead the actual locked rotor values are used.

Prior to interpolation of speeds using the zero speed curve, the lower three speed curves were removed (as these were probably extrapolated in any case), then the original characteristics were converted into the parameters as described in the above paragraph. The approach of extrapolating the beta lines of the original characteristic to pressure

ratio of 1 was used prior to interpolation and the torque beta was extrapolated by ensuring a smooth curve continuation from the original characteristic curves.

As the theoretical zero speed curve is created by running calculations at a range of non-dimensional mass flows, both the torque and pressure ratio locked rotor curves produced are a function of non-dimensional mass flow. Therefore this approach requires only the range of WrT/P26 to be defined to obtain the HPC A compressor zero speed curve and interpolation of the characteristic, like that described in Figure 11. b).

Therefore this approach reduces the amount of guessed unknowns compared to that of the extrapolation approach described in chapter 4. The surge beta line is set to around zero WrT/P26 and then the lower beta line non-dimensional mass flow is guessed. WrT/P26 was guessed until the low speed curve of 12%N/rT aligned with ATF test data. Although in using this approach the desire was to avoid the use of ATF data and thus produce a more predictive approach, it was found that to produce accurate characteristic the use of ATF data could not be avoided.

9.3.3. CFD STUDIES

9.3.3.1. Introduction

The second of the three objectives, required analysis of a range of engine compressor designs and test data to compare against. As the research developed it was realised that the individual blade analysis in CFD required comparison against test rig results, which had never been tested in any known literature at the conditions of windmilling and locked rotor. Thus a test rig was design for study later on to compare the CFD results with an validate and align the CFD modelling, as discussed in chapter 9.3.4

Although the primary aim of this area of research was to produce predictions of locked rotor values, in some simulations the windmilling (spool rotating) torque and pressure losses area also analysed. Much of the CFD prediction does have to bear in mind some caution from the results, as CFD is more a qualitative rather than quantitative analysis. However, as the flows are compressible and rotors almost stationary, oneself can have more confidence in the results. The large wakes produced at the large incidence angles flow regime, produce a discrepancy in these assumptions of reasonable accuracy, as separation wakes is one fluid behaviour CFD still has difficulties with simulating the real life conditions, though the low Mach numbers simulated should alleviate any serious errors.

The CFD studies of the compressor for locked rotor studies consisted of three main steps as discussed below.

- *Step one was to analyse previous work as described in the literature review. Then to assess 3D CFD and other approaches such as the theoretical calculation described in section 9.3.1.*

- *Step two was to produce actual blade modelling of engine C and have these available for analysis with a CFD model of the rig and then compare with test data. Also from this work the equivalent ATF data was used for windmilling runs and locked rotor runs to put some degree of reference to the flight conditions required to create these flows. However, in the locked conditions of increased pressure drop, this would actually affect the upstream compressors and the downstream turbines (albeit the HPT would obviously be in the locked condition too, whereas the IPT and LPT would be rotating). CFD analysis of the cascade test rig was also carried out.*

- *The third step was to model Engine A compressor blades through CFD steady state simulations. The torque and pressure losses from these simulations could then be used to define the zero speed curves on the Torque characteristics for engine A. Also combined with engine D results to create generic loss coefficients.*

The approach of these three steps are described in the following chapters. From all these three steps the results could be combined to provide overall blade profile data for locked rotor conditions, but also providing knowledge and data for the losses of the rotors at high negative incidences and low Reynolds numbers.

The work was restricted to compressors, though the study of turbines would be very useful.

Transient simulations would provide far better results in all the above CFD analyses, however, the time available and the direction of this work to only provide an approach not the fully worked solution, is the reason this was not taken further. Therefore full

analysis and maybe even a complete component CFD analysis would be required to validate the work here, though would be a significant size of research work.

The study has the advantages that at windmilling conditions the flows are incompressible, the rotational speeds are low or zero in locked rotor conditions, all favourable to simple analysis and more reliable results from CFD analysis.

In addition to the locked rotor studies simulations in CFD also applied a rotational speed to simulate the windmilling induced spool speed. Therefore providing some data of the individual blade performance at windmilling, and analysing the possibility of also using CFD for low speed curve prediction. Which could improve the speed curve definition in the extrapolation of component maps to the sub-idle region.

The following discussions of the research using CFD are based on the assumption the reader has a basic understanding of how CFD works. The simulations were not advanced, although the boundary conditions are not the typical conditions users would apply within CFD turbomachinery simulations, one example is the high negative incidences.

9.3.3.2. Evaluation of 3D CFD Capabilities [Step 1]

The 3D CFD package available at the time called TASCFlow, was utilised within this research. Later during the course of the EngD research TASCFlow was replaced by CFX which utilised some of the core elements and capabilities of TASCFlow. It was however, later found that not all the data from a TASCFlow simulation could be read by the CFX post processor.

As discussed in the literature review in chapter 9.2.2, previous 2-Dimensional CFD analysis was performed within the UTC based on Engine D HPC geometry. The geometry was basic mid tip and hub, inlet and outlet angles with the chord and thickness were available and combined onto a C7 profile to define the aerofoil. To create the geometry coordinates and introduce the individual blade camber arc and stagger angle, a tool was developed by the author and Bittan [3]. The tool was able to provide the geometry in Cartesian coordinates including for the blade height changes for the reducing compressor annulus. This could then provide basic 3D blade profile geometry for the 3D model.

The research considered the following effects on the locked rotor simulations, as performed by Bittan [3];

- Perform stage analysis of both rotor and stator.
- Perform multiple stage analysis.
- The effect of the Position of blade relative to stator.
- Percentage windmilling Speed effects at 5% and 10%, using locked rotor flow condition data.

Engine D was not a typical and modern compressor therefore it would be difficult to analyse and transfer the results to other engines. Therefore although useful as a study the work does not add value to future design or predictions.

Another area of work performed by [3], was to compare the CFD results for torque with that of the theoretical early calculation (Eq. 57), described in chapter 9.3.1. The results of these results are discussed in chapter 11.4.3.1.

9.3.3.3. 3D CFD studies for windmilling cascade test rig [Step 2]

It was agreed with the sponsor that HP compressor blades from a recent engine should be used in this study. Thus the sponsor provided HP1 and HP6 rotor blades from Engine C. The rotor blades were requested as these could provide data on the torque on what would otherwise be a rotating part and it can provide loss data for both rotor and behaves similar to a stator in the locked rotor condition. The simple analogy of a locked rotor being like a stator is not true as the stator geometry and angle would be designed for diffusion.

The sponsor's requirement was that this research aim should was to align CFD predictions and not perform an actual cascade aerofoil simulation and tests. Due to confidentially reasons the geometrical data for the blades could not be obtained. Therefore it was agreed that blades for both HP1 and HP6 could be digitally measured. Measurements along the 15 measurement planes of the chord for hub to tip for HP1 and 10 measurement planes for HP6, resulting in geometrical data to define the blade profile. A typical profile generated for CFD simulations is shown in Figure 40.

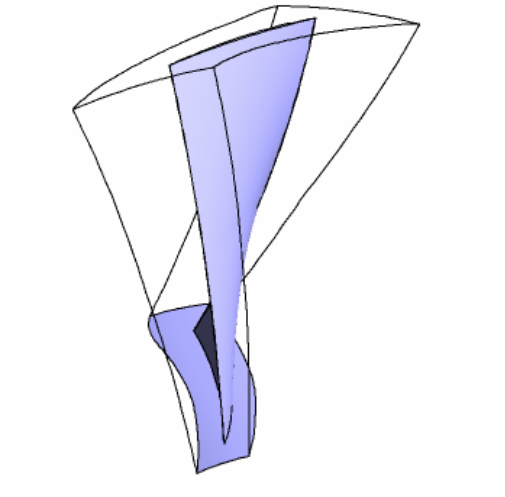

Figure 40. Generated Blade model, highly twisted geometry for Engine A LPC Rotor 1.

Initial 2D studies of the proposed cascade test rig for HP1 of engine C, were performed to understand the flows within the rig and any interference on the flow results from the rig geometry. The blade geometry used at that time was basic measurement from the blades. From this data and consideration of incompressible flow the rig design was completed.

Studies using CFD were required to further evaluate the rig design for a range of windmilling conditions in 2D and construction of a 3D model. This was carried out by an MSc researcher Perceval [47]. By comparing the 3D CFD model simulations of the rig against the results of the future rig runs, correlation factors can eventually be defined. These correlations will primarly be valuable in correcting the limitation of CFD simulations at predicting separation and wake losses. Future simulations can then use these correlations, to enable CFD to be used as a fully aligned predictive method, and thus defining the zero speed curve on component characteristics.

The cascade rig runs and CFD results are for a linear blade row, whereas the true configuration within an engine is annular. A 3D CFD turbo-machinery package such as CFX can produce annular geometry, as shown Figure 40. and simulation can be run either locked or rotating. To correctly model the locked rotor case the annular configuration would be desirable, to produce realistic losses from the geometric and rotational effects on pressure losses. In addition, secondary flow effects could be modelled such as tip leakage. This work was carried out by Kendrick [30] in which simulations of engine C windmilling conditions, were applied to a locked rotor and the windmilling rotor speed. Therefore from this work and comparison of the flow conditions, and such parameters as torque and pressure losses could be used to understand their transition from windmilling to locked rotor conditions, with their

implications on individual stage performance and the effect on the component characteristic.

The rotor speed has to be set in the CFD modeller by the user. In locked rotor simulations this would obviously be zero, but for windmilling simulations ATF data spool speeds were used and the equivalent flow conditions applied. CFD cannot be used for predicting windmilling speeds. thus the use of windmilling data for locked rotor conditions to provide some equivalent windmill speed for the same conditions.

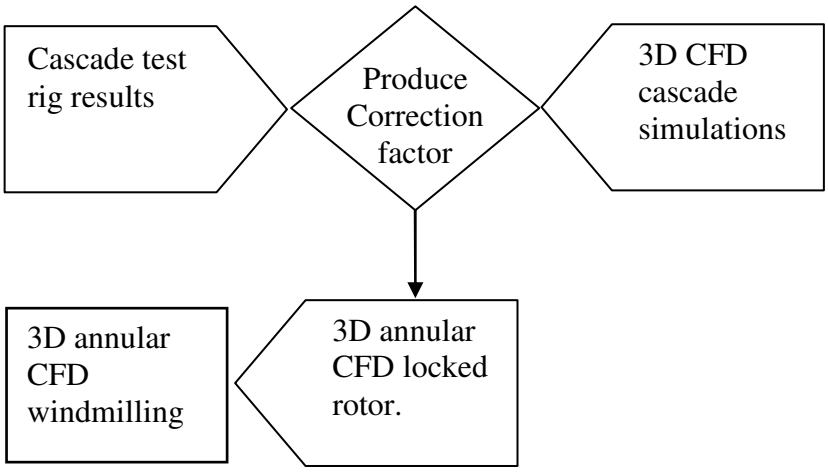

Figure 41. Process of CFD data use in the definition of locked rotor data.

Figure 41. describes the flow of the CFD areas of research, how they relate to one another, and how they can be used to obtain and correlate actual compressor data.

9.3.3.4. 3D CFD for creation of Engine A torque maps. [Step 3]

To generate a fully geometric and complete compressor simulation is far beyond the scope and time available for this portion of the whole thesis research. What was needed was a quick approach to provide a zero speed curve and at least promote that CFD to is a viable approach. The study of one isolated blade to understand the aerofoil losses is useful, even though it ignores the affects from the downstream blade, which forms the complete stage. It was decided by the author to only model the important stages within the compressors, to minimise time and allow for comparison and cross-over with theoretical methods. A simple approach of individual blade analysis was attempted and the averaged data from one, passed to the related stator or rotor. Within this area of research both the fan and HPC compressor torques were required. Table 3. explains the blades modelled for engine A, and how the boundary conditions were setup based on the windmilling station conditions available to apply to the simulations.

Blade	Boundary conditions			Source of Boundary conditions
LPC 1 Rotor	Ptotal in	T total in	Wout= Win	ATF Data station 1
LPC 1 Stator	Ptotal in	T total in	Wout=Win	LP1R result
HPC 1 Rotor	Ptotal in	T total in	Wout=Win	ATF Data station 26
HPC 1 Stator	Ptotal in	T total in	Wout=Win	HPC 1 Rotor Out
HPC 5 Rotor	Ptotal in	T total in	Wout=Win	HPC 5 Stator in
HPC 5 Stator	Pstatic out	T total in	Wout=Win	ATF data station 30

Table 3. Boundary conditions used for CFD Engine A blade analysis.

As can be seen from Table 3. the more desirable approach of setting the total pressure in and static pressure out, was not used. This is the most correct approach as the Mach number and flow balancing allows the results for find the relevant mass flow for that flows density. However, as the flows are typically all incompressible, this should be less of a problem.

A grid dependency check was made by using approximately 250,000 nodes on one simulation and then 500,000 on another. The boundary layer was defined in the simulations as a y + calculated by CFX, based on Reynolds number. A mixing rotor steady state set of analyses were performed. A frozen analysis would have been the most appropriate. The Reynolds number for most of the windmilling conditions is typically around $x10^{-4}$. A stage calculation (blade and stator) was performed and found to take twice as long as a single calculation even with the total elements only being 500,000.

Generic blade data for the compressors on Engine A were provided by the sponsor, this included inlet and outlet blade angles, S/C, thickness, at the mean, tip and hub blade heights. Drawings were used to determine the radius of each blade height and the compressor annulus. The tool developed alongside [3] was used to create the 3D geometry of each blade for application in the CFD modelling.

Bleed flow is removed after the last HPC stage, therefore it will have no effect on the mass flows through the actual compressor.

The author realised no fan simulations had been carried out to date and thus the results would provide a good insight into very three-dimensional geometry at windmilling and much higher height to chord ratios. One thing not simulated, was the possible back-pressure difference from hub to tip, due to the resistance created by the core flow path pressure drop, effecting a high bypass ratio. A full fan analysis would be required to produce this kind of analysis, for which the time is not available. Therefore the fan has very complicated flow patterns and boundary conditions to model. However, within this simple analysis only the averaged boundary conditions were applied.

Grid generation was very difficult as the automated grid generator within CFD seems to have been designed for small ranges of negative incidences around the design point, and thus causes difficulties when trying to impose the high negative incidences. High negative incidences are imposed on rotor blades after the first stage where the flow is leaving the stator blade exit angle. It was found trying to impose a negative incidence, which went past the axial plane the grid, would become very corrupted. In some cases, a compromise of reduced incidence had to be accepted. This problem would be removed with a complete compressor stage analysis, as the program will calculate the flow direction leaving the upstream stator and apply it as a vector for the flow path.

9.3.4. LOCKED ROTOR CASCADE TEST RIG

9.3.4.1. Introduction

The third of this research areas three objectives was the validation of CFD results required that a test rig be built to measure the pressures, velocities across compressor blades at the conditions of windmilling and particularly locked rotor. Therefore a test rig was designed and constructed to test an actual row of compressor blades in a linear rig, simulating the inlet flow conditions and the negative incidence at inlet to the blade occurring at windmilling. With a test rig, the CFD results could be validated if not aligned to represent the true pressure drop at conditions.

It was agreed with the sponsor to test a modern blade from engine C, and the most useful would be an HP compressor blade. Normal cascade tests use a 2D blade representing the blade mid-height. Instead a 3D blade was used, for two reasons; to reduce costs and time, but more importantly the 3D affects of the blade flow needed to be understood at windmilling conditions. This research was not a blade performance study more of an alignment of and validation of CFD results. Ideally the last stage

(HP6) would be more useful as the expected pressure drop would be higher. However, the chord to height ratio (aspect ratio) would be unity, and to avoid top and bottom cascade wall influencing affects this value should be at least 3. Due to the blades available, a compromise of a blade to chord ratio of just over two was chosen, therefore the first stage rotor (HP1) was used.

9.3.4.2. Operating conditions and performance design

The entry flows at windmilling are typically incompressible and as the upstream compressors are providing a pressure drop, depending upon the ram pressure from the flight Mach number and altitude, the entry pressure will typically be below ambient. The inlet temperatures will also be a strong function of the windmilling altitude condition. The velocity ratios presented by the CFD design studies expected at a range of windmilling conditions are typically in the range of 1.1 to 1.2.

A distinguishing feature of windmilling cascade test rig from typical design cascade rigs is that the velocity will increase across the cascade row. As in windmilling, the blades experience a pressure drop with the compressor behaving like a turbine/stirrer.

At a locked rotor condition the oncoming flow to the HP1 rotor would be axial with some amount of deviation. The sponsor agreed the flow should remain axial particularly with the influence of the upstream swan neck straightening the flow. Therefore the incidence angle would be around -32 degrees.

The rig design would enable the flow Mach number at entry to the blade flow to achieve similar conditions as that in the engine. However, the Reynolds number could not be achieved. Table 4. below highlights the error between predicted rig and the engine conditions for a range of flight conditions. Reynolds number can be achieved by decreasing the rig massflow and therefore creates an error in entry Mach number

(although this is half of the error of Reynolds number when matching entry Mach number).

	Matching Mn			Matching Re		
Flight case	**Mass flow Kg/s**	**%error Mn**	**%error Re**	**Mass flow Kg/s**	**%error Mn**	**%err Re**
3063	0.5	-4%	108%	0.24	-54%	0%
3036	0.6	-1%	140%	0.24	-60%	-4%
3048	0.6	-4%	131%	0.25	-60%	-4%
1490	1	-4%	60%	0.6	-42%	-4%
2426	0.7	3%	129%	0.3	-56%	-2%

Table 4. Predicted error of cascade rig for matching Inlet Mach number and then matching Reynolds number.

The same windmilling engine ATF data was used to define the approximate conditions in the test rig and provide some relation back to the CFD model. A similar CFD simulation could then be run as locked rotor and then run at the desired windmilling, speed and identify the losses correction for windmilling speeds by using the CFD to Rig correction factors, developed from the cascade test rig.

The cascade row consisted of nine blade flow paths, with only 9 blades a dummy surface was created on the rig walls. Total pressure loss was expected from the plenum chamber downstream, from some recirculating flow. However, the plenum chamber is not really a plenum chamber. Instead, it provides sufficient volume for the separated flows leaving each blade at the angle the flow so chooses and then mix.

A fan was available for supplying air to the test section could be bolted on to the inlet. Using suction was desirable for meeting the ambient pressures and temperatures actually apparent at windmilling conditions. Ideally to provide cascade results with the

least interference on the exit and main measurement plane of the rig, discharge arrangement would be preferred. However, as the rig was for a validation of CFD model rather than purist cascade tests, it is argued that a suction configuration is acceptable. To assess the suitability of the fan, its pumping characteristic of the air supply fan had to be considered.

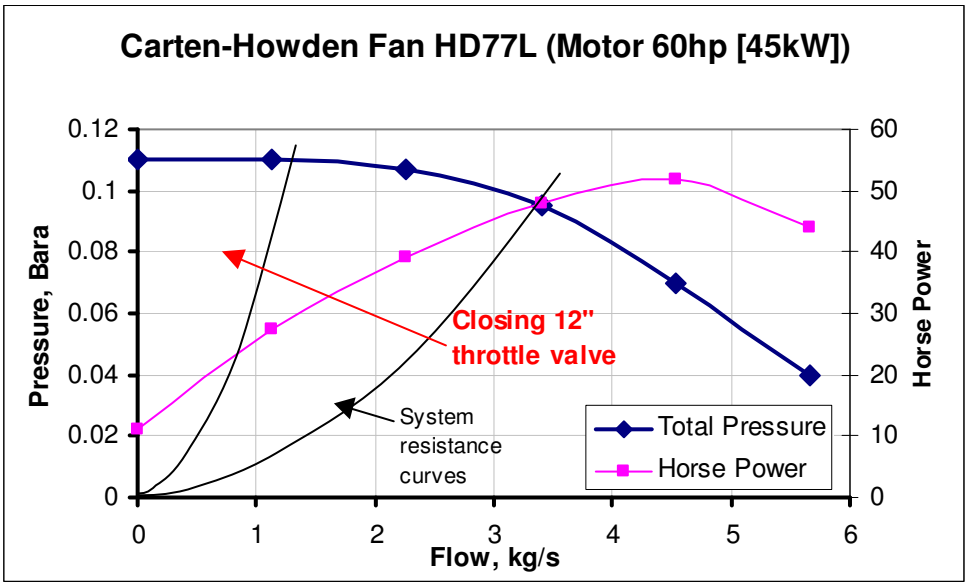

Figure 42. Air supply fan, pumping characteristic.

The flows required for the rig are low ranging from 0.5 to 1.5 kg/s. It can be seen from Figure 42. , the maximum pressure ratio can easily be achieved. To control the flow a 12" throttle valve is used, which on closing will increase the system loss curve, thus reduce flow through the test section. It was assumed that the fan discharge would be to the static ambient air pressure, thus through the rig a suction pressure equivalent to the pressure from the characteristic minus rig losses could be attained across the test section. The losses would be a summation of many losses through the rig as these are a function of V^2, these losses will vary according to the operating flows thus mach numbers required. The main losses are described in Eq. 76, and although it is easy to

try and break down these losses into the equivalent sections, in practice it is harder to actual define values for these losses, particularly in the plenum chamber as there will be swirl losses in the non-symmetrical geometrical.

$$\Delta P_{cascade\_row} = P_{fan} - P_{intake} - P_{plenum} - P_{Transition\_piece} - P_{Piping} \qquad \text{Eq. 76}$$

As the pumping characteristic in Figure 42. shows, the flows required are very small. To remove the possibility of stall in the fan, a 3" butterfly valve is placed between the fan and the 12" throttle valve to allow additional air to be drawn into the fan, bypassing the rig. This allowed additional flow control to increase the overall air and pulling the fan away from likely hood of surge. As the fan acts as like a pump, with increased flow the pressure rise will decrease and with increased flow the dynamic pressure loss increases.

9.3.4.3. Measurements

The total pressure and static pressure change over the stage is required. Also the velocity is required at inlet to outlet to understand the momentum. This can be derived from the total pressure and static pressure using the temperature.

A claw probe at exit of the cascade flow will measure the total pressure and the exit flow angle. As the blades will not have probes inserted within the blade to understand the Cp loss and not withstanding the fact that the blade is too thin, the static profile from inlet to outlet between two blades shall be measured instead. Calculation of total and static pressure with the claw probe will allow calculation of the velocity relative to the blade exit.

9.3.4.4. Design and manufacture

A design was conceived where the downstream section of the rig would be connected to the suction of the flow supply fan. This would produce necessary low pressures and temperatures at inlet to the cascade section.

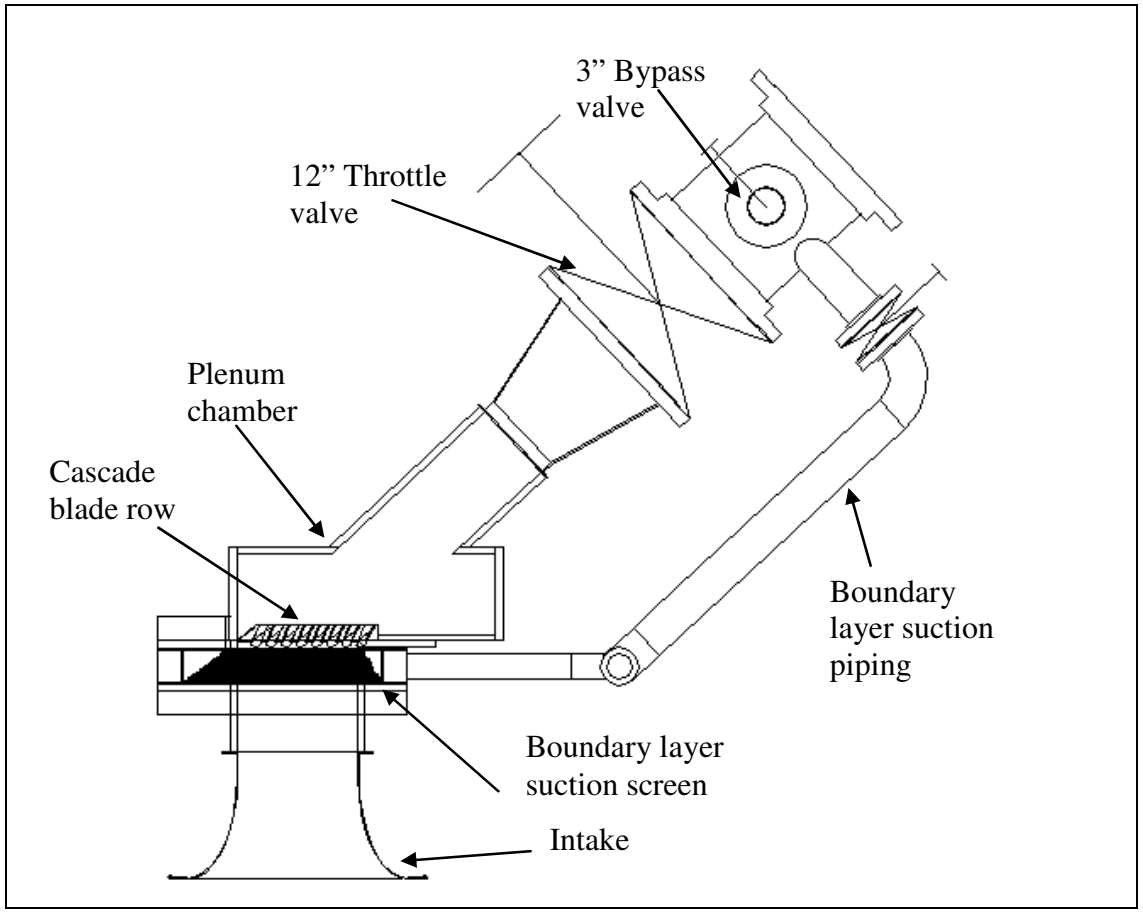

Figure 43. General Arrangement drawing of the windmilling cascade test rig design.

Due to the low blade chord to height ratio it was essential to alleviate some of the upper and lower wall effects in the rig, by providing boundary layer suction from these inlet surfaces before the blade row. This was achieved by perforated surfaces, with the suction flow taken from a tapping further downstream at entry to the suction fan, which is controlled by a 3" butterfly valve.

10. Technology Transfer and Project Management

10.1. INTRODUCTION

One of the most difficult tasks within the research Doctorate was to manage the various and the breadth of the topics covered, as well as the data, tools and contacts required. The information data and findings then required feeding the results, methods, modified programs, tools and findings developed back into the sponsor company and to be incorporated into their design process. This process is thus termed the 'Technology Transfer', and was an important aspect of the research as this Doctorate was more involved with the sponsor than any previous performance UTC project. Placements within the sponsors company, at Bristol, Dahlewitz (Germany) and Derby sites, are also discussed and the impact this had on accelerating the research and flow of communication.

Within the execution of any project, the needs and goals of stakeholders, all require management. These needs and goals are examined and the change during the course of the research.

The nature of the research work produces a network of tacit knowledge building. Therefore it is essential this knowledge be conveyed via this thesis and technology transfer activities approached in this thesis. Management of the project and the technology transfer between the Cranfield Performance UTC and the sponsor, Rolls-Royce, is discussed within this project. The chapter discusses the work and the benefits from MSc projects linked and supervised within this Doctorate.

This chapter also looks into how a sub-idle modelling capability within the sponsor could change the design process.

10.2. MANAGEMENT OF RESEARCH

10.2.1. INTRODUCTION

This was a very different research project than most, one aspect of this difference is the split number of research areas and also that the research area is such a large and continuing subject. Therefore planning and management of each research area was essential throughout the research.

Research planning is very unlike normal project planning, however certain analogies are easily transferable, such as;

Delivery of products	- On-time delivery of thesis (submission date)
	- Delivery of knowledge/reports to sponsor
Costs	- Those entailed in enabling research
Quantity	- Depth to which areas are researched
Quality	- The error of the results.

However, planning of research is difficult as the definition of research explains that there are inherently many unknowns as the outcomes or the time it will take to achieve suitable results, is not like say a project to build a set of offices blocks. In which tried and tested engineering designs and practices will be employed and some degree of certainty of schedules can be gained from experience.

Research is considered by [55], to be a high uncertainty and low complexity in terms of size, value and number of people involved. The only arguable point is that of complexity but only through the eyes of a technical viewpoint and that the size of the research area is large.

The financial benefits of the ability to predict sub-idle performance have already been considered by Rolls-Royce and thus providing the justification for the sponsorship of

this research. These benefits are expected to be a significant reduction in engine ATF testing due to control system testing being completed in a sub-idle model first.

The main players were the sponsor, Rolls-Royce and the Cranfield UTC in performance. However within these players structures there are further players that influence the research. The sponsor can be split into the industrial supervisors requiring an added benefit from their investment and there also the different departments with which contact is required and the results of this research may affect. Likewise within the UTC there is the author of the thesis, his supervisor and the head of the UTC, also other researchers particularly the MSc's that also have an active role.

10.2.2. ROLLS-ROYCE

The UTC relationship with Rolls-Royce is akin to a strategic alliance, where knowledge experience, abilities, tools and resources are shared to produce an added benefit, not achievable separately.

To ensure the sponsor's expectation, requirements and objectives for the research were covered, within the first month in November 2003 a meeting was held at Rolls-Royce Derby with heads of performance departments. In this meeting the research areas to be covered by this thesis research were outlined and agreed. These areas form the research areas as structured within this thesis. Additional scope was added in the second year which is discussed in chapter 10.2.7.

The author of this thesis had to manage the expectations of the sponsor. One example of this is that previous sub-idle performance modelling was quick, however, the scaling of previous data was used rather that creating a whole new set of data, methods to produce component characteristic data and code changes. The work being carried out in another

location also meant that data was not always freely at hand, as it would be to a Rolls-Royce employee.

Initial time periods proposed to Rolls-Royce were based on the time-frame of previous modelling. However, the main change was that the extrapolation of component maps was required for this modelling, which developed into a huge task with no tools available these had to be developed and ideas shared with Dahlewitz development work in this area. Without sharing of tools by Rolls-Royce Dahlewitz this work could have been delayed much further, as although the tool was not a complete finished method it allowed at least an approach to be used and developed and modified ad required. Empire building could have stopped this, thankfully Dahlewitz were willing to share their developments.

The same sponsor's overall objectives from this line of research, as described by Jones [29] are also the same for this research, as these two research projects are a continuation of a research area into sub-idle modelling.

10.2.3. DOCTORAL RESEARCH WITHIN CRANFIELD UTC

The author of this thesis has personal goals in studying for this research Doctorate. The first goal was to improve the author's technical knowledge to an advanced level and a mental challenge whilst working in a stimulating area of research. Secondly there is the qualification itself, improving the author's resume and personal pride. There are also the financial and career gains, attracting rewarding salary and interesting positions.

The experience of working in research within Cranfield and Rolls-Royce has been a large learning curve, coming from an industrial background in another industrial area of oil and gas. However, the rotating machinery subject aligns well with past and developed technical skills. The attitude to approaching research has also been a steep learning curve.

10.2.4. THE STUDENTS

This research involved the author of this thesis supervising five MSc researchers taking projects based on this research, as devised by the author to complement the research studies, see Figure 44. In some cases MSc researchers would undertake projects critical to a research area, or others are undertaken to discover if there is merit in a side avenue of research or to close out this line of investigations.

Additionally in the final year a hand over period took place to successor in this research, Pavlos Zachos a PhD.

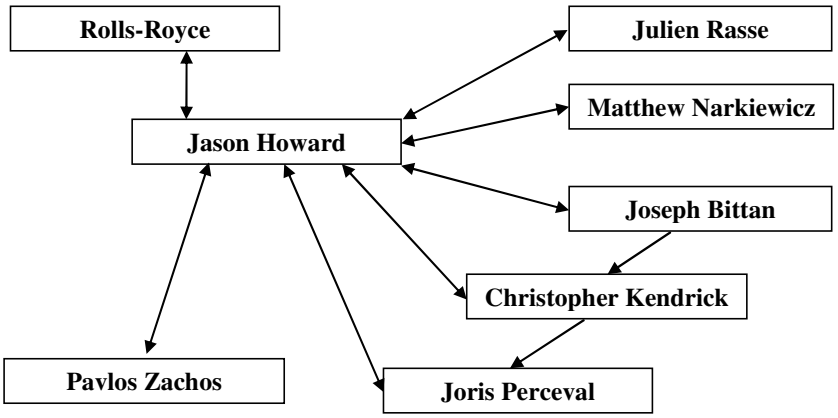

Figure 44. The flow of knowledge during the research project.

In the second year, two MSc researchers were supervised. Rasse [49] who worked on CFD simulations of engine exhaust mixing, Bittan [3] who produced the first 3D CFD locked rotor studies of compressors for this research. In the third year Kendrick [30] was supervised on another 3D CFD compressor locked rotor study, work which related to the build of the cascade test rig. In the final year two MSc's were supervised, Perceval [47] worked on CFD analysis of the cascade test rig, while Narkiewicz [43] worked on a very different area of combustion relight efficiency analysis.

10.2.5. REPORTING AND MEETINGS

Meetings with supervisor allowed the monitoring of progress of the research and steering the emphasis of the research considering such a large number of research areas. Meetings also have the beneficial effect of time keeping and keep the momentum of progress through the long duration of the research period.

Meetings with Students were kept open and honest, trying to build the partnership of the research area so that both the supervisor and the student benefited. Gaining partnership and honesty also promotes responsibility of the student to have ownership for their work, i.e not to say I was told to do this but upon discussion with my supervisor it was decided that. This is an important step for the student to become independent and build confidence. Meetings were held weekly if not more upon the MSc's request, however, it was important not for the student to come straight to the supervisor when they became stuck, so unplanned meetings were avoided where possible to allow the MSc to think over the problem, therefore gain interdependence.

Some students required a lot of assistance on the physical understanding, and easily became confused by trying to understand all of the engine issues taking place, at sub-idle conditions rather than focusing on their areas. An interesting time during the supervision of MSc's was when the author of this thesis was away nearly a month on placement Dahlewitz, coordinating the MSc's work by email. The progress by the MSc's upon return was one of the most significant of any of the MSc's. This was probably partly due to a large preparation period before the placement allowing the MSc's to proceed with little assistance. However, another important understanding gained, was how written explanations, such as those communicated by email during the course of the authors placement, seemed to be very beneficial to the MSc. Upon quizzing the MSc's about the email correspondence they agreed that details discussed within conversations could easily be forgotten, whereas written advice could be read again and commented upon. Whereas when the supervisor is available within their

office too easily is it for the MSc to gain assess, discuss some questions/ issues leave and forget.

Within the UTC quarterly reviews are held in the form of a presentation to Stephen Brown and others from the sponsor. In these reviews results, methods, progress and planning are presented and discussed. These meetings were good experience and helped to motivate and advance the research. An interesting aspect to the presentations was presenting problem results for discussion. In most other environments this would be highly sacrificial, however, within these meetings problems could easily be discussed and advice given or activated.

Annual reviews were held to report the UTC progress and areas of research and development to Rolls-Royce Performance community and the company as a whole.

10.2.6. WORK BREAK DOWN STRUCTURE

To gain perspective on the wide ranging issues for a sub-idle modelling of a gas turbine engine the following work break down Work Breakdown Structure (WBS) was created Figure 45. By no means does the WBS meant to represent the interdependency of each element. Creation of a spider diagram to link the activities and cross interdependence would show how the areas relate.

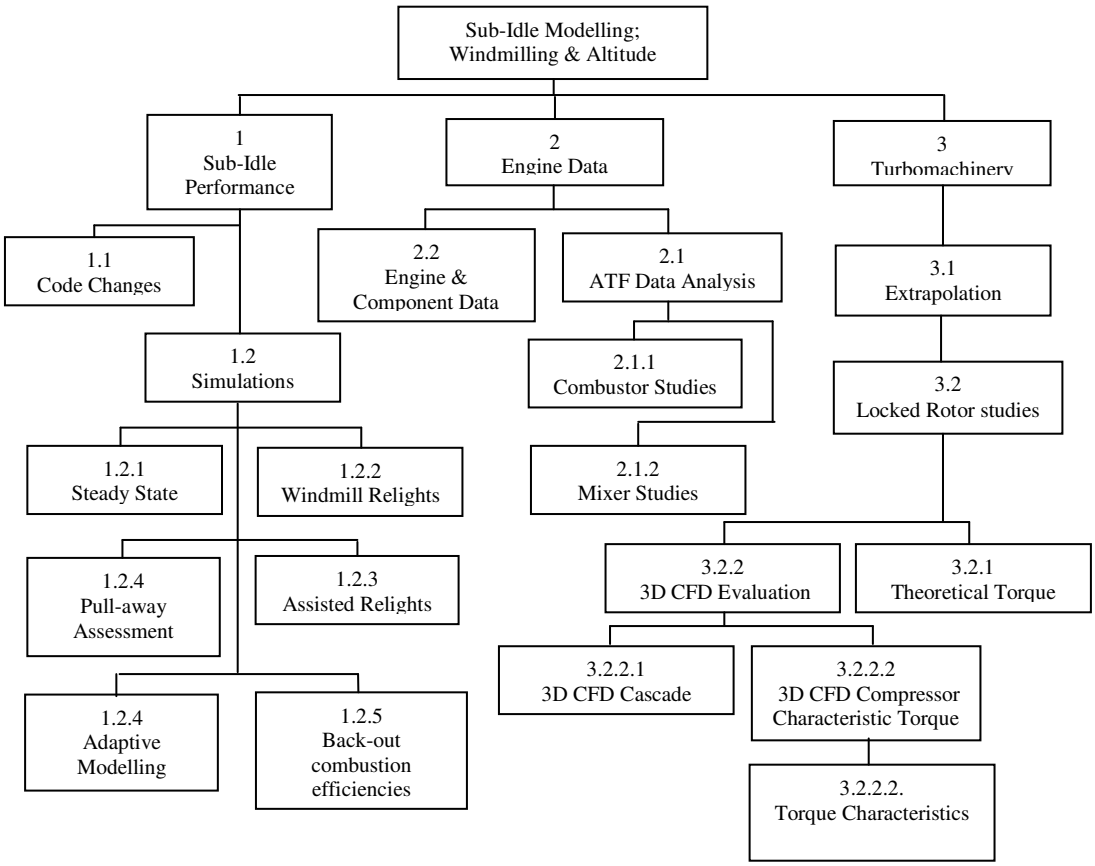

Figure 45. Work Break Down Structure of Research

For the research to complete its objectives the components of the work break down structure may rely on completion of other components. The research experienced two

root causes of either delay in lack of data, or number of occasions with the MSc projects. Therefore the experience gained Jones [29] was acknowledged, whereby to complete the work either; the scope of the work was reduced to a cut-down version, the supervisor assisted the MSc or the supervisor completed the work. Obviously the MSc's requirements of gaining their qualification also had to be considered.

With the research of Narkiewicz [43] the scope had to be reduced to analysis of one engine instead of the two planned, for the research to be completed within the time frame available. As a result the objective and outcomes of the projects research were completed and a useful conclusion was obtained, although for one engine. In the case of Kendrick [30], the scope was met and his results were then corrected by the Author for one set of cases where an error had occurred. All of this MSc's work was then later used to define the loss coefficients for comparison of different blade types, blade angles and engine windmilling conditions.

10.2.7. THE RESEARCHER'S DILEMA WITH ADDITIONAL RESEARCH SCOPE

During the second year of the research the sponsor requested that the CFD analysis of locked rotor discussed in chapter 9 required a cascade test rig to validate the results. Inevitably this added to the scope and workload of the research and as the research has not possibility of extra manpower resources

Managing the change to scope was crucial, as research does not have the luxury of additional human resources to carry out increased scope. Therefore the researcher has to manage not just the increased resource, but the implications on other research areas, the schedule, and the sponsor's expectations.

Knowing that the core items of research cannot be sourced out to MSc's, the researcher has to accept the squeeze on the other research areas.

A great learning for the author of this thesis was the influence of the rig criticality to a research and the reflection of the prioritisation within the manufacturing schedule. As the rig was not deemed priority, the manufacture would be pushed to the back of the workshop schedule, and the longer this happened, the momentum on the delay increased. The momentum is lost as it is hard to pick-up a piece of manufactured work and reset jigs, and the manufacturers knowledge also has to be refreshed. Small items to finish become a big job to familiarise with again. It was not just the manufacturing group which had difficulties, due to the time frame the author also had difficulty in remembering the design status.

Communication was key, and the problems which can be experienced by separate sites was encountered. Although the manufacturing site was relatively close it would be a 15 minute walk or a short drive, however, when other research is ongoing it can be difficult to break away from this for what may only be 5 minute discussion or inspection.

The author personally learnt to provide realistic timescales, agree these and then manage any delay by expediting the problem personally to whatever level, and if need be negotiate new deadlines.

10.3. TECHNOLOGY TRANSFER

10.3.1. INTRODUCTION

There are two aspects of technology transfer into Cranfield, such as data, tools and knowledge, and the other is transfer out, developments findings, models, reports.

An important aspect of this work is the use of Rolls-Royce tools for easy transfer of the knowledge and learning's of this research back into the company. Figure 46. explains the current knowledge and methods status, along with what the research develops and offers in terms of new techniques.

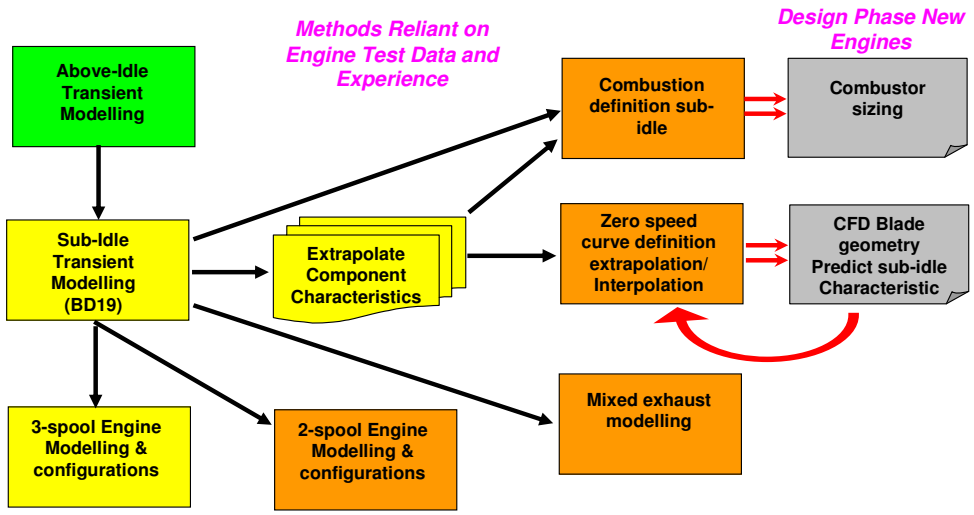

Figure 46. Development phases of research areas (green=current, yellow=further developed in research, orange=new methods, grey=new engine design abilities).

One of the most important results from this research, is creation of a predictive method for generation of engine compressor characteristics.

10.3.2. IN-COMPANY PLACEMENTS

The author completed over three months placement in Bristol and altogether one month in Dahlewitz, working on and collecting data for engines A and B respectively. Further placement was spent at Derby for engine C data collection. These placements were in addition to any visits and meetings at the sponsor's offices.

Placements within the sponsor allowed not just data to be collected by the author, it provided a chance to learn tools and create valuable relationships within the company. One of the most noticeable differences from working within the company, was that questions could be put to and answered by peers around the office.

An important aspect of the different placements, were that the author was free to carry out just his own research and not be placed with other work not relevant to the research area.

10.3.3. HANDLING THE FLOW OF DATA

Transferring data from the sponsor is very much a 'Pipeline flow', where data is requested and an unknown time for the sponsor to assemble and send the data. Other parties may be required or more priority jobs means waiting.

Using Rolls-Royce tools and the Alice Workstation at Cranfield University UTC, provided integrated transfer of research, from the sponsor to the researcher and vice versa. Also prior experience of using these tools, made in-company placements simple as no training was required. The sub-idle model simulations were run on the workstation, along with analysis of engine test data.

Within the first year of the studies the UTC UNIX workstations software required updating to the equivalent update as in Rolls-Royce to Solaris 12. This entailed the

author liaising with Rolls-Royce and department for the sponsors IT department to load up and install new software.

Compiling of BD19 sub-idle simulation model changes, had to be completed within networked workstations at Rolls-Royce, and although a cumbersome approach, this meant that the sponsor always maintained a copy of the code changes.

Discussions with the sponsor debated regarding which design group the sub-idle model would be placed. It was decided the model would be owned by the steady state group, as it is at this stage of the design and information, where it would be more useful, even though the model can run transient simulations for development of start-up control logic and systems.

10.3.4. TECHNICAL REPORTING

To record the changes to the sub-idle model and the creation of engine A model, a large technical report was issued by the author to the sponsor [25]. Within this report the code changes, design parameters used, definition of component characteristics, engine data, and results of model simulations, were described. This report formed part of the technology transfer along with electronic model code and data to run the model. This electronic transfer of data is aided by using the same tools and systems as the sponsor.

10.3.5. CHANGE TO THE DESIGN PROCESS

Recommendations were made to Rolls-Royce, how this research could change and advance the design process, with benefits in cost saving, time saving, and improved data for the sponsor and the airframe manufacturer (customer), as shown by Figure 47.

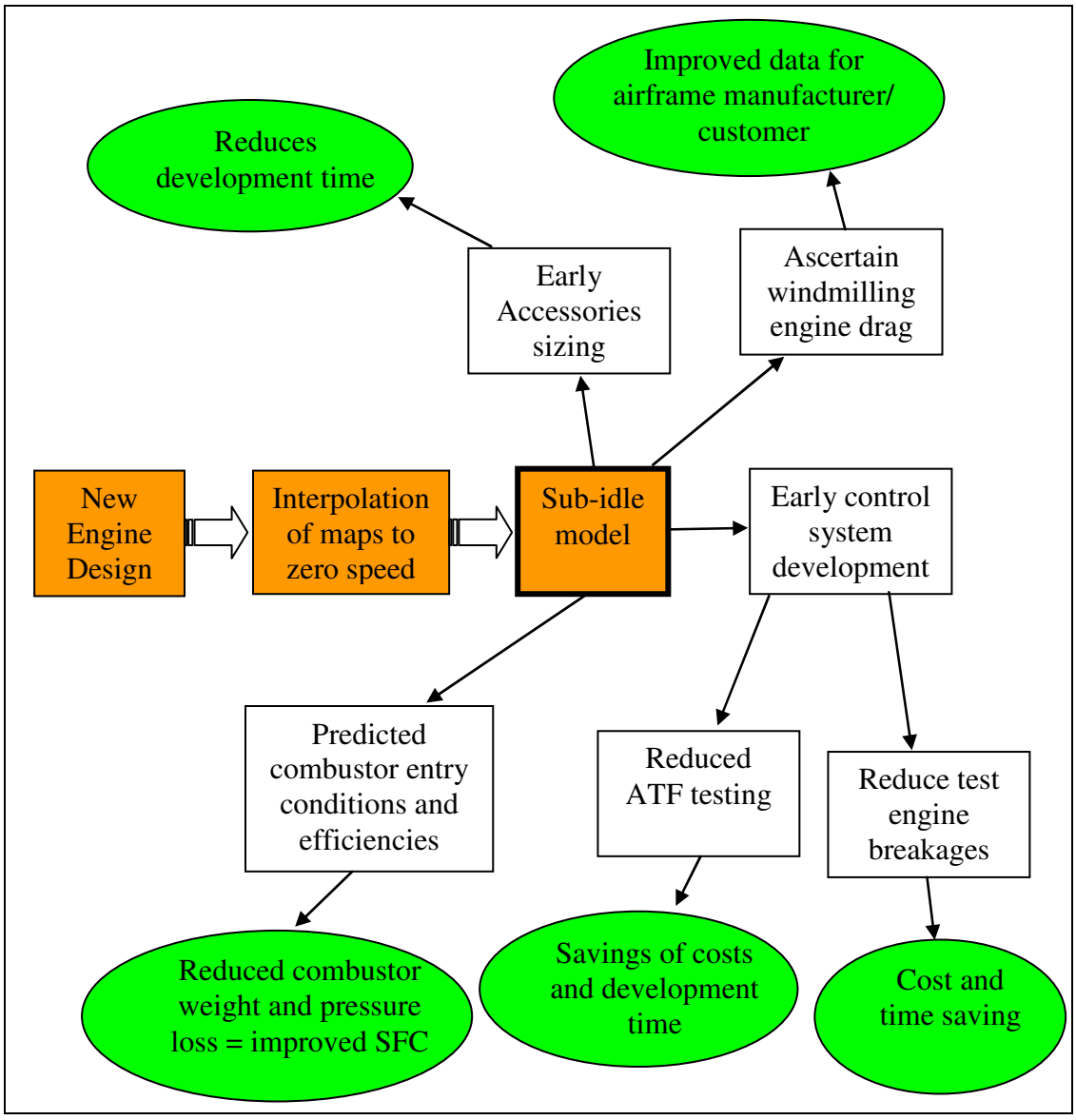

Figure 47. Design process change from introduction of sub-idle modelling and the possible benefits.

11. Results and Discussion

Within the first section of this chapter the sub-idle modelling along with related mixer and combustion studies are presented and discussed. In the later section the results from the locked rotor studies are presented and discussed, with the resulting characteristics produced from the developments made within this area of research.

11.1. ENGINE SUB-IDLE SIMULATION RESULTS

The reader should note that the each sub-idle simulation result number is not chronological.

Engine ATF data is used to compare some of the sub-idle simulation results thus allowing further validation and critique of the results. The ATF data itself however, may contain error due to measurement errors at these sub-idle off-design conditions, therefore caution should be applied in all critique of results. Another problem of the anomalies in ATF test data time steps can add error to percentage difference analyses.

11.1.1. RELIGHT SIMULATION RESULTS OF ASSIMILATION OF ENGINE TEST DATA

Within a one dimensional model one cannot simulate all fluid and thermodynamic effects, for example some relights use only the port side igniters and check the light-up performance, this is not possible with the simple definition of the combustor within the model.

11.1.1.1. Windmilling Steady state

To ascertain a models alignment to steady state windmilling speeds and component operating conditions, simulations for a range of windmilling flight Mach numbers were applied. The results below discuss these results along with other analyses such as sensitivity analysis of power offtake loads and mixer representation effects on windmilling performance. Engine A is typically shown in this results section.

The results for model alignment to engine windmilling and power offtake sensitivity studies are shown below in Figure 48. in which the most sensitive component to power off-take loads, the HPC to which the offtake loads are coupled, is presented. The results form in every case a curve similar to a choking or swallow capacity curve.

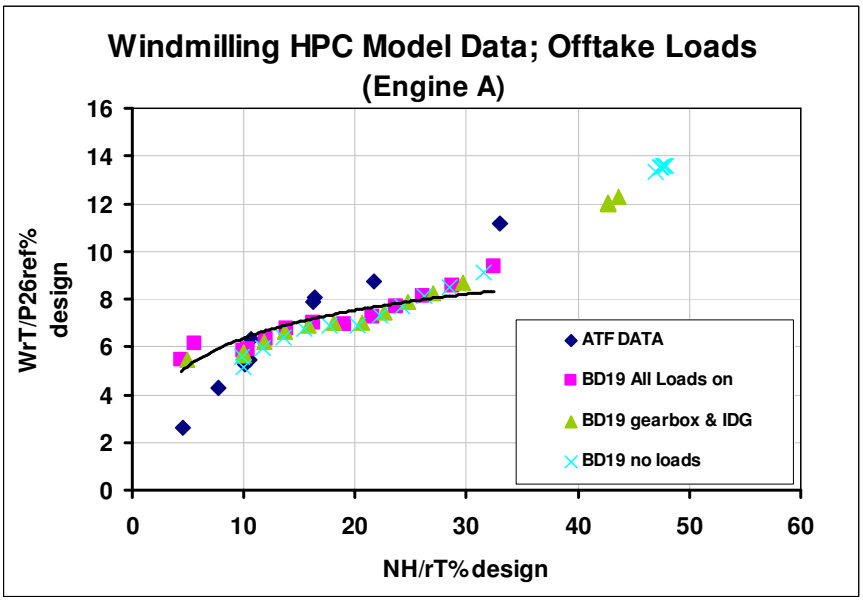

Figure 48. Model alignment to test data and sensitivity study of offtake loads on steady state windmilling performance, Engine A HPC.

When observing the match of the model (with all loads on) against ATF data (through a range of flight Mach numbers where lower speeds are lower flight Mach numbers), it can be seen that the model has a slightly lower WrT/P than the test data down until

around 10%N/rT, then below this a higher Wr/T/P. Some of this error may be due to model matching and some may be the error in the test data. However, below 10%N/rT it is the limitations of the extrapolation technique on the compressor characteristic in this speed range, where no definition of a zero speed curve forces a selection of high WrT/P. Therefore this engines model simulations are limited to N/rT greater than 10%, and for Engine B it was found this was not an issue.

The speed range of the results seems a good match from low to high windmilling speeds for the applied Mach numbers. However, we can see that reduction of offtake loads to just gearbox and IDG (pumps removed), and then no loads, the N/rT increases significantly. Thereby reducing power offtake reduces the drag on the HPC and total power of the HP spool, thus for a given momentum from the air flow the spool speed will increase. Though the WrT/P has no significant change from these power offtake effects at low N/rT, as the N/rT increases the WrT/P increases and follows along the swallowing capacity trend, as higher non-dimensional speed allows increased flow.

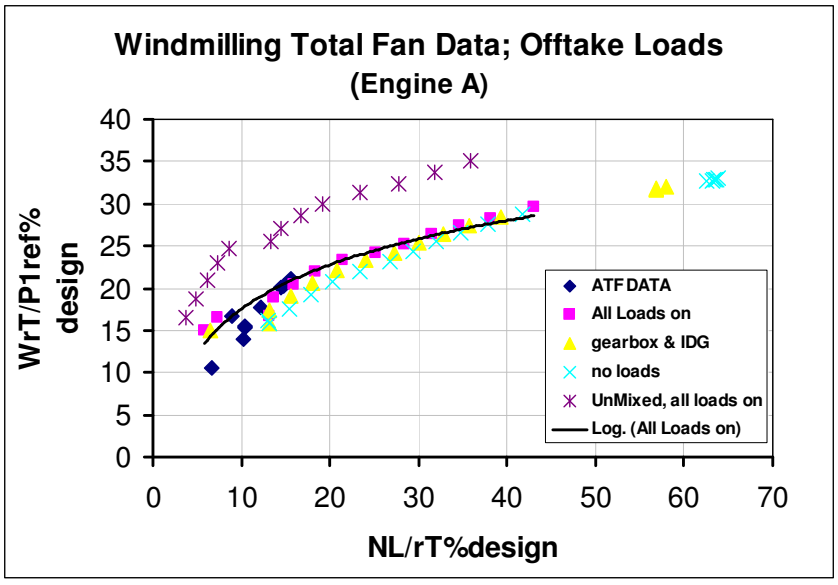

Figure 49. Model alignment to test data and sensitivity study of offtake loads on steady state windmilling performance, Engine A LPC (fan).

The fan on Engine A is of low BPR, compared to higher BPR engines such engine B, its steady state windmilling performance is more affected by the variation of the power offtake, and the core performance. As shown in Figure 49. the fan steady state windmilling results also show a swallowing capacity curve. With the fan it can be seen at low N/rT the power offtake does have a significant influence on the WrT/P. Decreasing the power offtake increases the spool speed, which in the fan is a result of the increased WrT/P in the core, which produces greater work out of the LPT from increased flow momentum, for driving the LPC.

As with the HPC at speeds less than 10%N/rT the WrT/P is higher than the test data, indicating same extrapolation limitation with the compressor characteristics.

Also shown in Figure 49. is the effect of having an unmixed engine, which shall be used for study in chapter 11.2 discussion of results.

The plot of WRTP versus N/rT would seem a good representation to validate the matching of the model and particularly the characteristic for a range of steady state windmilling conditions, however, this representation is not enough. The flow and speed can be easily matched, whereas it is the pressure ratio, thus the losses, which are the harder to match. Therefore at some point in the analysis of results the pressure ratio versus non-dimensional mass flow requires study. However, this representation is useful in studying sensitivity analysis as it presents any change in mass flow and also the change in non-dimensional speed, thus relates to the momentum of the air flow to that of the drag of the engine spools

If the compressor swallowing capacity steady state windmilling trends, as shown by the results in this chapter, could be predicted/ calculated in some way, then this would greatly assist the extrapolation of characteristics in defining the limits of flow and thus a steady state windmilling working line which could align speed curves for a given flow.

11.1.1.2. Windmilling relights transient simulation results

To manage the analysis of the model improvements when considering the large volume of data and simulation cases to be dealt with, a base case was used of windmilling relight case 1360 for Engine A. The case was considered useful as flight conditions were central in the relight envelope see Figure 2. thereby avoiding other complications of edge of relight boundary affecting the sensitivity studies.

Results of working lines for case 1360 windmilling relights transient sub-idle simulations on the HP compressor characteristic, are shown in Figure 50. The engine actual working line obtained from ATF data is also shown for comparison.

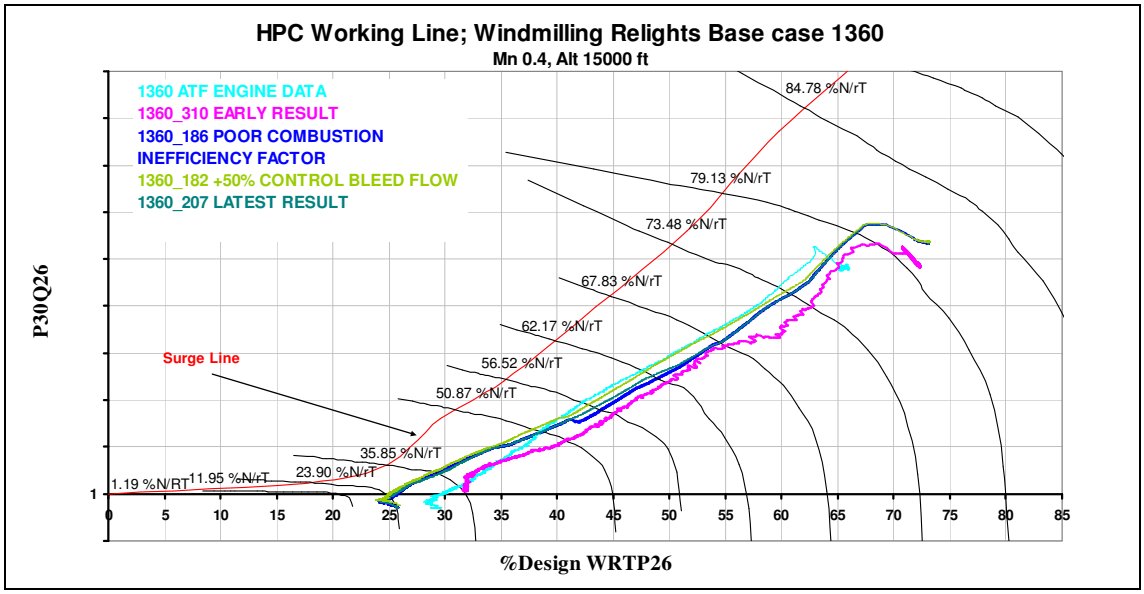

Figure 50. Working lines on HPC characteristic for Windmilling Relight transient sub-idle simulation result (case 1360)

As the engine model matches on pressure and it is important to simulate that the windmilling operation is at pressure ratios (with this engine) are less than one, the characteristics were modified to ensure this from the earlier model results (1360_310) are shown by Figure 50. Throughout the research, the idle speed curves were removed and re-extrapolated characteristics, particularly a lot of time spent on the Psi versus

Isen_Psi characteristic which were the greatest influence on the pressure drop, though non-dimensional flow is a factor due to its strong influence on momentum flow onto the blades in the actual, and in model at windmilling. Also through most of the relight transient the control bleed valve is open thus the HPT sees less flow than the HPC and will affect the shaft power balance. In consequence to these changes the later simulation models produced lower non-dimensional mass flow at windmilling, with good alignment on pressure ratio.

The original characteristics idle-point inaccuracy becomes apparent by observing the model error to ATF data in the idle region, considering that the characteristic extrapolation to lower speeds starts from 68%N/rT. In response the model matches at a higher idle non-dimensional mass flow. Early simulations had the bleed closing, where in fact the bleed was still open on the actual engine, although the valve flow choked. Therefore the later simulations included the bleed open resulting in the difference in pressure ratio between early and the latest result.

The method for running the simulation described in chapter 5, required the author to observe the model HP spool speed match with engine data over time and alter the acceleration rate by modifying the heat input from the combustor, via a combustion inefficiency factor. These speeds are shown in Figure 51. below.

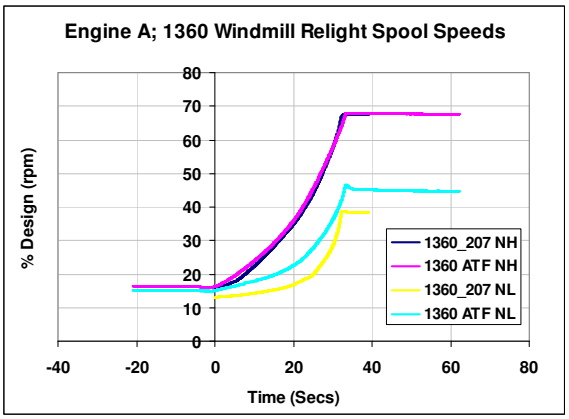

Figure 51. Windmilling relight simulation spool speed matching

The change in speed over change in time is the spool acceleration, thus when looking at the results in Figure 51. the model accelerates slower than required. It was found hard to accelerate the model any quicker, without the model failing on matching due to the large acceleration light up torques. Speed matching was even more difficult to achieve on the LP spool, some of this has to do with the power balance issues of how the LP power balance is calculated and the effect on the operation point in this engine A, as described in chapter 4.3.5.1. Other causes of this are the sensitivity of the mixer characteristic back pressure effect which has a significant effect on not just LP but HP spool speeds.

The working lines with the latest model 1360_207, produced during the acceleration transient an improved match with engine test data. However, study of the non-dimensional mass flow against speed indicates a swing from negative to positive error as shown in Figure 52. for latest case 1360_207.

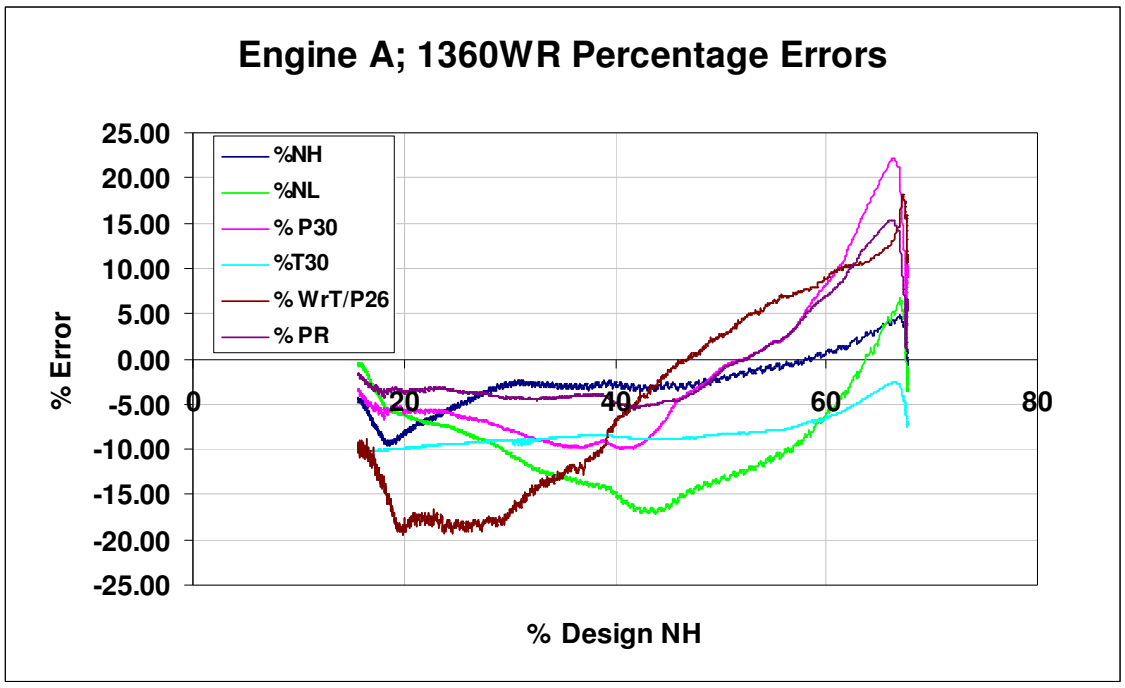

Figure 52. % errors of windmilling relight transient simulation, case 1360_207.

In the latest model errors at this windmilling speed of 22% NH, are very reasonable at less than -5%, it is only the non-dimensional mass flow which has an unreasonable error at -10%. Though the non-dimensional error is more to do with the limitation of extrapolation technique where the pressure ratio and N/rT could not be achieved without some sacrifice to the non-dimensional mass flow.

The errors shown in Figure 52. for the latest model may seem large, however, considering that operating conditions where a very small percentage change in pressure, say from an error on the extrapolated characteristics and the escalating effect of this on the other components downstream, the results are in fact very reasonable. The results could have been improved particularly the error in non-dimensional mass flow at windmilling if not limited by the extrapolation limitations. Which led to the improved methods for extrapolation, developed in chapter 9 and results of which shown in chapter 11.4.5.

The error comparisons are based on individual time steps data, in consequence instrument measurement lag (for example temperature thermocouple) for a given time step will be delayed, whereas modelling data will be instantaneous. Therefore error calculations should be treated with some reservation and may actually be better than presented. As speed is directly measured its accuracy would be expected to be accurate in the results. Model heat soakage representation limitation may also be a factor of error in the modelling transient results.

The results indicate how even though steady state windmilling conditions can be suitably matched for a range of flight conditions and operational light-up requirements, representation of the transient behaviour, as well as comparison with test data, is much more difficult to achieve.

11.1.1.3. Comparison of relight types

The trajectories of different relight engine operational relight conditions can be very complex and work in entirely different areas of the component maps. These results present and discuss the working lines on an HPC and HPT characteristic from all three relight operational conditions.

In Figure 53. the sub-idle model results are shown along with ATF engine test data for comparison. The windmilling relight is discussed in the preceding chapter, therefore lets consider the quick windmill relight, showing the deceleration through to light-up almost along a constant speed curve and accelerates to idle. The model working line generally lines up with the test data, however the deceleration error is likely due to an error in the map extrapolation, and acceleration error is more related to inaccurate fuel scheduling within the model.

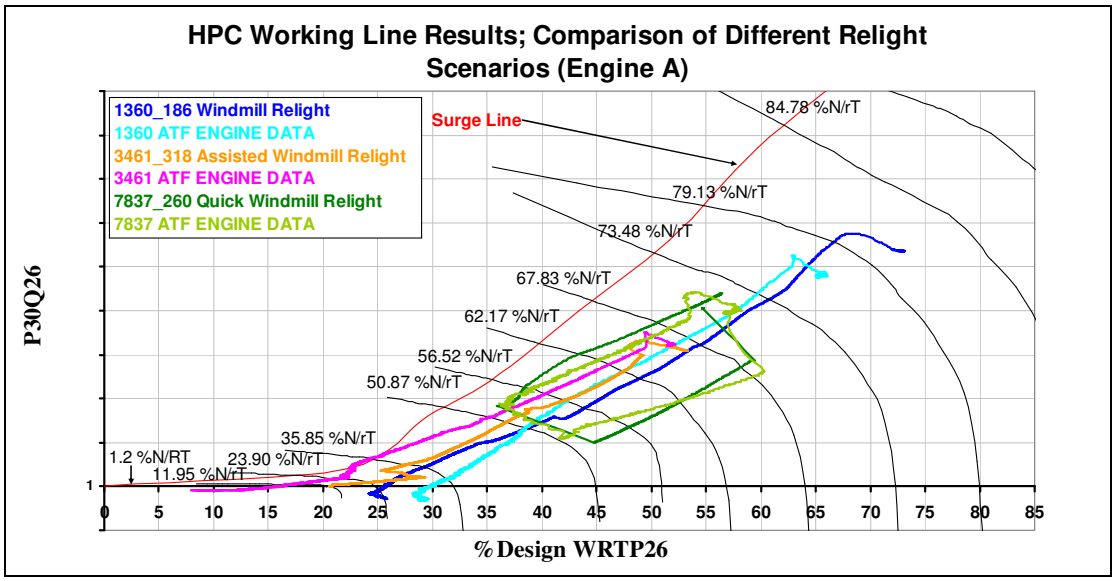

Figure 53. Comparison of HPC working lines for a range of relight conditions, Engine A.

In considering the assisted the most obvious difference between the model and the ATF data is at the windmilling start. The model cannot operate down to the low non-

dimensional mass flow due to the limitations in the extrapolation of the characteristic in this low speed region. Instead the model starts on the PR=1 lowest speed curve which has no variation in PR, thus the model moves closer to the next speed curve of 12%N/rT to try and achieve some pressure ratio drop, creating even a larger error in WrT/P. These results were the greatest impetus on creating a zero speed curve and improving the compressor characteristic in this region.

Assisted ground start simulation does match well, however, at its idle point indicating some regions of the characteristic match well, while other areas are very erroroneous.

The resulting trajectories of the simulations discussed above on the HPT characteristic are shown in Figure 54. below. Steady state simulated windmill points are also shown to highlight the initial range of windmilling starting points, as the transient curves shown are for an instant at when the engine lights, thus some temperature effects increase parameter values increasing the position of the working line.

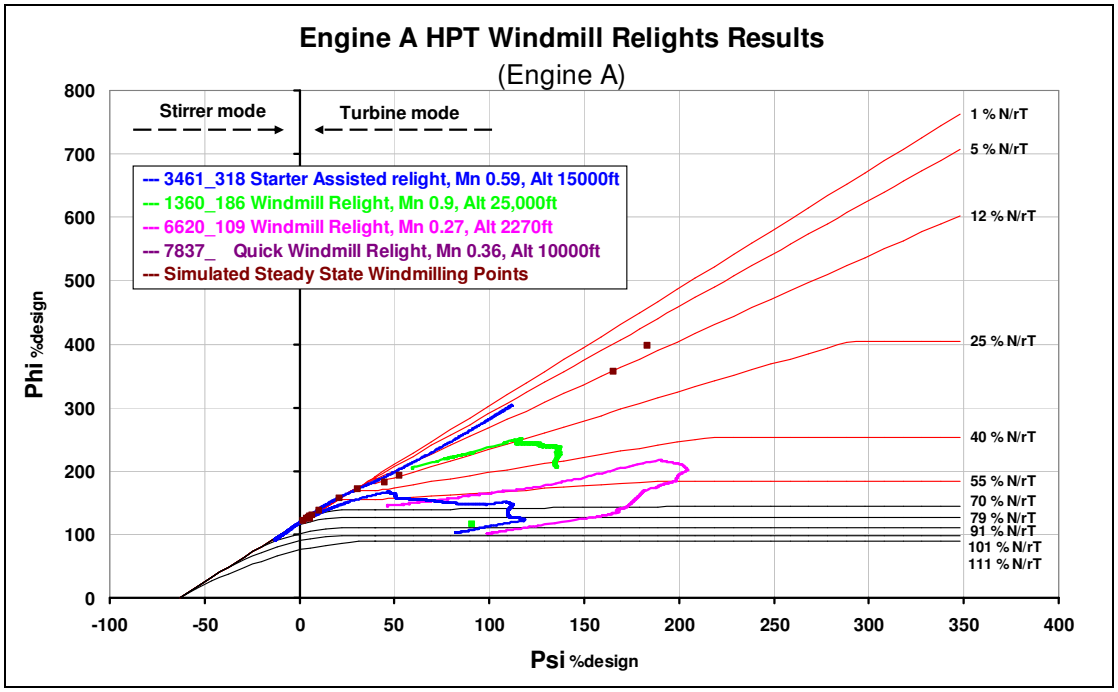

Figure 54. Working lines on Turbine characteristic for a range of relight conditions.

The steady state windmill operating points are typically on or near to the incompressible limit speed curve. Upon light-up the T41 at entry to the turbine increases rapidly thus significantly affecting the temperature terms in N/rT, WT/NP and DelH/N^2, with little change in the other terms of these parameters. The result is a large initial movement to higher values of Psi and Phi and then decrease as idle is approached. The assisted windmill relight is much different, as the initial starting phase is the dry-crank from the starter motor, which drives the HPT working line into the stirrer mode, until light-up increases T41 and PSi and Phi values increase, as the turbine begins to provide work input to the spool.

These characteristic also help to highlight that the turbine has little influence on the resulting windmilling speed as the speed lines converge trajectories long a constant speed curve. In fact these are converging to one line of the incompressible limit line. It is the compressor non-dimensional mass flow, thus the momentum and resistance through the compressors which is the greatest influence in determining the windmilling speed.

11.1.1.4. Heat soakage simulation results

Within the sub-idle model lumped sum heat soakage values are calculated. For an example of the magnitude of the temperature difference in the core engine components the results for two extreme cases area shown in Figure 55.

The smaller engine A during a windmill relight the most significant degree of heat soakage takes place within the combustor which initially extracts heat energy from the combustion into the surrounding liner walls. For the large two spool engine modelled, engine B, results from a quick windmill relight show the large heat input from the component materials to the flow, particularly within the Combustor and HPT. Upon

relight the heat soakage reverses to an even higher magnitude of heat energy absorption within the combustor. The HPC lags the HPT and combustor soakage and remains in adding heat energy to the flow through much of the light-up phase, which can seriously effect surge limits as discussed by author in previous research Howard [24].

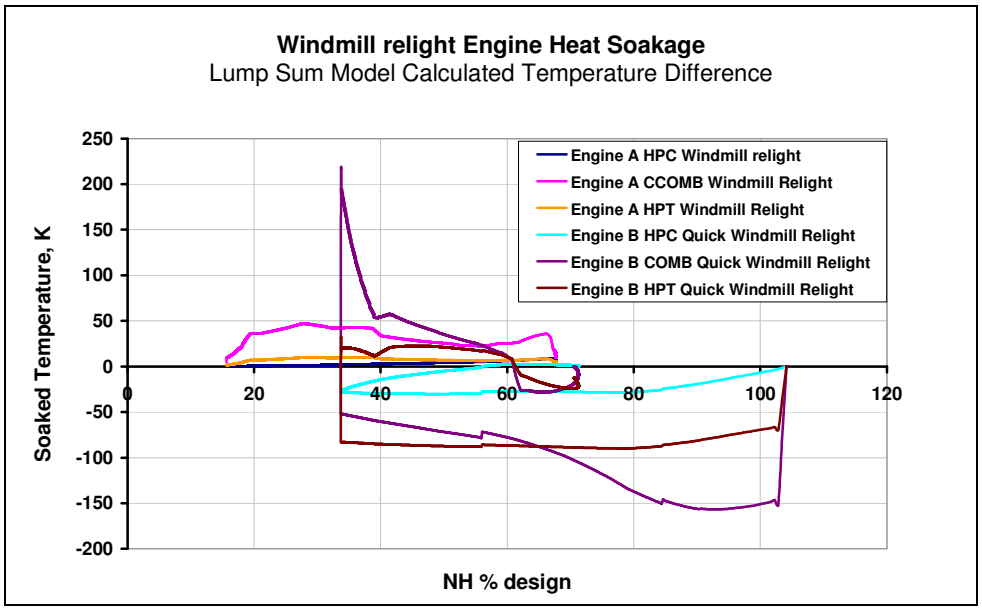

Figure 55. Model calculated heat soakage temperatures for two extreme windmilling cases and engine size.

The simple heat soakage calculations will produce some errors within the results, as with compressors a much more stage by stage heat soakage analysis is required to model its performance during large transients and heat soakage effects.

11.1.1.5. Pullaway

From the modelling results the resulting net thrust can be extracted, as presented in Figure 56. For a range of windmilling relight conditions the net thrust can be seen to be affected by both the Altitude and Flight Mach number, with high flight Mach number and low altitude producing the largest drag at windmilling (simulation of this case could not achieve a full acceleration to idle).

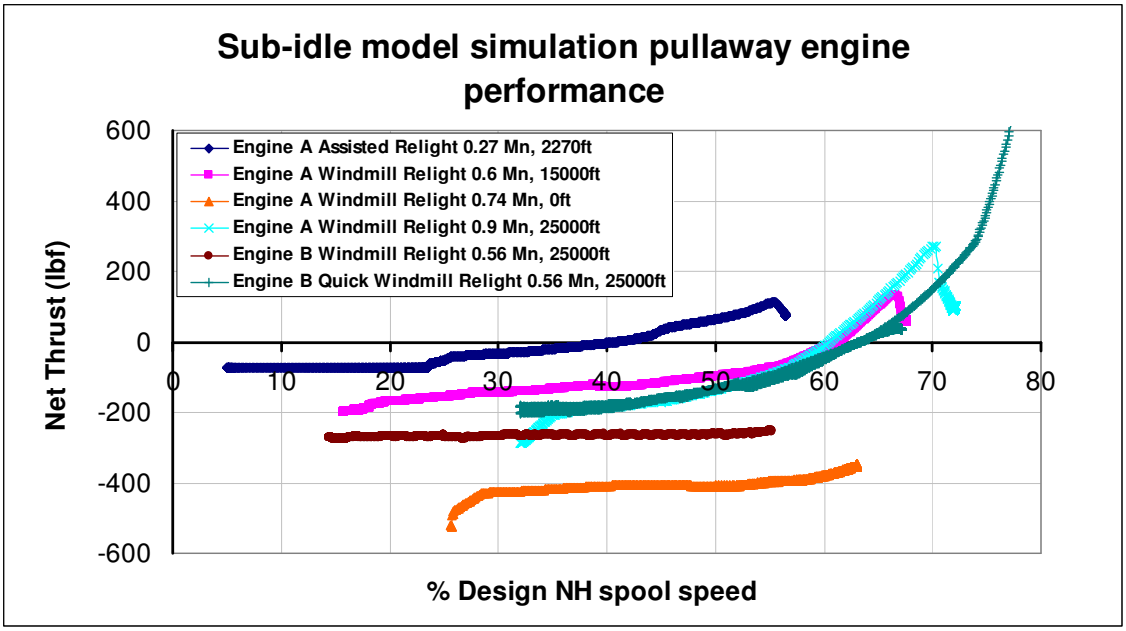

Figure 56. Relight pull-away net thrusts resulting from sub-idle simulations.

In the initial light-up phase the net thrust to spool speed gradient is very small and only past idle does the net thrust increase more rapidly.

Depending upon flight conditions the engines simulated will only produce a positive net thrust, thus accelerating the aircraft, after spool speeds of 40% and greater are achieved. Surprisingly the lower flight Mach number case of assisted windmill starts can achieve a positive net thrust at earlier spool speeds than other relight cases.

11.1.2. SIMULATIONS OF SUB-IDLE ENGINE SENSITIVITIES

11.1.2.1. Effect of Compressor map low speed extrapolation

As the extrapolation technique for compressors struggled to achieve low speed non-dimensional flow a sensitivity analysis was performed on modifying the 12%N/rT speed curve non-dimensional surge line flow by 5%. The result of this study found that although steady state windmilling speeds were affected, the acceleration trajectory region was also affected and decreased acceleration rates.

11.1.2.2. Turbine incompressible limit line

Turbine characteristics based on calculated and an approximated (from windmilling data) incompressible limit line were compared within the model simulations. The data derived curve has a less steep gradient. The calculated incompressible curve provided the best windmilling match for all conditions, however, the data based curve assisted engine acceleration rate with reduced fuel flow.

11.1.2.3. Control bleed valve

Steady state light-up the control bleed valve flow is very influential. As the core flow is small the control bleed valve flow influences the steady state windmilling operating point. For light-up reduced mass flow lowers the velocity and prevents flame blow-out limits and stability limits being reached. It was found that the Steady state speed from +/-50 bleed could change windmilling steady state speed by 5%.

Influence of control bleed flow on relight transient performance is like any other transient performance situation. An increase in control bleed flow by -50% on windmilling relight transient performance are shown by the working lines in Figure 50. as a result the working line is higher closer to surge line. Increased bleed valve flow actually caused the model to not converge. If the bleed valve is closed during acceleration the working line again becomes higher and closer to surge.

11.2. MIXER STUDIES

The results of the mixer analysis are shown and discussed within this chapter, in which the sub-idle model was used to study the influence of Static Mixer Pressure Ratio (SMPR). Separate theoretical calculations were performed to understand the mixing equations and turbulent mixing influence. At the end of this chapter CFD studies of Engine A mixing process are studied.

11.2.1. SUB-IDLE MODEL SIMULATION MIXER ANALSYSIS

The results from the mixer analysis using the sub-idle model are shown in Figure 57. Alignment of ATF engine data and model SMPR's is good, indicating the model is suitably selecting the correct SMPR from the mixer characteristic. Also shown are results where the SMPR is set to one, to simulate the typical suggestions that the Static pressures should balance at the mixing. The aim of this result was to indicate the mixing process is much more complicated, where separate streams do not fully mix due to the velocity ratio between the streams as discussed in chapter 7.2.2. As the results show an SMPR=1 slightly reduces the compressor NH/rT and the same is true for NL/rT.

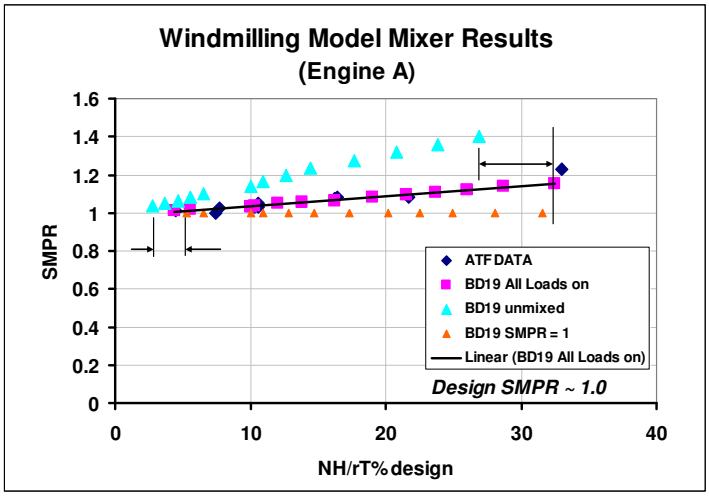

Figure 57. Sub-idle model mixer investigations, effect of SMPR and resulting core non-dimensional speed.

With SMPR=1 there is also little effect on WrT/P only the decrease from that of the speed moving the capacity trend, therefore with high non-dimensional speed there is high non-dimensional flow error through the HPC (engine core).

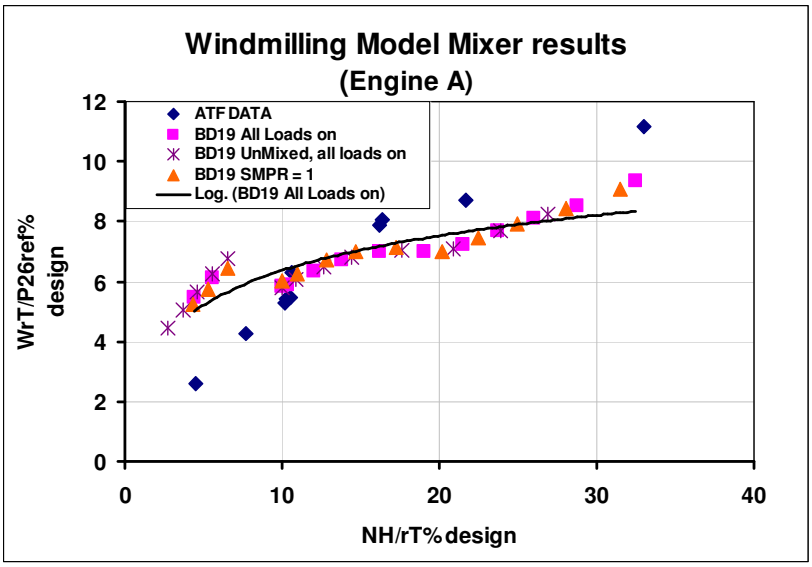

Figure 58. Sub-idle model mixer investigations of effects on core flow capacity.

Unmixed configuration creates a very drastic change to the engine performance in terms of both ~6% reduced LP and HP speeds. Therefore it would seem that when mixed, it is the bypass which is pumping the core flow thus increasing spool speeds in engine A. In engine B the opposite was found as the core mixer area is much smaller than the bypass and velocity is comparatively high thus the core pumps a small region of bypass duct flow. Also as a result of the higher bypass pressures a back pressure is created on the core from this mixed bypass flow and in tern reducing engine B spool speeds.

For unmixed condition, although core WrT/P is only changed along the flow capacity curve, from Figure 49. it can be seen that the fan flow capacity curve increases by ~5% design WrT/P. This is due to the back pressure on the fan is free to ambient and the change in nozzle area. As a result the unmixed configuration has a higher bypass ratio.

Using the SMPR characteristics compiled from ATF test data, it was found that the core total pressure at entry to mixer matched well > 10%N/rT. Bypass total pressure at inlet varied widely, though this is not all accountable to the mixer, part of this is apportioned to the LPC characteristic accuracy and the power matching of the total fan work as discussed in 4.3.5.1.

11.2.2. THEORECTICAL MIXING CALCULATIONS

To understand the mixing calculations applied within the mixing bricks used within the sub-idle model, the following analysis was performed with results shown in Figure 59.

ATF windmilling data was used as the inlet conditions to each mixing stream, also the static pressure at entry to the bypass duct was recalculated by iterating upon conditions upstream of fan exit conditions. A further calculation also included shear mixing effects into the momentum equation. Also another calculation set the static pressure ratio to one, with the core using the test data value and all other parameters remaining the same.

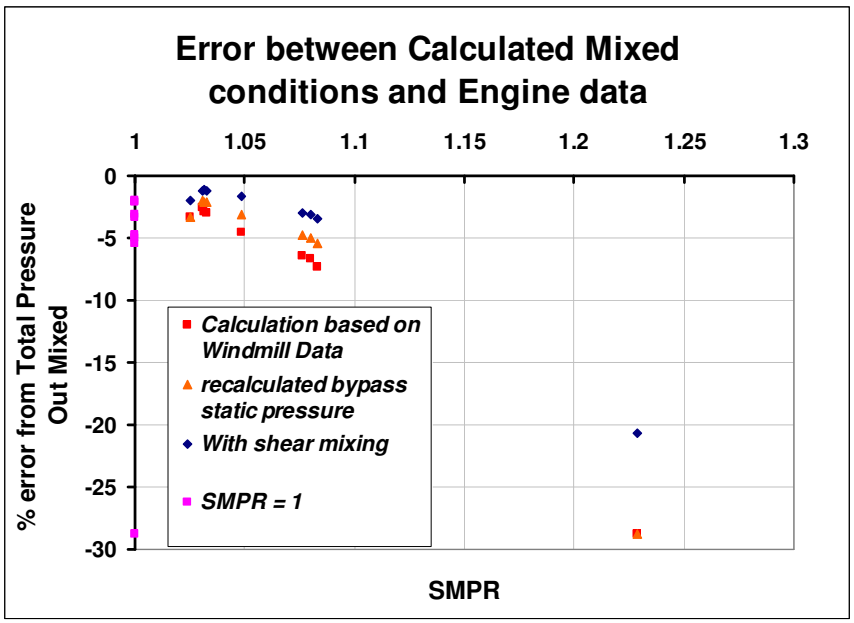

Figure 59. Theoretical Mixing calculations influence on mixed outlet total pressure.

These results show that the error of the outlet total mixed pressure calculated can be reduced by more accurate accounting of static pressures and inclusion of the shear mixing formula. However, as SMPR and by virtue flight Mach number increase the error becomes much greater and the mixing equation cannot account for the full mixing effects taking place.

The result of this error must be that the models matching process, to achieve exit mixed nozzle total Pressure matching ambient, recalculates mixer entry conditions and thus changes core and bypass operating conditions or in other words the model results are forced to deviate from those within the actual engine to achieve correct outlet total pressure. This inability to fully calculate the mixing process causes another possible error in the model results.

At windmilling the mixer significantly influences the spool speeds, and within the model these depend upon the accuracy of the mixer SMPR characteristic. Therefore this makes the modelling assessment and adaptive process of constructing the maps much more difficult. With a mixer the model engine matching core and bypass is much more coupled than an unmixed engine.

11.2.3. MIXER CFD INVESTIGATIONS ENGINE A

The following work was performed by Julien Rasse, an MSc Student at Cranfield University, supervised by Professor Pilidis and the author of this thesis.

CFD modelling was performed to investigate mixing of bypass and core streams at windmilling conditions of high bypass ratio, significant static mixer pressure ratio and the low practically ambient pressure exhaust conditions. 2D and 3D models results were achieved in this research, in which the latter included swirl effects. To improve the understanding of the static pressure difference between the two streams, with

windmilling conditions applied from ATF engine data, the results show that the static pressures do balance in the mixing zone., as shown in Figure 60. However, the difference in static pressures is maintained upstream of the mixing plane.

If we think of the bypass duct area changes little from the fan to the mixer duct, however, the core has significant area changes particularly at the LPT exit to the mixer, resulting in lower core static pressures than the bypass duct. One would then expect the bypass to imply a back pressure on the core, however, examining the momentum balance equation fully the mass and velocity are equally important. As shown in Figure 61. the bypass duct has a large flow energy, which seems to act as an ejector pump on the core flow.

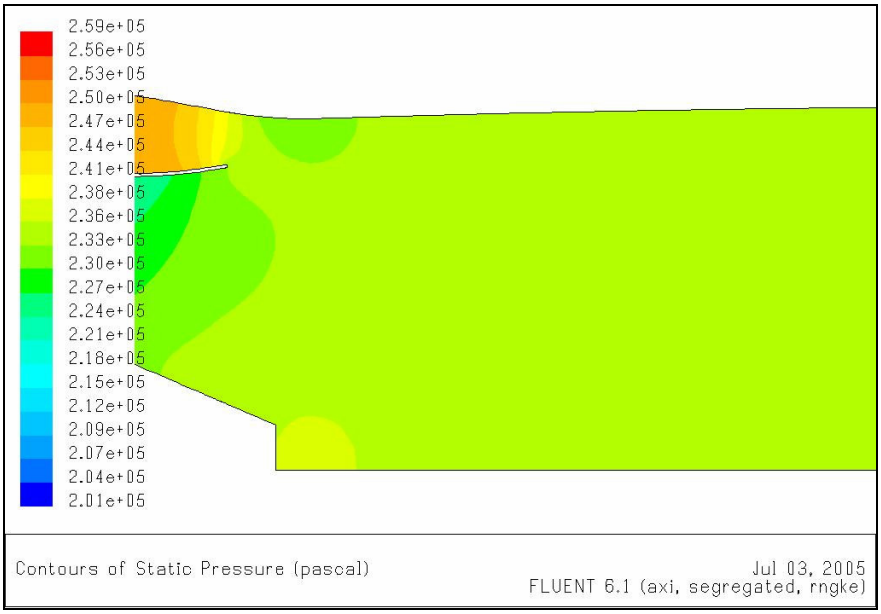

Figure 60. CFD analysis of engine A mixer, static pressures at mixer entry [49].

A large recirculating mixing region was shown by the results to be taking place in the jet pipe. At the end of the jet pipe at the nozzle the total pressures were almost equal, indicating a fully mixed stream. The jet pipe confines the flow and forces the two

streams to mix, although the bypass flow is initially in its own segregated region, with only what appeared to be a shear layer mixing taking place nearer the mixing plane. The jet pipe basically inadvertently provides a mixing length thus benefiting the mixing of the two streams.

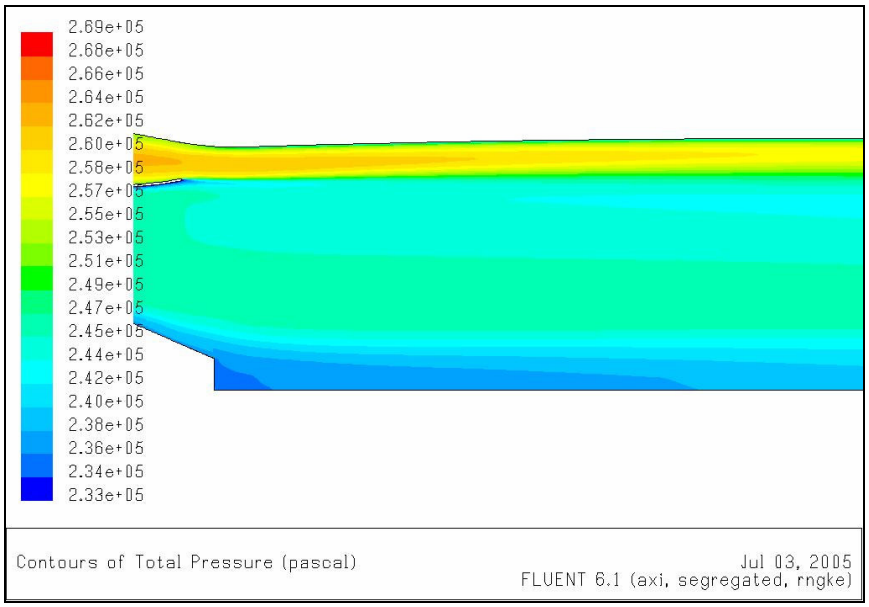

Figure 61. CFD analysis of engine A mixer for high flight mach number windmilling case, total pressures in mixing zone [49].

The 3D model with swirl applied to the results, increased mixing, and created a much more dramatic recirculation zone within the jet pipe. The results overall showed that the mixing depends heavily on the mixing length of the jet pipe, and that the mixing effectiveness depends upon the flight case, where higher Flight Mach numbers produced larger velocity ratios and reduction in mixing.

11.3. COMBUSTION LIGHT-UP EFFICIENCIES RESULTS

Within this chapter the results of investigations of the first ever combustion efficiencies (backed-out) from a sub-idle model, the change of liner pressure loss, and the evaluation of whether evaporation becomes a limiting factor on combustion efficiency at light-up.

11.3.1. SUB-IDLE MODEL DERIVED COMBUSTION EFFICIENCIES

Taking results from sub-idle simulation and comparing the effect of windmilling conditions and engine starting conditions, Figure 62. was produced.

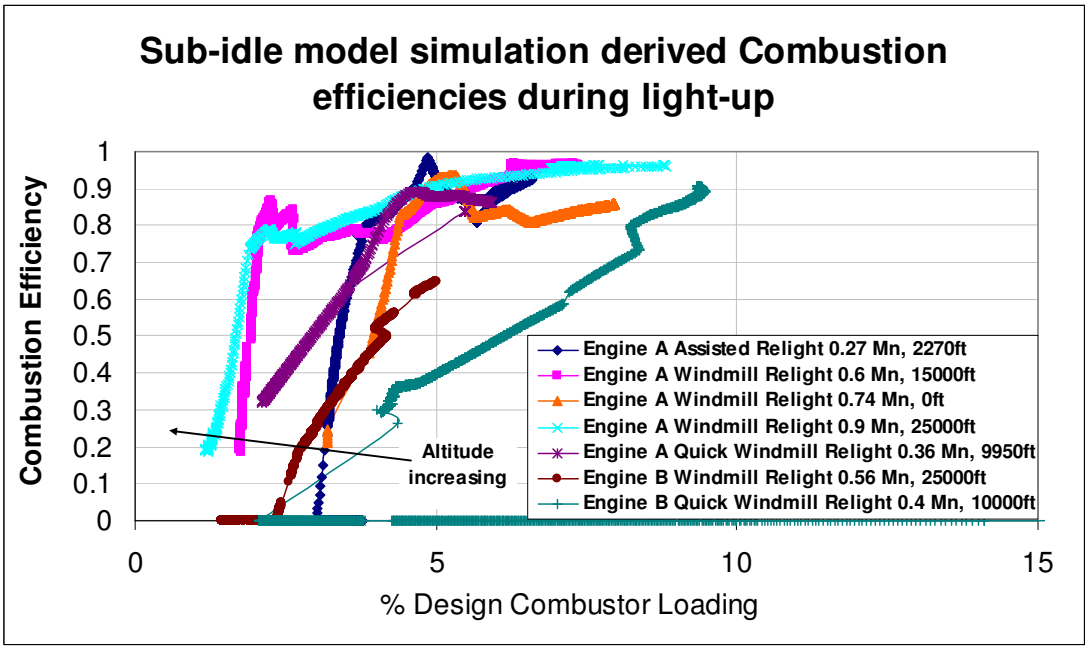

Figure 62. Sub-idle model backed-out combustion efficiencies for a range of light-up conditions, Engine A and B.

All combustion efficiencies for windmill and starter assisted windmill relights tend to be around 20%, with engine B a slightly lower value of 15%. Quick (immediate) windmill relights tend to have a light-up efficiency slightly higher at 30%, likely due to the heat soakage effects of the remaining heat in the combustor prior to light-up assists more fuel to burn upon light-up.

The trends of relight efficiencies would all seem to lay within a region as described by Lefebvre [37], for designing combustors using the loading versus efficiency chart.

In Figure 63. the trends for a windmill relight are described, and in discussions with the Rolls-Royce combustion department agreed that the results seem very indicative. The bump after the acceleration up the constant speed curve, signifies the break away acceleration up the transient working line towards idle. Also this figure highlights the smoothing of combustion inefficiency factor, where the dip at around 3% loading was removed by smoothing the gradient of the inefficiency factor with an improvement to the acceleration alignment with test data.

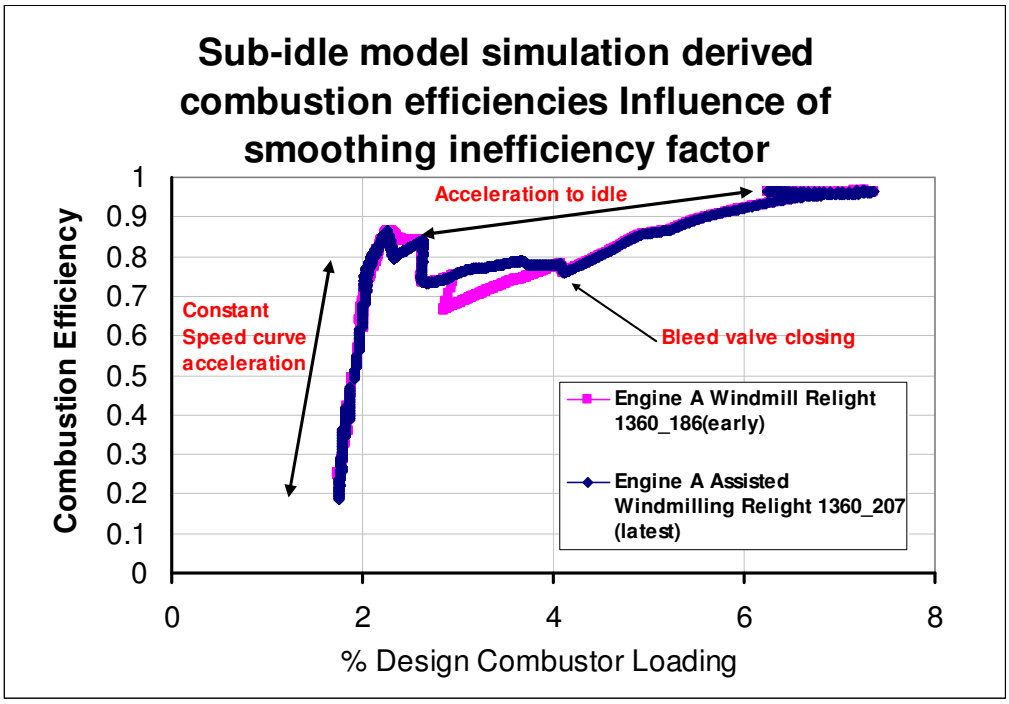

Figure 63. Influence of combustion inefficiency factor smoothing on sub-idle model backed-out combustion efficiency, with negligible effect on engine acceleration.

Attempts were made to use a single combustion inefficiency factor schedule versus HP spool speed for all windmill relights. However, it was found this not to be possible, with each windmilling case simulation requiring an individual schedule. This would tend to indicate either the combustion characteristic (particularly the extrapolation) is poorly defined, or there are other effects within light-up and pullaway within the combustor that cannot be captured by the current definitions, or modelling errors of other components have an adverse effect on the combustion conditions. The following two chapters present what may be contributing factors to limitations of the combustion definitions.

Another limitation of the combustion definitions and the characteristics, is that transient combustion behaviour is not modelled, which would have a very influential effect at light-up and pull-away.

The results of this work provide useful information indicating the light-up efficiencies are typically around 20% and quick windmill relights have a higher efficiency of around 35% due to heat soakage within the combustor. This data and trajectories will be useful for comparison with combustion light-up efficiency rig tests taking place within the sponsoring company.

11.3.2. COMBUSTOR LINER PRESSURE LOSS AND INFLUENCE ON EFFICIENCY EQUATION

Here the research was to ascertain whether the combustor liner pressure loss variation is significant over the operating range of an engine into the sub-idle windmilling region, as this is neglected from efficiency equation.

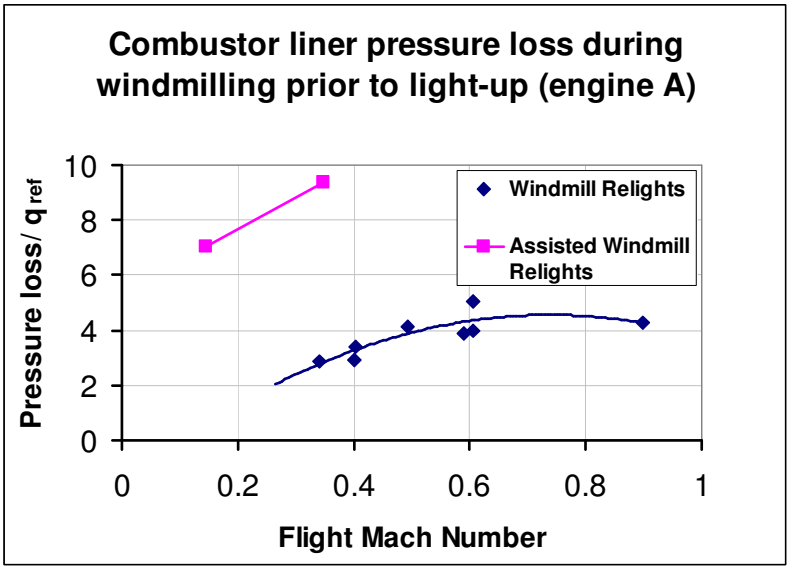

Figure 64. Approximate calculation of combustor liner pressure loss variation at windmilling conditions.

The design value for the liner pressure loss was unknown to the author of this thesis, however, Lefebvre suggests a design value of around 20 for annular combustors and assuming value in comparison there is a large variation in liner pressure loss from design to windmilling. As can be seen from Figure 64. there is also an apparent significant variation even for a range of windmilling conditions.

Although these calculations are approximate using engine ATF data, the findings would indicate that the liner pressure loss does not remain a constant value into relight region, therefore the loss probably should be included within the combustion loading equation.

11.3.3. EVAPORATION INFLUENCE ON COMBUSTION EFFICIENCY

The following work was performed by Matthew Narkiewicz, a MSc Student at Cranfield University, supervised by Dr Pachidis and the author of this thesis.

This research found that combustion efficiency, limited by the reaction rate, is not fully defined at high altitude conditions where the combustor inlet pressure is low and atomisation of the fuel is poor. In fact the results indicate that combustion evaporation (rate of the fuel evaporation) is the limiting condition in combustion. Past research by Lefebvre [37] in where gaseous fuel was added to improve ignition limits indicating the main obstacle is the lack of evaporated fuel.

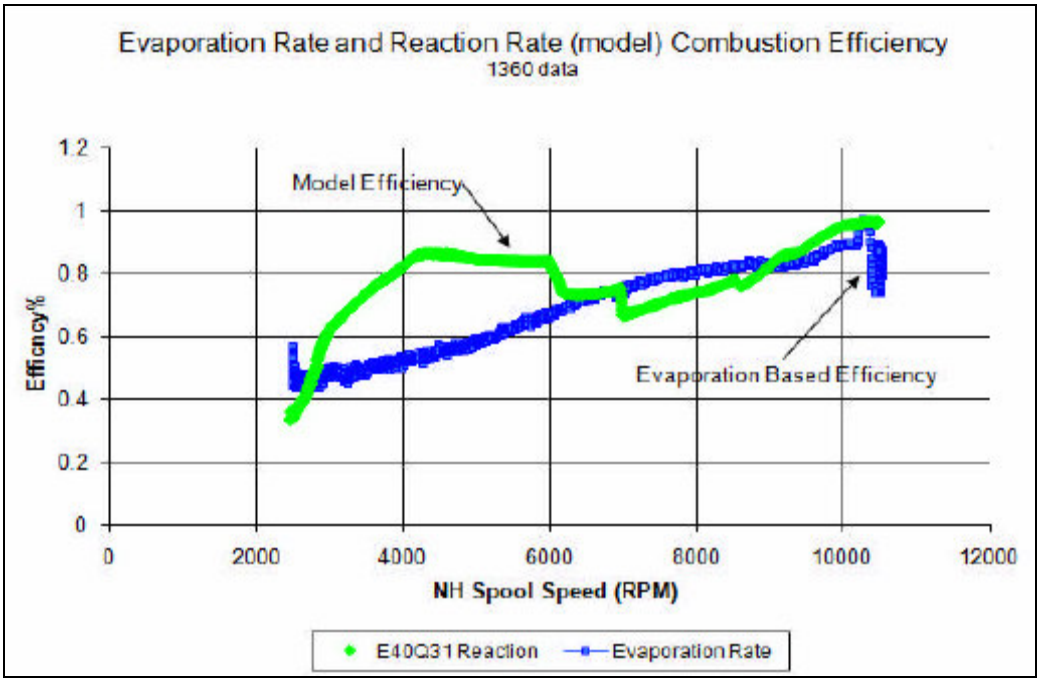

Figure 65. Evaporation based efficiency model versus model reaction rate derived combustion efficiency [43].

The results indicated light-up efficiency was dominated by evaporation based efficiency (as shown by Figure 65.), and dominated even more of the light-up trajectory with higher altitudes and flight Mach numbers.

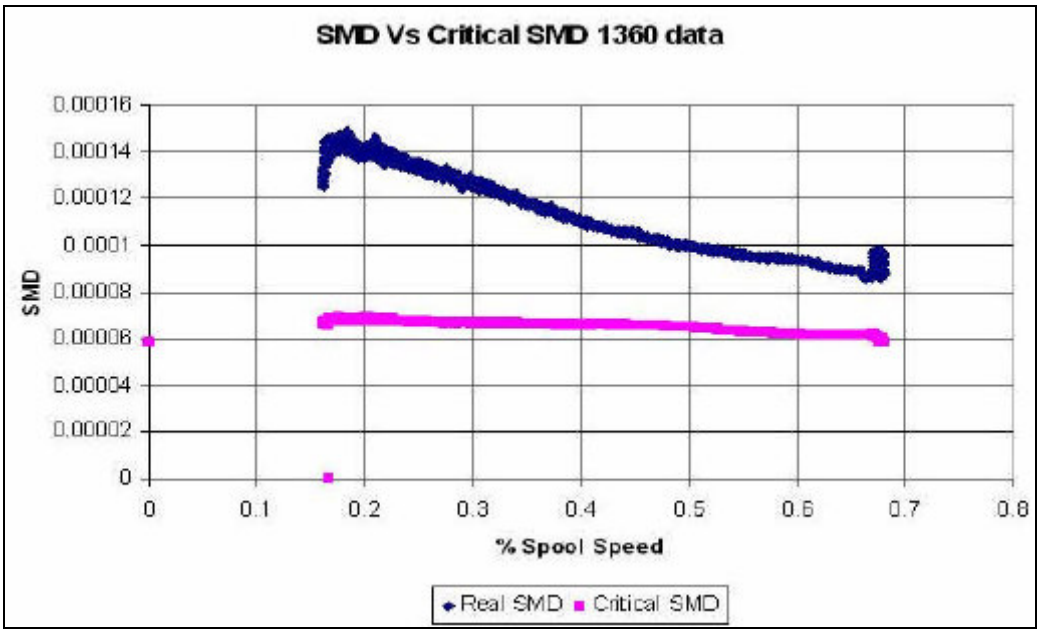

Figure 66. Comparison of Critical and Actual combustion SMD [43]

Another indication of the evaporation rate limiting combustion was the study of the SMD versus the critical SMD. [43] found that if the SMD value is above the critical value (as in Figure 66.) then evaporation rate can be limiting to combustion. Most of engine A cases indicated SMD values around or above the critical SMD value.

Therefore the research suggests combustion evaporation and reaction rate calculated efficiencies are multiplied to obtain the overall combustion efficiency and typically at light-up, particularly at high altitude cases, evaporation based efficiency is dominant. The sub-idle model would benefit from application of this calculation.

11.4. LOCKED ROTOR STUDIES RESULTS

Presented within this chapter are the results for the Locked rotor analysis and prediction of the locked rotor characteristic approached using techniques with CFD, theoretical and a combination of both methods.

The theoretical results chapter combines the first approximation method and then the theoretical method utilising the loss coefficients developed from the CFD studies.

11.4.1. CFD STUDIES

11.4.1.1. Evaluation of 3D CFD Capabilities and Results.

Initial CFD results for Engine D analysis, were performed to understand the process of creating simulations for windmilling and locked rotor conditions, the difficulties in representing the particular conditions. Form these results it was also important to understand the capabilities of CFD and the important phrase that CFD results can only be used to any certainty as 'qualitative rather than quantitative' information.

The following work was performed by Joseph Bittan, a Degree Student on Project placement at Cranfield University, supervised by Professor Pilidis and the author of this thesis.

Bittan investigated the HP compressor of engine A at windmilling and locked conditions using the locked rotor engine data for some comparisons. The 3D CFD package used was TascFlow, a commercial CFD package with turbomachinery simulation capabilities. The package provided the ability to create annular 3D compressor geometry either single blade, stage or combination of stages and could simulate the rotation of the rotor blades.

Parameters of torque and pressure loss (or pressure ratio) allowed definition of the zero speed curve against either blade entry Mach number or preferably non-dimensional mass-flow.

It is unknown at locked rotor conditions within a stage what the rotor position is relative to the stator, thus Bittan performed an analysis of varying this position. The red line (Torque 2) in Figure 67. shows the position of rotor trailing edge aligned to stator leading edge, and the other blue curve for an offset position.

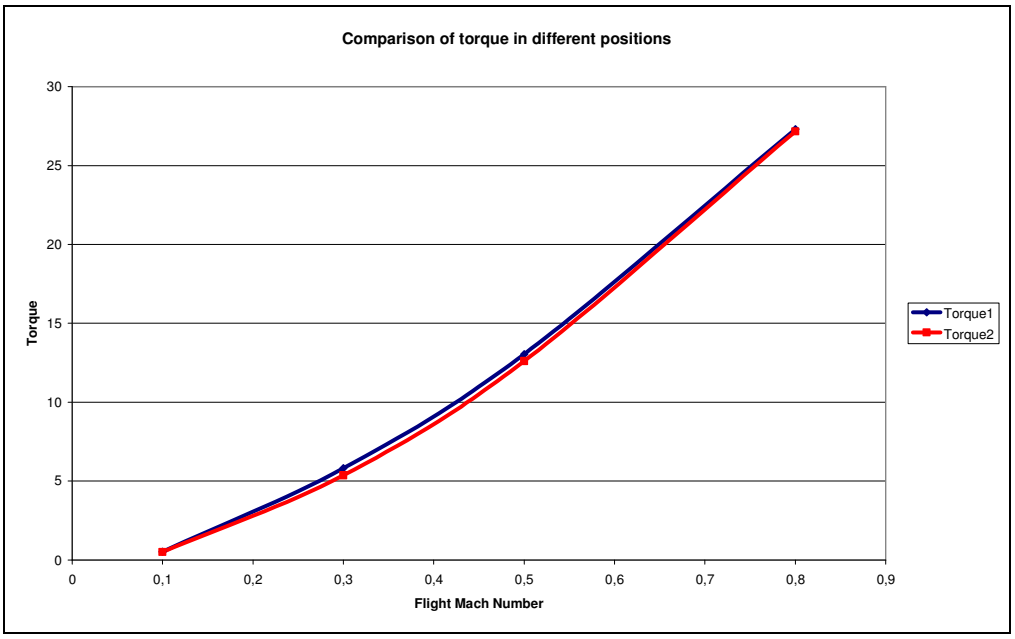

Figure 67. CFD Results Engine D, Locked rotor stage analysis of rotor trailing edge relative to stator leading edge positions [3].

As can be seen from Figure 67. the variation in torque is negligible at the locked rotor condition, however, Bittan found and intuitive result that at for pressure ratio the offset position created the largest pressure drop. Studies for the windmilling condition are not required as the relative position of the blade to the stator is not required as this is constantly changing from the spool rotation.

Bittan created results at locked rotor, 5% and 10% spool speeds at representative windmilling conditions obtained from engine test data. Furthermore results for compressor stages 1, 2 and the stage 7 were combined to investigate the effect of stacking the CFD stage results (shown in figure 68 below), with an aim to align and predict the total compressor performance. The last stage 7, was considered to be important, as it is this stage where the Mach number would be expected to be highest. Therefore the losses likely to be greatest, as was shown by Bittan's results.

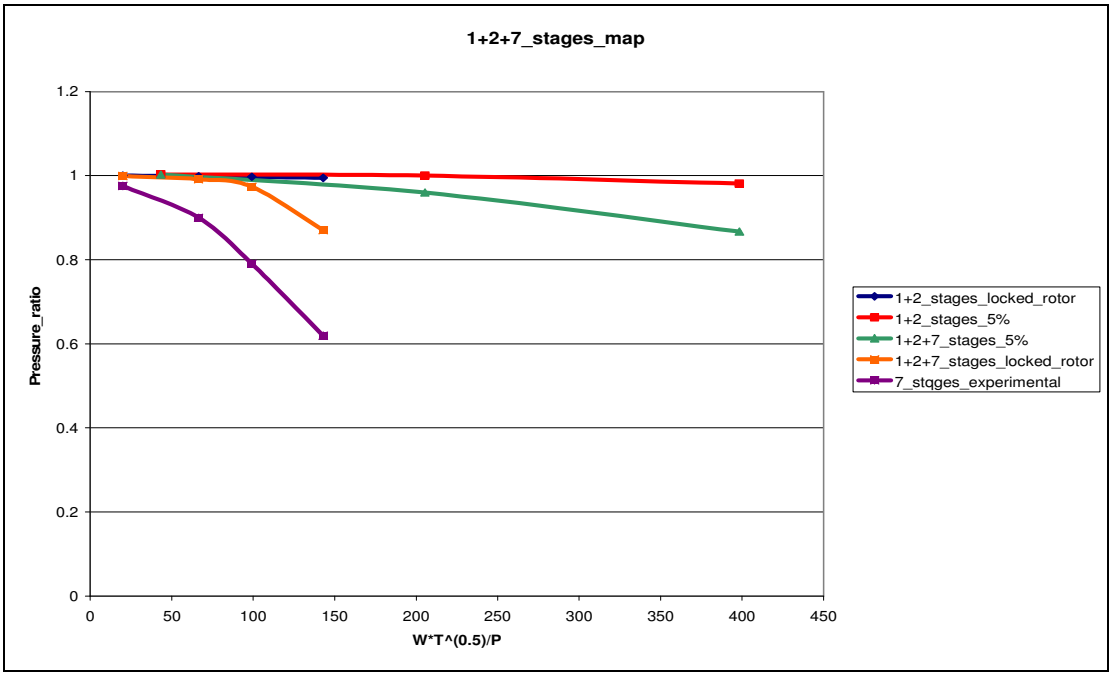

Figure 68. CFD results for Engine D Locked Rotor and 5% windmilling spool speed Pressure Ratios with summation of stage pressure ratios [3].

Within this research a whole compressor simulation was not possible with the time or computer resources available at that time. In the following year the CFD software package TascFlow was replaced by a newer commercial code called CFX. This code contained many more functions which also allowed easier extraction of torque data.

The greatest difficulties were with the geometry, and Bittan highlighted that with a single blade analysis it is difficult to represent the high negative incidences of blades

following other blades with the geometry package TurboGrid. The periodic region created around the blade is setup to accommodate variance around design flow angles and not the high negative incidences required in windmilling and locked rotor analysis. However, stage analysis allowed the stator inlet flow angle for example to be imposed by the upstream modelled rotor blade exit flow angle.

This research paved the way for confidence in CFD ability for representation of the locked rotor conditions, particularly as the flow conditions were incompressible. From assumption of incompressible flow behaviour, for further work a few major assumptions and notes of caution were drawn up;

- The flow angle leaving a blade was approximately the same angle as the blade exit angle.
- Static pressures can reasonably be predicted by CFD at incompressible conditions.
- Total Temperature ratio is zero, as derived from no work done on the fluid, however, the static temperature difference is very small, though very important.
- The large separation wakes and vortices produced at locked rotor and windmilling conditions are known to be a problem for representation by CFD codes and these separation vortices may reduce the accuracy of the CFD static pressure values.

11.4.1.2. Results for Rotor Blade Engine Annular Configuration 3D CFD Analysis for Cascade Test Rig Comparison and Rotor Behaviour Studies

Future windmilling cascade tests as proposed and designed within this thesis, will use the rotor blade from stage one of the HPC on Engine C. It is required to translate the cascade rig test linear data into data which represents the actual annular configuration of the engine for representation of the zero speed curve. Therefore CFD simulations were

performed at a range of windmilling conditions and equivalent spool speeds and then locked rotor for the same windmilling conditions, thus providing data for comparison with cascade data in an annular configuration and the possibility of transposing this data to windmilling rotational conditions.

The cascade rig data could be used to align these CFD results to more accurately represent the engine using CFD prediction for future compressor designs. The aim of this work was also to form the basis of understanding for the rotor and flow behaviour from windmilling to locked rotor conditions. With this aim in mind in addition to HP1 rotor, the HP6 rotor was also modelled in CFD at windmilling and locked rotor conditions. Therefore allowing the compressor rotor response and flow conditions to be studied from entry to exit of the HPC compressor.

The following work was performed by Christopher Kendrick, an MSc student at Cranfield University, supervised by Dr. Ramsden and the author of this thesis. Further work was undertaken by the author to utilise the data for the theoretical and further CFD studies for creation of locked rotor curves discussed in later chapters.

The results of this analysis showed that the pressure loss for both windmilling and locked rotor conditions was always less than a pressure ratio of one. However, when describing the rotor performance in terms of torque as shown in figure 69, the HP1 rotor at only windmilling conditions produced a positive non-dimensional torque, thus a drag on the engine. Therefore studying figure 69, if a even spread of the windmilling torque for each stage between 1 and 6 is assumed, then the overall torque windmilling torque of the compressor would be only slightly positive, therefore forms a small drag (this assumption neglects the drag torque of the power offtakes).

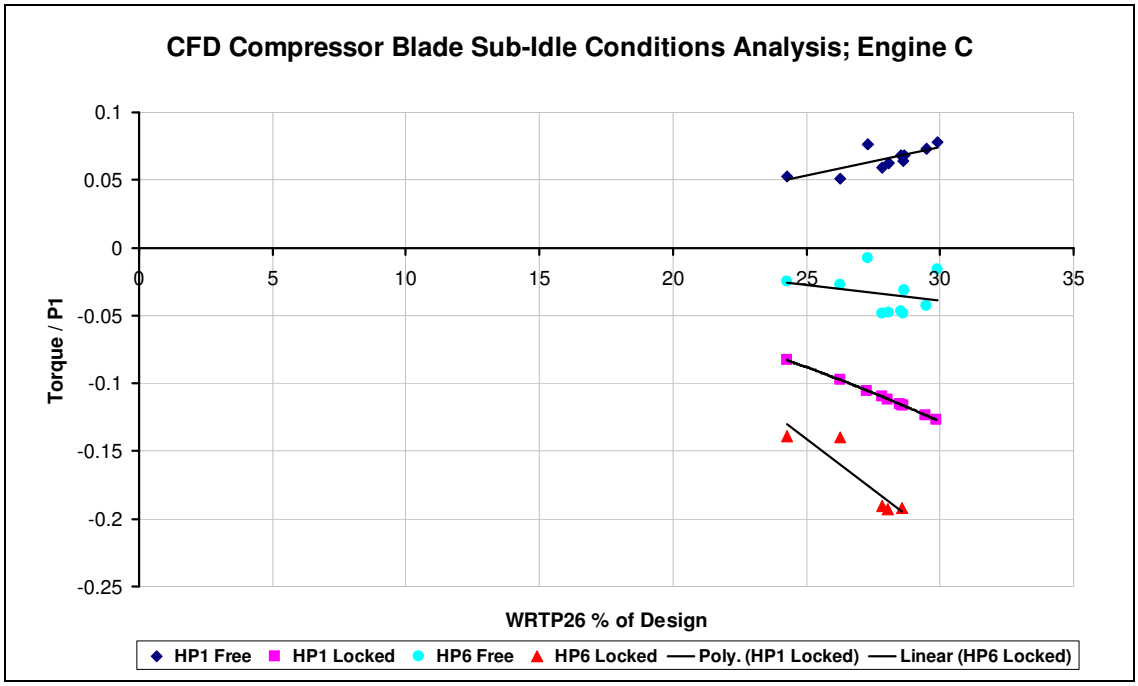

Figure 69. CFD results for Non-dimensional torque at range of windmilling and locked rotor conditions. The same windmilling flow conditions are applied to the locked rotor conditions (adapted from [30]).

As observed from Bittan's work, this research identifies that the last stage, which in this engine is HP6 rotor, produces the greatest torque. An explanation of these observations is discussed in chapter 11.4.2.

The results in Figure 69. are all presented with respect to the non-dimensional flow at inlet to the HPC compressor, not at inlet to each blade. The author of this thesis decided this reference was required for any future use of the data to create a whole compressor locked rotor component characteristic, such as a conventional compressor characteristic is referenced to the inlet non-dimensional flow.

Kendrick found that while producing the range of data other secondary flow effects were playing a large part in the pressure changes. As shown by Figure 70. graphical representation of the flow stream lines over a rotor blade indicates the amount of vortices and created by a locked rotor blade. More importantly, however, a strong tip leakage influence is shown, which flows in the opposite direction to the tip leakage direction at design. The direction is intuitive from the inlet flow incidence and turbine or stirrer operation creating a favourable pressure drop, instead of a pressure rise across the blade which at design conditions would create a reverse flow and stalling effect.

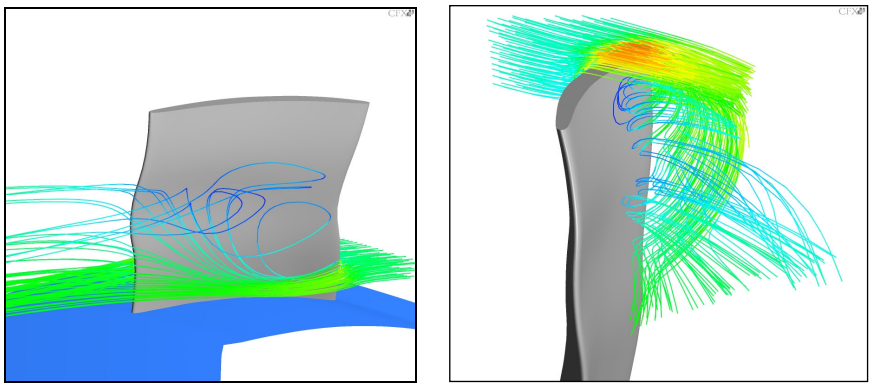

Figure 70. Blade vortices and tip leakage vortices, at locked rotor conditions [30].

The research on Engine C rotor blades by Kendrick [30] provided a valuable insight and confirmed intuitive ideas on flow and rotor behaviour, as well as providing the useful information of the HPC first stage positive torque drag at windmilling conditions.

11.4.1.3. Results of Engine A Compressor Blade CFD Analysis

The analysis used generic blades geometry provided by the sponsor for the compressors in Engine A and used a double circular arc profile. With geometry for every stage and now stator and fan geometry, the intention was to develop generic loss coefficients from analysis for every stage. However, a complete compressor CFD study was not practical within the constraints of this research, therefore LPC 1st stage, HPC 1st and 5th (last stage) were modelled.

In these simulations modelling of a compressor stage was not required, instead results for the blade profile and design blade angles (thus the incidence) were required for application in the chapter 11.4.2. However, some effects such as blade to stator interaction from hub to tip lost as averaged values from rotor exit are applied to stator inlet. Rotor torque was also extracted from the results as shown in Figure 71.

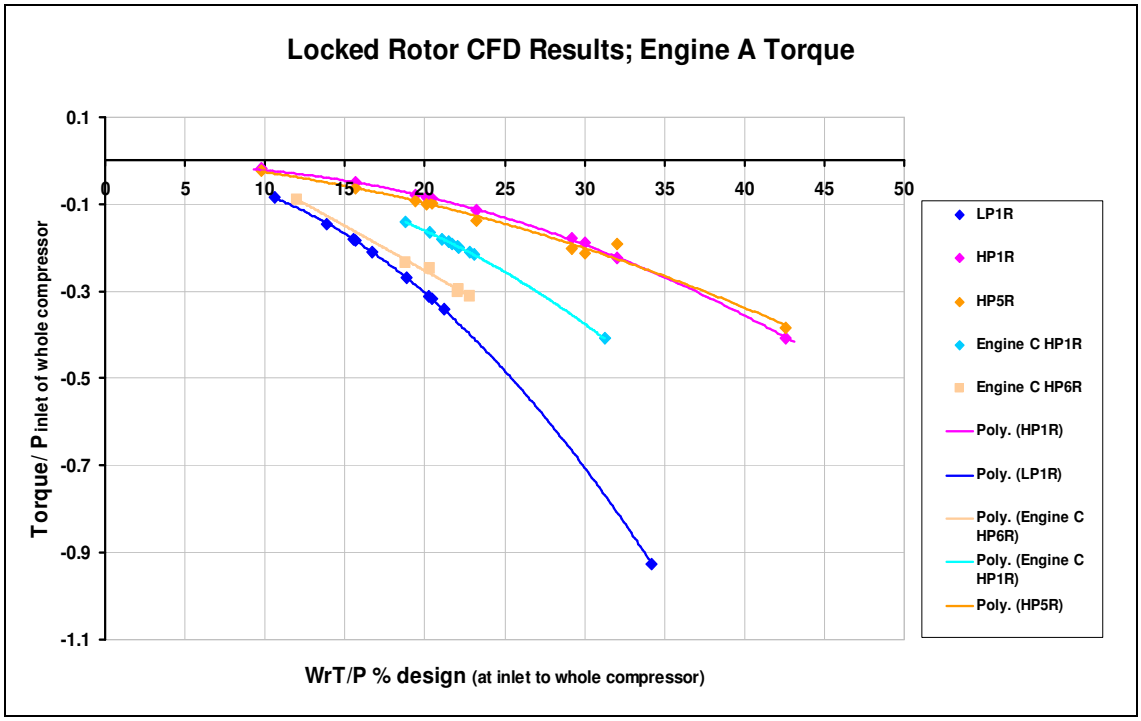

Figure 71. CFD results for Torque curves and trends at locked rotor conditions.

The locked rotor non-dimensional torque results for each blade in Figure 71. present smooth polynomial curves. Engine A HPC inlet and outlet rotors practically provide the same amount of torque, whereas in comparison engine C would indicate that the last HPC stage produces a greater torque. The fan with its larger surface area and experiencing all of the momentum of the air engine the engine at windmillling conditions produces the greatest locked rotor torque.

The 1st stage fan rotor is shown in Figure 72. with plots of velocity at a locked rotor condition, which indicates the large variations from hub to tip. There is an increasing area of stagnation from hub to tip on the leading edge of the blade suction surface. Which forms the static pressure force, as discussed in previous chapters, as being around 1/3rd to 2/3rds of the blade surface. Also the CFD results confirm the flow leaves the trailing edge with approximately the blade exit angle.

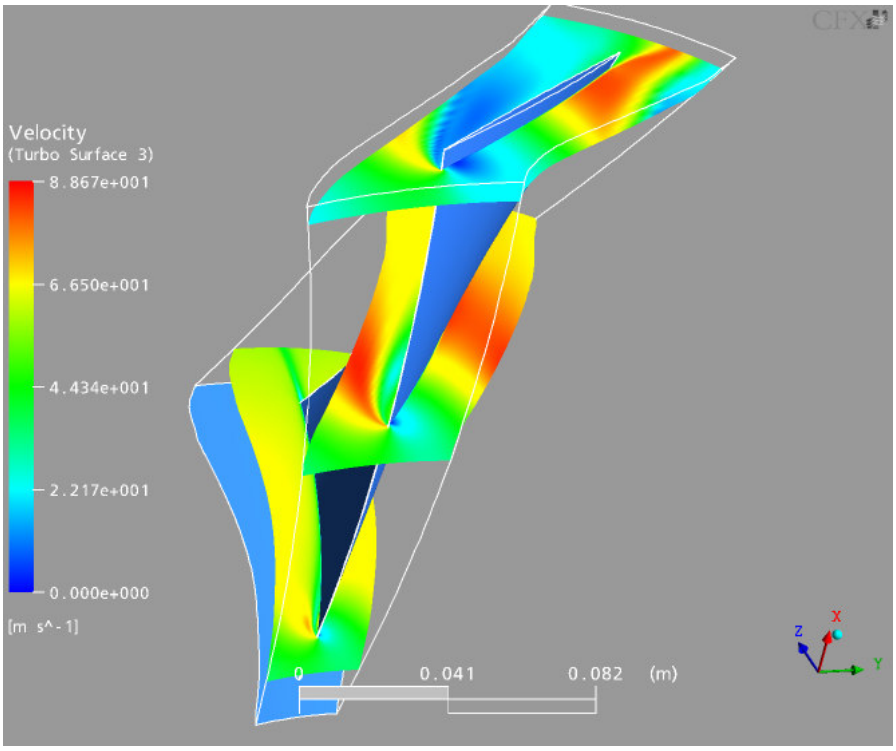

Figure 72. Engine A Fan rotor 1, CFD locked rotor results, for velocity flow sections near hub, tip and at mid height.

In Figure 73. the pressure ratio results are shown for both the rotor and stator blades. All results again provide smooth trends, with the exception of the fan stator which is likely showing simulation errors. Another cause in the spread of the LPC stator 1 results could be to do with the very 3-dimensional flow patterns taking place from hub to tip. In fact on observing the flow patterns within CFX there are large swirl patterns travelling up the blade from the root.

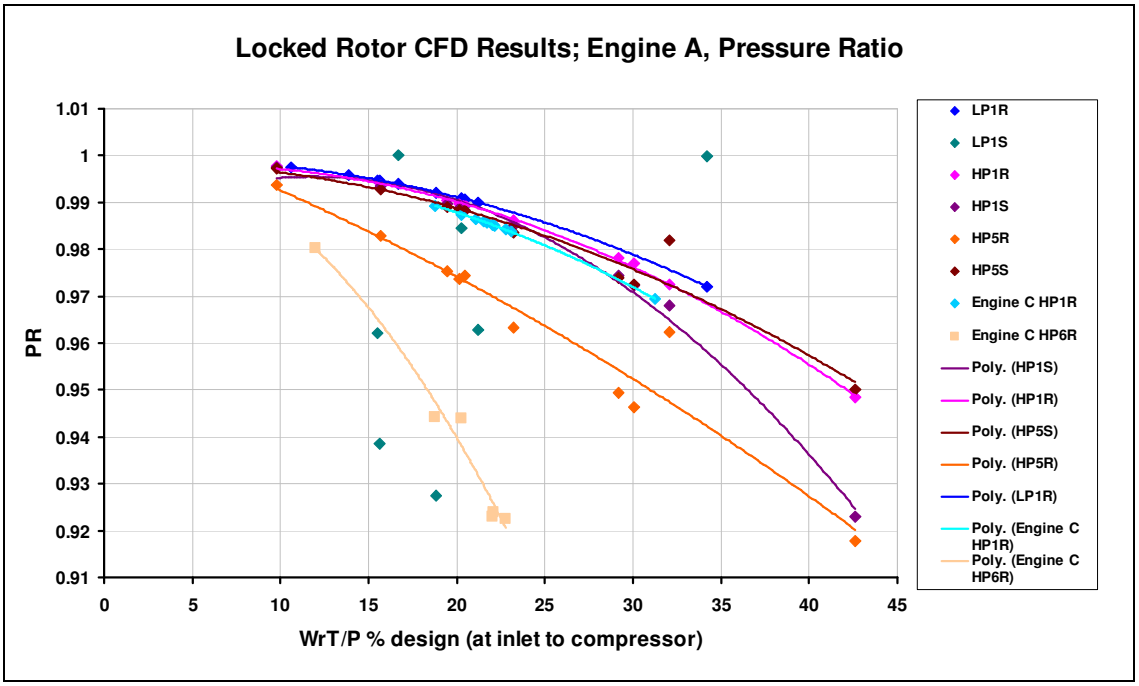

Figure 73. CFD results for pressure ratios and the trends of the locked rotor curves.

The author would suggest that Engine A HP5 blade losses are much higher as the actual blade inlet flow incidence could not be applied in the CFD analysis. Those incidences simulated in the CFD results for Engine A compared to those expected to actual occur in engine at locked rotor conditions are shown in Table 5. Therefore from this table a judgement of the degree of the CFD predicted loss to what would be expected in the engine can be seen although this is not a thorough method.

Blade	Incidence simulated	Incidence in engine	Incidence at 1360 Windmilling case
LP1R	-39	-39	-11
LP1S	-37	-66	-28
HP1R	-57	-57	5
HP1S	-31	-77	-19
HP5R	-61	-70	7
HP5S	-31	-83	-17

Table 5. Engine A compressor inlet flow incidences for locked rotor and windmilling conditions, achieved in CFD simulations and those in engine.

As the actual incidences could not be achieved within the CFD results it becomes difficult to understand how to apply these results to creating an actual zero speed curve from this data. Also time was not available for further stage construction and analysis or a construction of a whole compressor CFD simulation, which would be difficult, time consuming and in it self be another PhD. Therefore the following chapter describes how this data is useful to derive loss coefficients for any incidence and construct a zero-speed curve.

During many of the simulations for the stators convergence entered a cyclic mode in which the residuals took a long time to converge. All results converged within 200 iterations, and windmilling simulations would converge in under 70 iterations, probably as a result of the reduced flow separation from the respective lower windmilling incidences.

11.4.2. RESULTS OF CFD FOR FORMATION OF COMPRESSOR BLADE LOSS COEFFICIENTS

11.4.2.1. Locked rotor results and discussion

The locked rotor CFD results from Engine A and D analyses, were combined to find a generic correlation between the blades, therefore the loss coefficients were plotted against each other for their respective incidences simulated.

The total pressure loss coefficient, described by equation 72 in chapter 9.3.1 is shown in Figure 74. below, for a range of windmilling conditions with the rotor locked. For comparison a windmilling condition and the resulting total pressure loss for all engine A blades is shown. Also shown is the effect of various windmilling conditions around engine A fan rotor blade 1. These last two results are discussed in the following chapter.

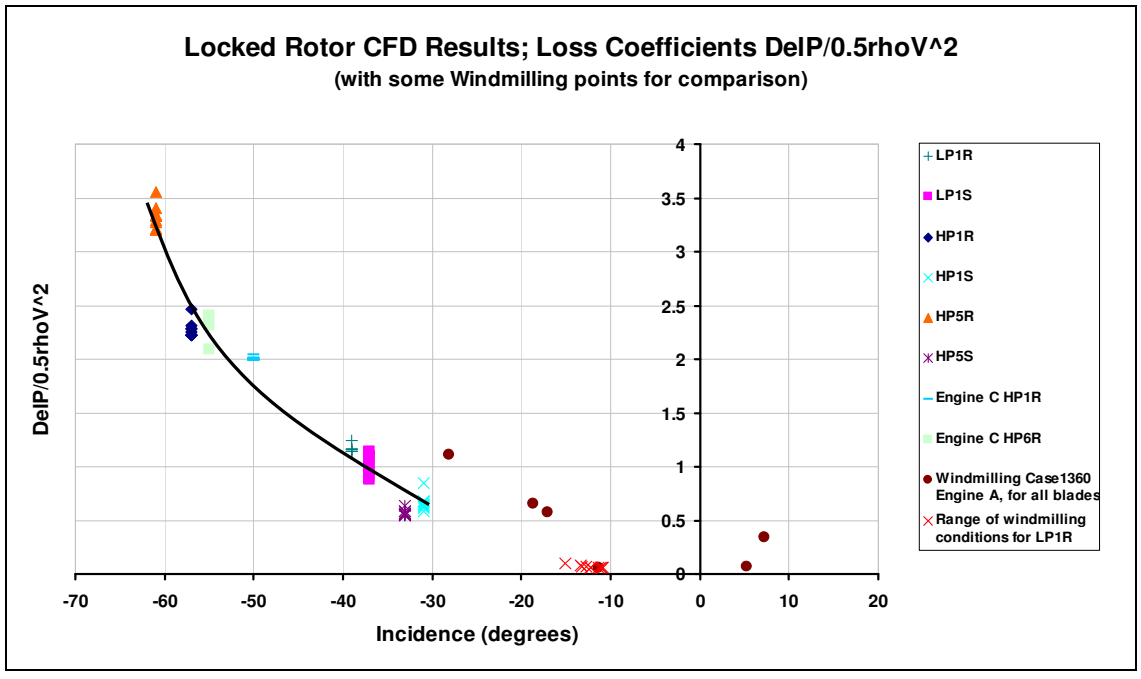

Figure 74. Formation of compressor blade total pressure loss coefficients relationship, derived from CFD results of Engine A Fan, HPC and Engine C HPC.

The total pressure loss coefficient for all compressor blades rotor and stator and even different engine, seems to produce a general trend, which can be represented approximately by a polynomial.

Also for each blade, as the rotor is locked, there is no variance on incidence, only a small variance on total pressure loss. This highest total pressure loss for a blade represents the highest flight Mach number condition, thus the highest ram pressure and resulting in the highest velocity and mass flow at inlet to the blade. The lowest total pressure loss represents the lowest flight Mach number. For example on engine A the range of widest range of flight windmilling flight Mach numbers the engine would experience was used, therefore that which is depicted in Figure 74. is the greatest windmilling range of total pressure loss for each blade.

As discussed in the preceding chapter, the actual incidences for the stators are in fact much more negative than could be simulated within this individual blade CFD analysis. Therefore, from the relationships shown in Figure 74. one would expect for stators to move along the trend line to higher total pressure loss coefficient and negative incidence.

Using the polynomial for the general trend from Figure 74. the exit total pressure of any compressor axial blade at locked rotor conditions (designed for the same operational envelopes as engine A and C), may be approximately obtained. This is applied in the results in chapter 11.4.3.3.

The Lift coefficient (CL) and the Drag coefficient (CD) were composed for the compressor blade CFD results as shown in Figure 75. The equations describing these coefficients are found in chapter 9.3.1. These results directly relate to the same simulation results in Figure 74. and can be compared based on the value of incidence.

Also shown is the effect of various windmilling conditions around engine A fan rotor blade 1. These last two results are discussed in the following chapter.

As with the results for total pressure loss coefficients, the CD and CL coefficients appear to produce general trends. The trends are suitably represented by a polynomial curve.

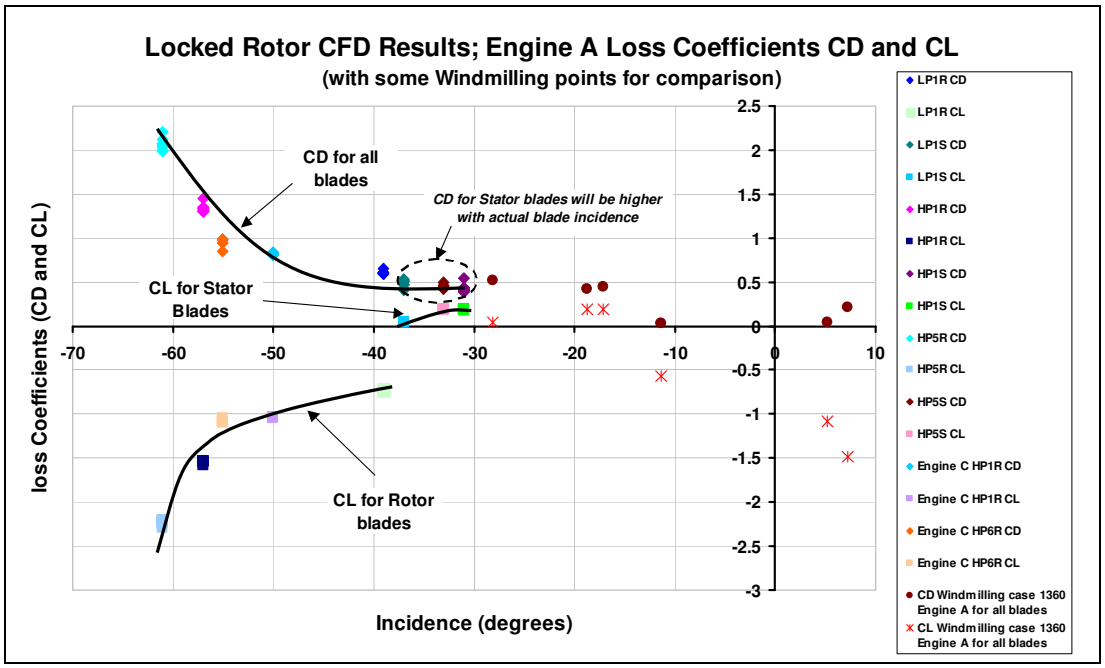

Figure 75. Formation of Compressor blade CD and CL coefficients relationships, derived from CFD results of Engine A Fan, HPC and Engine C HPC blade data

The values for CD coefficient are all positive and relate well to other published loss profiles as the incidence tends negative, however, I must be understood, these results are for windmilling conditions and where the Reynolds number is much lower than design (Reynolds ratio can be as low as 0.14). In the case of CD coefficient, a single polynomial trend fits well and the variation for the range of windmilling locked rotor conditions on each blade is small. The stator blades seem to be at a minimum on the polynomial, however, as discussed previously the stator incidences in the CFD

simulations were limited and will have much higher negative incidences in the actual engine. Therefore one would expect the CD values to be higher moving up the polynomial trend curve.

There seems to be two trends for the CL coefficient, one where the stator blades have positive values and the other where the rotor blades have a negative value. With some error to LP1 rotor, one trend line could be formed. Also, as the stator incidences would be far more negative in the actual engine, their trend dictates that at higher negative incidence their CL values will fall onto the trend of the rotors. The lift coefficients at high negative incidence have negative values as the blades are operating in a mode, where if considered like a plane the aerofoil creates a down force, in which the flow is approaching the suction side of the blade.

The CL coefficient trend also compares well with other published loss profiles, in which the CL becomes negative at highly negative incidences.

11.4.2.2. Summary

The blades for engine C are modelled as a full 3D profile representation of the actual blades and blades for engine A include profiles hub mid and tip cross section to create a 3D profile. However, it would seem from the results in both Figure 74. Figure 75. that the blade profile has little effect on the losses, instead the incidence is the dominant function.

These results would suggest the author's early opinion is correct, that the blades at these highly negative incidences are behaving like a flat plate thus the actual blade profile has little effect on the losses. Unlike at design incidences where the profile shape and thus profile loss is so important.

11.4.2.3. Windmilling Results and discussion

As in Engines D and C CFD studies, it was also found that Engine A rotor HP1 produced a small but positive torque in windmilling and HP5 rotor produced a negative torque. In which a positive torque is equivalent to the compressor in working a stirrer mode, producing a drag torque though with a pressure ratio less than one. With a negative torque, the compressor is in turbine mode providing torque to the compressor also with a pressure ratio less than one.

To provide some insight into windmilling and relate this to the locked rotor cases, windmilling ATF engine case 1360 conditions for engine A, were applied in CFD simulation only to engine A blades. The following discussion analyses these results.

With the aid of the windmilling points plotted in Figure 74. Figure 75. and using Table 5. to ascertain from the windmilling incidence in these figures, the stirrer drag mode of HP1 rotor in windmilling can be analysed further. In Figure 74. both HP1 and HP5 rotors are shown to have a positive incidence at windmilling, this is a result of the windmilling speed, which is not just a function of the compressor performance but also of the Turbine and power offtake drags. What differentiates the two rotors is the order of the total pressure loss coefficients. HP1 rotor has negligible loss, whereas HP6 rotor has significantly higher drag from the higher velocities (Mach number) it experiences from the culmination of the pressure drop and reduced annulus area.

The windmilling CD coefficient values are all positive with the minimum of the trend for those blades at this incidence windmilling condition tending toward a typical blade design incidence of around -3 degrees. Interestingly the windmilling CD values for those blades with windmilling incidence values around -15 to -30 degrees tend to line up with the trend for the locked rotor CD values.

Windmilling CL coefficient values for all rotor blades are negative, however, the stator blades are positive. However, with the correct higher negative incidences as within the engine, these values would be expected to become negative.

All windmilling discussions in the previous paragraphs have been for one windmilling condition. It would be interesting to gain some understand of the change in incidence and for example change in total pressure loss coefficient at a range of windmiling condition on a one blade profile. Figure 67. presents such an analysis for LP1 rotor. The more negative incidence case is for a lower flow momentum at entry to the blade (which is a function primarily of power offtake load, flight Mach number and Altitude) hence lower rotational windmilling speeds. As a result the variance in data for a blade at windmilling, is mainly that of incidence rather than total pressure loss coefficient.

11.4.2.4. Summary

From the windmilling results it would seem there are further trends for the windmilling coefficients with respect to incidence. Further CFD studies could set the rotational speed say at 5%,10% and 15% non-dimensional spool speeds and apply the same range of windmilling conditions to ascertain windmilling rotational loss coefficient trends, thus producing a generic map of loss curves for calculating a complete compressor locked rotor through to windmilling sub-idle rotational speeds. In fact if consistent results are found, this approach via a stage stacking technique for each non-dimensional speed could define the whole sub-idle region of the map removing the need for extrapolation. However, some caution must be added, as the compressor mode when the engine is lit may be different than the windmilling driven mode, producing different loss coefficients. This is a useful area for further investigation.

From the indication of the loss coefficients results one can conclude that compressor drag is higher for locked rotor conditions than windmilling, which is intuitive from the

higher the incidence the higher the wake, whereas windmilling rotational speeds reduce the incidence. Overall engine drag is likely to be the opposite of this statement and will be of a much greater order of magnitude.

11.4.3. THEORETICAL CALCULATION RESULTS

This chapter presents results and their improvement from the developments of the theoretical compressor zero speed curve prediction method and then the modified theoretical method using the locked rotor loss coefficient relationships developed from the CFD results from the preceding chapter. All methods are discussed in 9.3.1.1.

It was important to validate, if not check, the theoretical calculations, and as no test or cascade test data for a single blade or whole engine locked rotor data is available (except for engine D), the results of this chapter are compared against the CFD results for the specific engine and blade simulation used.

11.4.3.1. Results of Early Theoretical Method.

The result of the early theoretical method to calculate the torque and pressure loss of a rotor blade, formed by Bittan [3] and the author of this thesis as discussed in chapter 9, is shown in Figure 76. below. It can be seen that the result has good agreement with the CFD result at low flight Mach number however, error increases with increasing flight Mach number.

The torque is presented by [3] as being positive, where in fact this should be negative, it is only the positive sign which is wrong not the results. Although the engine flight Mach number relates the inlet flow momentum to the core flow (as engine D is a turbojet engine), to represent the results more indicatively to the compressor the inlet

non-dimensional flow should be used. Also this allows the results to be applied to a compressor characteristic using non-dimensional torque.

As the engine operational envelope is unlike typical engine designs, the data from this engine geometry is not suitable for creating generic understanding of engine blade results or compressor behaviour at windmilling and locked rotor conditions.

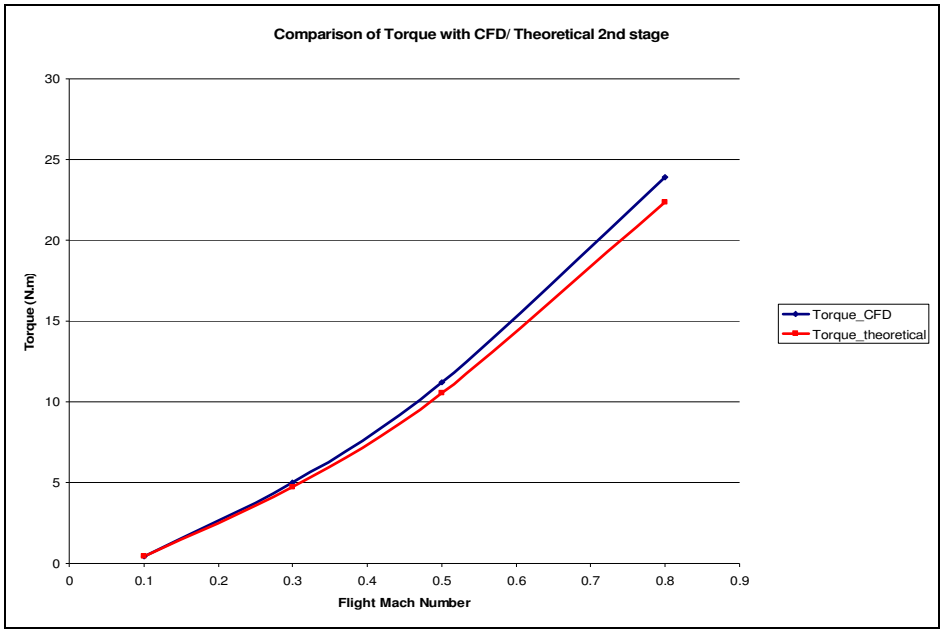

Figure 76. Result for 1st Locked rotor theoretical method plotting torque versus flight Mach number for engine D 2nd stage rotor [3].

The main problem with this method and its results, is the formulation of the method assumes that the axial velocity is constant from blade inlet to outlet, as in the case of a cascade. Whereas the blade in locked rotor and windmilling has a accelerating flow from the pressure drop thus $Va_{out} > Va_{in}$, therefore the approached will have an error. This led to the development of the method to account for this velocity change and the results of which are shown in the following chapter.

11.4.3.2. Later Theoretical Method Results.

The results for the 2nd improved theoretical method, as discussed in chapter 9 are shown in Figure 77. and Figure 78. The theoretical results could be calculated for a range of non-dimensional mass flows, thus creating a single stage zero-speed curve. The first analysis of results were based on Engine C HP1 rotor and then further calculations on HP6 rotor.

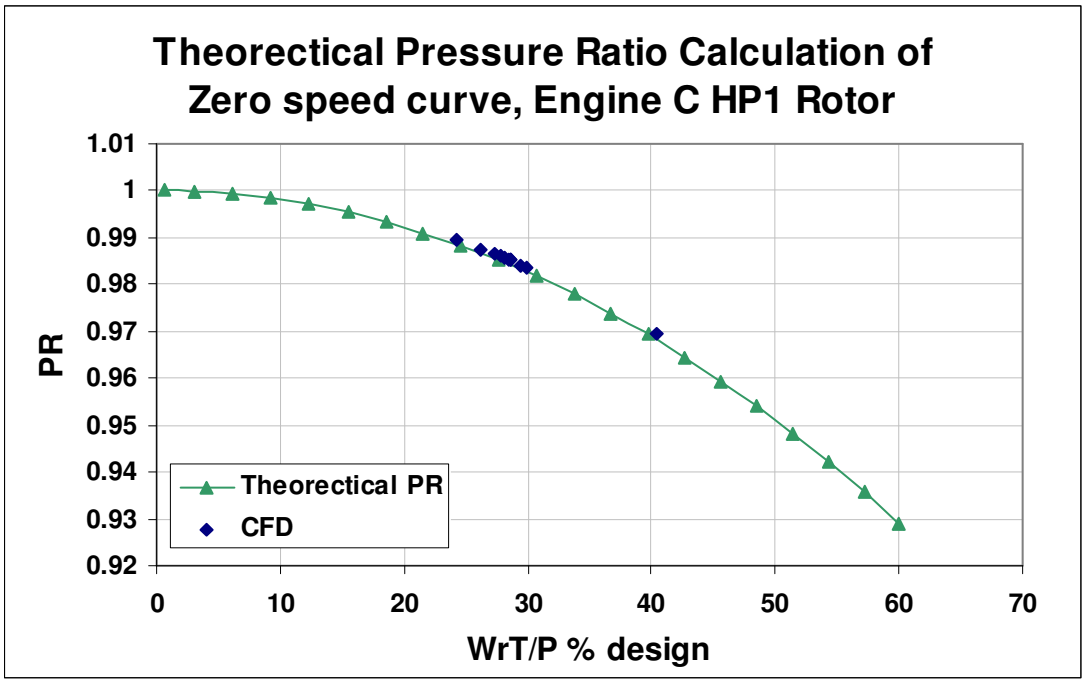

Figure 77. Results for 2nd Theoretical approach for $Va_{out}>Va_{in}$, pressure ratio results compared to CFD result.

With this improved method there is good agreement for the predicted pressure ratio and non-dimensional torque. However, upon calculating HP6 rotor it was found the results did not predict the pressure loss or non-dimensional torque very well. The results were not producing low enough pressure ratios, or higher enough negative torques.

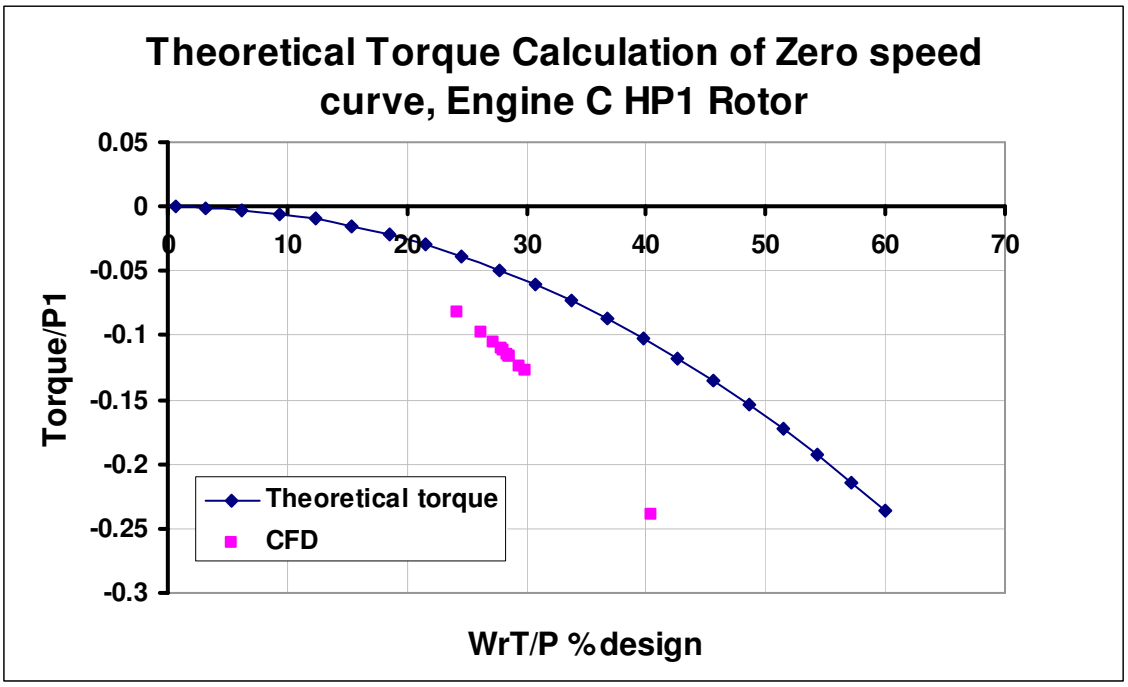

Figure 78. Results for 2nd Theoretical approach for $Va_{out}>Va_{in}$, non-dimensional torque results compared to CFD result.

It was decided that the complicated losses particularly the conditions entering and acting across HP6 rotor could not be calculated by this simple approach. HP1 rotor results benefited by simple flow at entry and across the blade, thus producing good results. Instead the theoretical method required incorporation of some loss models to determine the pressure drops across the blades. The following chapter's results answer this requirement.

11.4.3.3. Results of Theoretical method using CFD derived loss coefficients

Using the generic geometry data available for engine A, the stage stacking approach could be used to combine each stage calculation to create a whole compressor calculation of the locked rotor curve. This data could then be used to define the zero speed curve on a compressor characteristic for extrapolation/interpolation.

Within the whole compressor theoretical calculation the pressure losses were determined using the polynomial curve from CFD derived loss coefficients results in chapter 11.4.2. In using the loss coefficient curve equation, it was possible to determine the correct incidence and relative loss to apply to every stage. The results of these calculations are shown in Figure 79. and Figure 80.

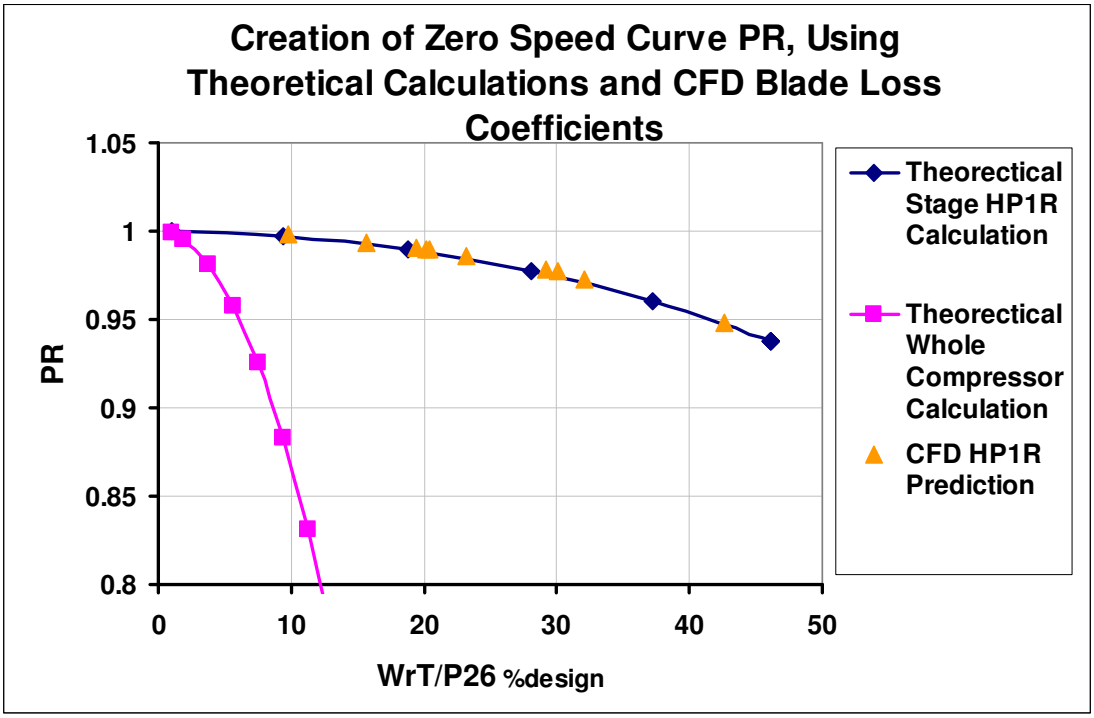

Figure 79. Zero speed curve creation for engine A HPC, pressure ratio versus non-dimensional mass flow.

Validation of results is difficult as no engine data is available, therefore the theoretical results for the first blade were compared with the CFD results for that blade. With the results for the first blade aligning well with the CFD as shown in Figure 81. Figure 79. and Figure 80. , the results for the whole compressor prediction were accepted.

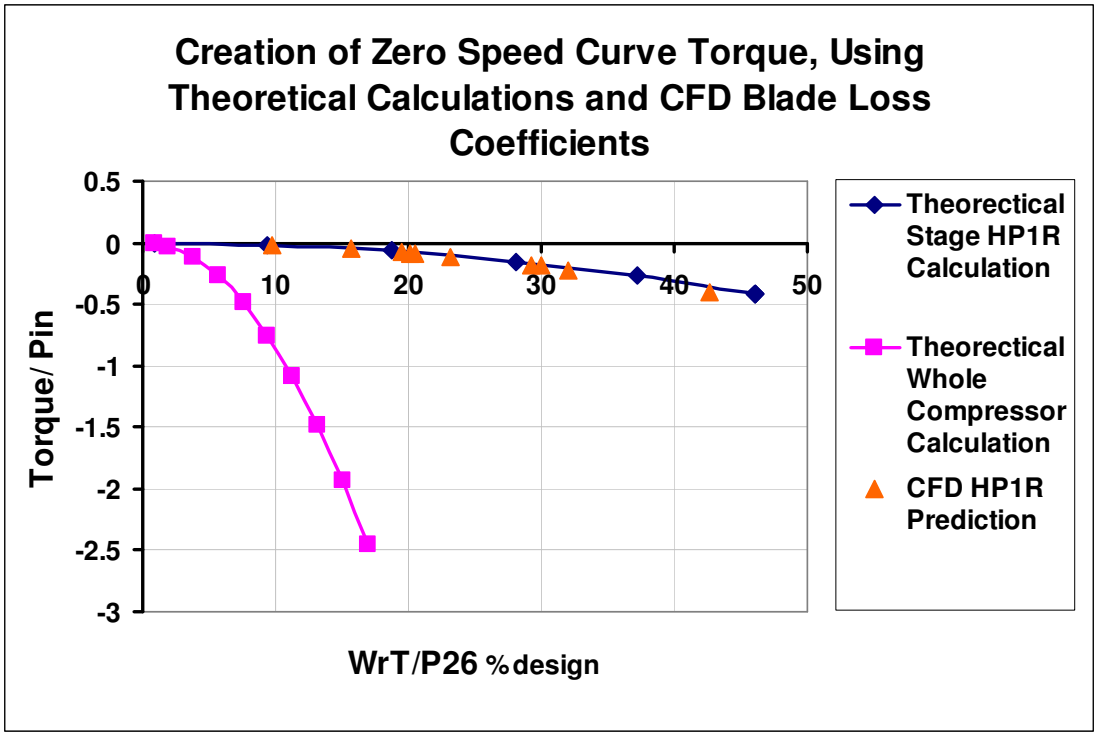

Figure 80. Zero speed curve creation for engine A HPC, non-dimensional torque versus non-dimensional mass flow.

The results seem very intuitive of lower pressure ratios and higher non-dimensional torques than a single stage, and the curves seem sensible. Observing the zero speed curve shape on the whole compressor characteristic would provide a greater appreciation and validation of resulting curve. This comparison and interpolation for the characteristic using the zero speed curve is shown in chapter 11.4.5

11.4.4. TEST RIG

Unfortunately there was only time available to design and build the test rig. Time was not available to run the test rig to gain some cascade results, this work shall be continued by the next researcher.

The results will be evaluated against the CFD simulations of the Test Rig and then transposed to the annular actual engine configuration results. A delta or coefficient factor will be applied between these the test rig and CFD of test rig, and between the CFD test rig and the annular CFD simulations. A further analysis other than locked rotor would be to derive the equivalent windmilling CFD correction factors required as the windmilling conditions were used to create equivalent locked rotor runs.

The loss coefficients result in chapter 11.4.3.3 are defined by CFD, which require validation and maybe alignment to test data, thus the main purpose of the future windmilling cascade test rig results.

11.4.5. TORQUE CHARACTERISTICS

The results for the torque characteristics developed and interpolated from the zero speed curve, which was defined by the results in chapter 11.4.3.3, are presented and discussed within this chapter. The approach and method used to obtain these characteristics is described in 9.3.2.

Figure 81. and Figure 83. show the resulting interpolated characteristics for engine A HPC in terms of non-dimensional torque and pressure ratio both versus non-dimensional mass flow. Interpolation of speed curves was between 68%N/rT and the zero speed curve 0%N/rT, with the range of beta in the original characteristic extrapolated to pressure ratio of one prior to speed curve interpolation.

It can be clearly seen from these results that this approach defines an end limit therefore interpolation, but more importantly the lower speed curve shapes are more defined compared to those defined with the extrapolating approach as shown in Figure 13. The speed curves are very smooth in profile, although the choking limit may be a little too vertical on the lower speed curves. Further work either using the same techniques for each individual lower speed curve could be used to remove the need to interpolate altogether.

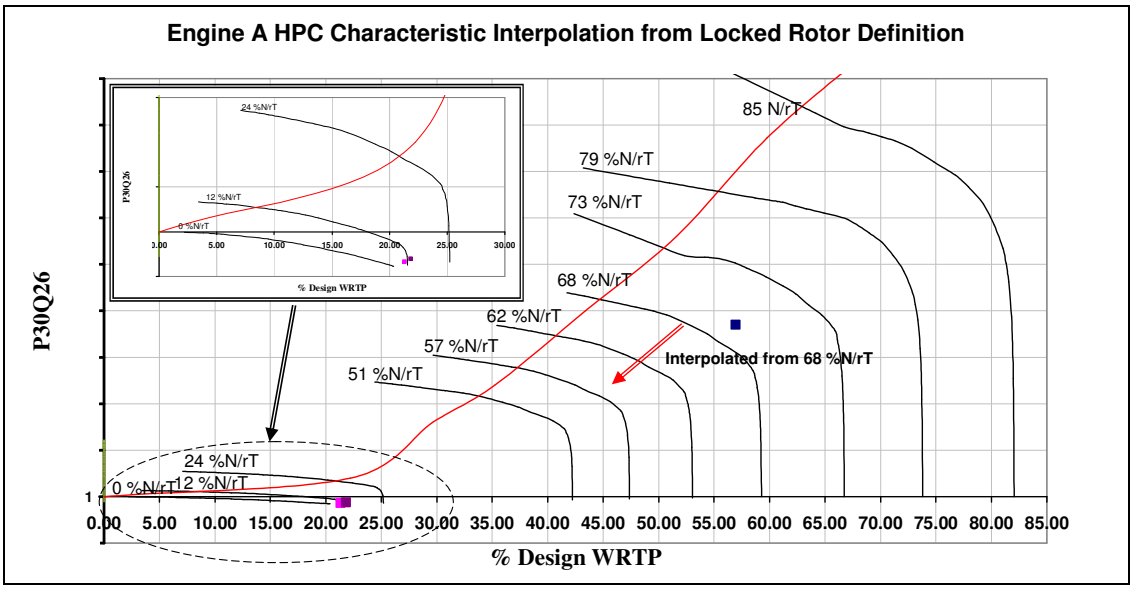

Figure 81. Interpolated Engine A HPC Characteristic using locked rotor defined curve, Pressure ratio versus non-dimensional mass flow.

The only guess required is reduce to that of the range of WrT/P for the zero-speed curve, as this affects the position of the N/rT interpolated curves, as shown in Figure 82. Therefore ATF test data still had to used, to align the interpolation by guessing the zero-speed curve maximum WrT/P until the 12%N/rT curve lined up with the test data as shown in Figure 81.

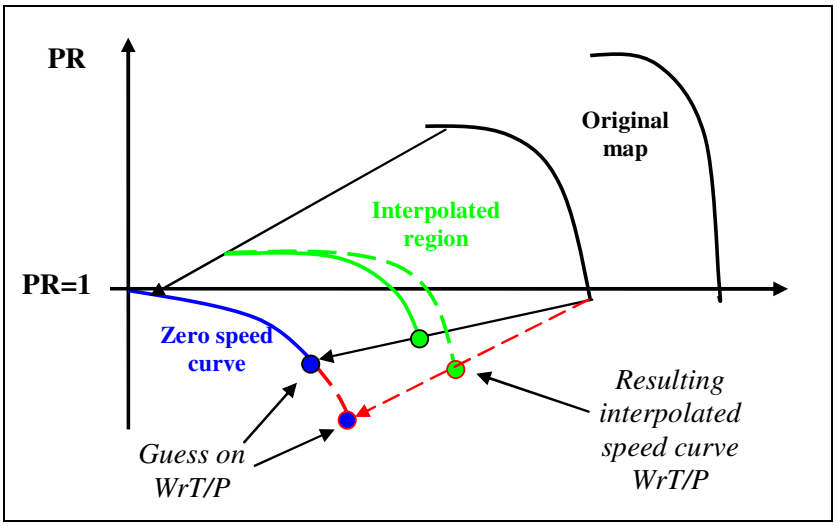

Figure 82. The effect of the guess of zero speed curve maximum WrT/P on the interpolated N/rT curves.

As a zero speed curve is defined in terms of torque rather than work, groundstart simulations would be possible with these characteristics. Future work would be to apply these characteristic within the sub-idle model with code changes to accompany the new arrangement of parameters and the new parameter of torque. Torque balance calculation will be made much more direct within the programming.

The torque drags from power offtakes and starter motor assistance drag can much more easily be compared with the component characteristic now the torque is a defining parameter.

To summarise this approach is much simpler than the previous extrapolation method, requires less guesses and is based on some physical representation. Also if the original Psi Isen_Psi and WT/NP parameters are still required, they can be obtained by transforming the torque parameter to specific work. This would still present a much more simple, repeatable and confidence gained approach, than the previous extrapolation approach. However, there will be no zero speed curve and groundstart simulations would not be possible.

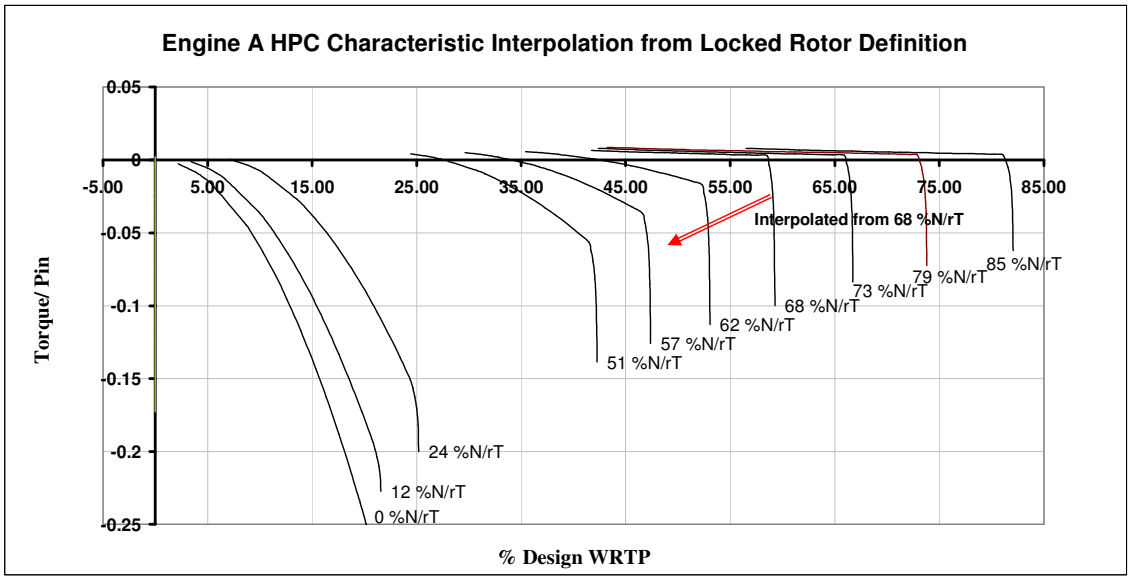

Figure 83. Interpolated Engine A HPC Characteristic using locked rotor defined curve, non-dimensional torque versus non-dimensional mass flow.

The compressor characteristic can be extrapolated in terms of torque with the definition of the zero speed curve, as shown in figure 83. This characteristic will replace the work definition and is expanded to sufficient negative non-dimensional torque values for windmilling and locked rotor conditions. The non-dimensional torque is the compressor torque divided by the inlet total pressure, which relates the torque to the inlet flow conditions of pressure which primarily influence the momentum force. Although the non-dimensional torque magnitude seems large at the lower speeds compared to design this is more related to the inlet pressure will be lower at windmilling and the losses within the compressor gas path are less towards design, creating less resistance.

The same approaches use here for compressors may be applied for turbines and would reinforce the definition of the incompressible speed curve. A full CFD analysis of losses probably isn't required as the turbine incidences are not as negative and Soderberg correlations can be suitably applied with Reynolds number correction.

12. Conclusions

12.1. INTRODUCTION

The main conclusions from the research work are discussed within this chapter, with regards to the areas of research discussed within the thesis. The chapter then presents a summary of the research work.

12.2. SUB-IDLE SIMULATIONS

The sponsor's development sub-idle model was evaluated and modified for two-spool engines and configurations. Engine models were created for two engines with widely different design parameters. From these engine models an improved understanding of sub-idle modelling was gained and knowledge passed on to Rolls-Royce. The research found that the smaller engine due to its lower design parameters was very sensitive to model compared to larger engines.

Steady state and transient model simulations were carried out, with sensitivity analysis, which partly evolved from the adaptive process of aligning and improving the model. In the sensitivity analysis, compressor and turbine extrapolated regions variations were studied, finding that the compressor was more dominant and it was this that selected the spool rotational speed at windmilling and not the turbine. Further sensitivity analyses involved, the, control bleed valve size, power offtake and then analyses related to other the research areas such as varying combustion volume, combustion inefficiency factor and mixer entry static pressure.

To understand the effectiveness of the linerarised parameters for component characteristics, the results of the simulations were studied, finding that the lack of definition of pressure loss in the very low speed region close to zero, made these

parameters particularly not suitable for low flight Mach number assisted starts and groundstart simulations.

Windmilling analysis is not enough to satisfactorily extrapolate and determine that the component maps are successfully extrapolated.

12.3. COMPONENT SUB-IDLE EXTRAPOLATION

This area of research investigate the extrapolation techniques of the linearised parameters making improvements to the method and extrapolating characteristics for engines A and B. The improvements to the extrapolation technique recommended and presented extrapolation of WrT/P first to obtain Phi, and presented smoothing methods for extrapolation of beta.

The best approach and method for obtaining characteristics with the large number of guesses required in the extrapolation technique is desccribed. Along with defining an iterative and adaptive approach of utilising the model to obtain suitable characteristics

Limitations of the linearised parameter extrapolated characteristics were studied through model simulations.

An approach to extrapolating combustion characteristics is shown using the steady state unlit combustion loading to define the end limit. Also recommendations are made to use the parameter WrT/P31 to replace AFR for sub-idle models to improve both light-up simulations and extrapolation.

12.4. SUB-IDLE MIXER STUDIES

The mixer sub-idle operation and how to represent its behaviour in a performance model has been studied, from the use of engine ATF data, CFD analysis and engine sensitivity analysis to the off-design mixing behaviour.

Test data was limited to a low bypass ratio mixed engine, from which it was found SMPR was greater than one and a strong relationship of increasing SMPR with engine flight Mach number. A characteristic for definition of the SMPR was built into the sub-idle model to understand its influence of improving windmilling speed matching, where SMPR of 1 would slightly reduce core spool speeds.

The research with model simulations found that the mixer increased core windmilling spool speeds on low bypass engines, where the core stream is pumped by the ejector effect of the bypass stream. Mixing slightly decreased core spool speeds on high bypass engines, where only a percentage of the bypass flow mixes the core flow.

12.5. COMBUSTOR STUDIES

The sub-idle model was used to back-out combustion efficiencies at light-up for a range of flight conditions. This data provided approximate efficiency values of 20 for windmill relights, with the transient data presented provide intuitive results, which can later be used for combustion test rig comparisons currently being undertaken within Rolls-Royce.

Through work by an MSc student an analysis was performed on the suitability of reaction rate combustion loading definition used at present for combustion efficiency calculation. The findings proposed that evaporation rate can be limiting at light-up and through light-up at high operational altitudes, therefore the combustion efficiency

should be calculated by the sum of the reaction and evaporation rate defined combustion efficiencies.

An analysis of combustor liner pressure losses at the low Reynolds number conditions of windmilling were studied, and showed a marked difference from typical design loss values. Therefore it was suggested that the combustion loading parameter, possibly should not neglect the pressure loss term, as the liner loss would seem to vary considerably from design.

12.6. LOCKED ROTOR STUDIES

An analysis of the windmilling and locked rotor behaviour of compressors was performed with 3D CFD commercial turbomachinery codes, also assessing the suitability of CFD and how to model compressor blades at these off-design conditions.

A theoretical method was produced to calculate the torque of a rotor blade. This method was developed to fully calculate the blade exit velocity and via a stage stacking method calculate the whole compressor zero-speed curve, in terms of pressure ratio and non-dimensional torque.

The theoretical method derived above employed generic compressor blade loss coefficients which were created from the compressor CFD studies in this research. The CFD found that all blade profiles acted like an inclined flat plate at the high negative blade incidences in locked rotor, therefore the blade profile had little effect. Each blade loss coefficient fell onto and created a generic trend, with scatter becoming smaller towards lower flight Mach numbers (which are more akin to locked rotor engine operational conditions). A cascade test rig was designed and built for future validation of these CFD results.

From the locked rotor curve definition by the theoretical calculation, compressors characteristics were interpolated, with the amount of guesses reduced to only one.

12.7. SUMMARY

Research conducted within this thesis covers a wide range of issues related to sub-idle modelling, and discusses in some depth each problem at hand. This should provide an invaluable reference for future studies and creation of sub-idle models.

The research has led to an increase in sub-idle modelling knowledge, creation of methods, and engine models, all transferred into the sponsoring company.

Some of the sub-idle modelling areas have only been identified as problematic areas during the course of this research. These areas of research were preliminary studies which make some analysis and findings that require further research, these are outlined and discussed in the following chapter.

13. Recommendations for Further Research

The sub-idle performance model BD19 accuracy at low windmilling speeds (low flight Mach number), could be increased greatly by the improved characteristic definition created by the methods of zero speed curve and interpolation methods presented within this thesis. The code matching, to avoid multi-match points would also benefit by using the torque characteristics defined in this thesis. It is recommended by this author, that the BD19 code matching and component bricks be changed to incorporate torque characteristics and parameters as defined in chapter 9.3.2. The zero-speed theoretical calculation can be used to create the zero speed curve, with pressure losses and torque defined by applying, the locked rotor compressor blade generic loss coefficients created within this research and Soderberg correlations (with Reynolds number correction) for turbines. Then the component characteristics can be interpolated.

With regards to engine testing, the following is recommended, but not limited to;

- More cold windmilling tests need to be taken on the ATF engine tests. This could easily be achieved by the first test of the day and every day (when the engine is cold) is used for a windmill relight, thus producing cold data with no heat soakage influences.
- Pump pressures at inlet and outlet with flow should always be measured.
- If the engine has mixed exhausts, the static pressures in both ducts prior to the mixing plane should be recorded, along with the related total pressures and temperatures. This will aid sub-idle model mixer representation, and increase engine data in this area.

The complicated area of off-design mixer behaviour particularly at windmilling conditions was only touched on in this research. In which the influence of mixing on windmilling speeds and representation of the mixer in a sub-idle performance model, was studied. Further areas for study are listed below;

- To fully understand the mixing process it would be useful to conduct a test in a representation by simple ducts (in either scaled or full scale test) in which a range of bypass to core mixing area ratios and velocity ratios could be tested. The influence of a mixing length tube (representing variations in jet pipe length) could also be used to understand mixing length influences. The SMPR from these tests should be measured as well as any flow visualization to study the mixing regions. Also tests should be applied with varying duct static pressure to simulate this variation at windmilling conditions from upstream engine components.
- The BD19 code changes for implementation of Brick 60 to represent % of cold duct mixing with core, would not link when compiling. Therefore this needs to be fixed and then simulations and further analysis on the influence of mixing on engine B can be carried out.
- When using Mixer Total Pressure Ratio (MTPR) as a representation for one of the graphical axis in the mixer entry conditions graph in Brick 47, the model ignores this value and sets it to one. This is a problem with using the cold duct total pressure, the output from brick 47's iteration, as a match. This needs to be remedied as ATF data study of engine A, indicates MTPR varies significantly at windmilling conditions.
- The simple enthalpy and momentum balance used in the RRAP mixing bricks require further development to represent the off-design mixing conditions at windmilling. One example could be to include shear mixing calculation, as applied to the theoretical calculation study within this thesis.

In the area of the locked rotor and windmilling studies in CFD there are many areas that require clarification, extended CFD models, or more advanced rigorous CFD analysis, as listed below;

- A whole compressor locked rotor 3D CFD model would provide a more complete analysis of the compressor and CFD capabilities for representation of the compressor losses and torque at these conditions. The results could be used to compare the results from the theoretical whole compressor locked rotor calculation.
- The CFD blade analyses have only been steady state, a more accurate representation of the complicated flow separation and vortices at locked rotor, would be to run stage transient simulations. These could be used to generate a whole compressor stage by stage. It is recommended that the first and last stages be analysed first due to the findings within this thesis of the differences in losses. The stages in between could be constructed and all combined to form the complete compressor.
- The generic blade loss coefficients generated from this thesis, require further study. Using the transient analysis, as discussed above, a comparison of steady state to transient derived loss coefficients can be evaluated. A locked rotor analysis of a high BPR fan blade would be very useful and add to the data available, though simulating the BPR flow paths and difference in root and tip pressures at windmilling conditions may present a problem. Also all of these should be validated by the cascade test rig results.
- The cascade test rig for windmilling conditions, requires assembly and testing first with the incidence at the axial flow direction, and then at least two other incidences such as design and -80. These results can then be used to validate CFD derived generic loss coefficients, and produce correction factors and deltas for future windmilling CFD analyses.

To understand the combustor light-up efficiencies and influence of evaporation at windmilling light-up, a series of tests or even a study of the same combustor with liquid and gaseous fuel could be conducted. As the gaseous fuel is already evaporated the comparison would indicate, for the same range of operating conditions (particularly pressure), the influence of evaporation compared to the evaporation of the liquid fuel on efficiency.

The gearbox drag in terms of torque at windmilling requires greater understanding from either theoretical methods or a test on an actual gearbox. Driving the gearbox from an electric motor, the power requirements can ascertained, with increasing the load on the driven shafts (measuring this applied load in terms of torque). Also temperature changes to the gearbox oil would be useful, as the effects on the oil viscosity will dramatically effect the gearbox drag. This influence of oil temperature on gearbox drag causes significant scatter, to windmilling working lines.

References

[1] Agrawal, R. K. and Yunis, M. A Generalised Mathematical Model to Estimate Gas Turbine Starting Characteristics. ASME, Journal of Engineering for Power. January 1982, Vol 104, Pgs 194-201.

[2] Allan, C. Combustor heat transfer during start-up. MSc Thesis, Cranfield University, August 2002.

[3] Bittan, J. J. Study of a compressor during windmilling using computational fluid dynamic. MSc Thesis, School of Engineering, Cranfield University, 2005.

[4] Bradsaw, P. Topics in Applied Physics. Turbulence. Second corrected and updated Edition. Volume 12. Springer-Verlag Berlin Heidelberg New York, 1978.

[5] Bragagnolo, N. Ferretti, A. and Venanzetti. Initial Engine Relight Test on Eurofighter 2000. 22 October 1999.

[6] Braig, W. Schulte, H. and Riegler, C. Comparative Analysis of the Windmilling Performance of turbojet and Turbofan Engines. University of Stuttgart, Journal of Propulsion and Power, Vol 15 No.2 March –April 1999.

[7] Caines, B. N. Hicks, R. A. and Wilson, C. W. (Defence Evaluation and Research Agency, Farnborough, UK) AIAA-2001-3573, Joint propulsion conference and exhibit. 37th Salt Lake City, UT, July 8-11, 2001.

[8] Chambard, R. Study of a compressor during windmilling using computational fluid dynamics. MSc Thesis, Cranfield University, August 2002.

[9] Choi, M. S. et al. A Practical Method for Predicting the Windmilling Characteristics of Simple Turbo Jet Engines. ASME 96-TA-60, 1996 ASME Turbo Asia Conference, November 5-7, 1996, Jakarta, Indonesia.

[10] Curnock, B. Engine starting and stopping. In VKI, Gas turbine engine transient behaviour. VKI/LS-1993-06, 1993.

[11] De-You, Yan. And Zhong-Fan, Mai. A Dynamic Model of Turbojet In Starting at High Altitude. Beijing Institute of Aeronautics and Astronautics, Beijing, China. Sixth International Symposium on Air Breathing Engines. Symposium Papers June 6-10, 1983. American Institute of Aeronautics and Astronautics, Paris, France.

[12] Dixon, S. L. Fluid Mechanics and Thermodynamics of Turbomachinery. 5th Edition. Elsevier Butterworth Heinemann.

[13] ESDU, 81009a. Estimation of windmilling drag and airflow of turbojet and turbofan engines. April 1984

[14] ESDU, 81004a. Estimation of spillage drag for a wide range of axisymmetric intakes at M<1. April 1984

[15] Fawke, A. J. and Saravanamuttoo, H. I.H. Digital Computer Methods for Prediction of Gas Turbine Dynamic Response. SAE-71/0550. 1971.

[16] Frost, T. H. Practical bypass mixing systems for fan jet aero engines. The Aeronautical Quarterley, May, p141-160.

[17] Gaudet, S. R. and Donald Gauthier, J. E. A simple sub-idle component map extrapolation Method. GT2007-27193, Proceedings of GT2007, ASME Turbo Expo 2007: Power for Land Sea and Air. May 14-17 2007, Montreal, Canada.

[18] Gostelow. J. P. Cascade Aerodynamics. Pergamon Press, 1984.

[19] Gullila, A. Thrust and flow prediction in gas turbine engine indoor sea-level test cell facilities. PhD Thesis. Cranfield University. 2006.

[20] Haghrooyan, C. Combustor modelling for ignition under windmilling conditions, MSc thesis, Cranfield University, August 200.

[21] Harding, S. Meeting discussing BD19 backed-out combustion efficiencies and light-up data for MSc project. Derby, July 2007

[22] Hatch, J. E. Comparison of Experiementally and Analytically Determined Windmilling Characteristics of a Compressor with Low over-all Pressure Ratio. NACA RM E57L12a.

[23] Hawthorne. W. R. Aerodynamics of turbines and compressors. High speed aerodynamics and jet propulsion. Volume x. Princeton University Press, 1964.

[24] Howard, J. Altitude Relight; Analysis of compressor behaviour during quick-relight and corresponding effects on quick-relight performance. MSc Thesis, School of Engineering, Cranfield University 2003.

[25] Howard, J. Engine A sub-idle 2-spool modelling, BD19, Main Report. Cranfield Rolls-Royce UTC in Performance, Cranfield university. Report 121.1, 2006.

[26] Howard, J. Rolls-Royce report defining EngD Thesis, engine and parameters used. Report 121.2. Cranfield Performance UTC, Cranfield University 2007

[27] Jones, G. Pilidis, P. and Curnock, B. Extrapolation of Compressor Characteristics to the low-speed region for sub-idle performance Modelling. ASME, GT-2002-30649. Proceedings of the 2002 International Gas Turbine and Aeroengine Congress and Exhibition, 3-6 June 2002, Amsterdam, Netherlands.

[28] Jones, G. and Curnock, B. Compressor Characteristics in Gas Turbine Performance Modelling. 2001-GT-0384, Proceedings of ASME Turbo Expo 2001: June 4-7, 2001, New Orleans, Louisiana, USA.

[29] Jones, G. Performance Modelling of Windmilling Gas Turbines. EngD Thesis, Cranfield University, School of Engineering, Oct 2002.

[30] Kendrick, C. CFD analysis of a windmilling high pressure compressor from a three-spool gas turbine. MSc Thesis, School of Engineering, Cranfield University, 2006.

[31] Kerrebrock, J. L. Aircraft Engines and Gas Turbines. 2nd Edition. The MIT Press, 1992.

[32] Kupcic, M. Combustor performance modelling during altitude relight. MSc Thesis, Cranfield University, 2001.

[33] Kurzke, J. How to get component maps for aircraft gas turbine performance calculations. ASME 96-GT-164, International Gas Turbine and Aeroengine Congress & Exhibition, Birmingham, UK June 10-13, 1996

[34] Kurzke, J. Smooth C. User's manual. 1999.

[35] Kurzke, J. Smooth T 7.0. Users manual. 1999.

[36] Kurzke, J. Gasturb, version 8, users manual. 1999.

[37] Lefebvre, A. W. Gas Turbine Combustion. 1983 (1st Edition). McGraw-Hill Book Company.

[38] Leitges, F. Windmilling –validation of component characteristic diagrams in the partial load range. Thesis Diploma, Stuttgart University. November 2004.

[39] Lim, S. K. et all. Study of Windmilling Characteristics of Twin-Spool Turbo–Fan Engines. AIAA 2002-0376, 40th AIAA Aerospace Sciences Meeting & Exhibit, 14-17 January 2002. Reno, NV.

[40] Massey, B. S. Mechanics of Fluids. 6th Edition, Chapman and Hall.

[41] Mattingley, J. D. Elements of Gas Turbine Propulsion.1996. McGraw-Hill Book Company.

[42] Monticelli, M. Engine E BD19 sub-idle model. Report No. PTR23159. Rolls-Royce, 22 November 2003.

[43] Narkiewicz, M. Engine Relight Performance' a combustor analysis. MSc Thesis, Cranfield University, 2007.

[44] Naylor, P.H. Gas Turbine Transient Performance; heat soakage modelling. Cranfield University, Thesis 2004.

[45] Nixon, D. A Theory for the Mixing of a Compressible Round Jet. Department of aeronautical Engineering, Queen's University of Belfast, UK. AIAA 94-2193, June 20-23, 1994 / Colorado Springs, CO. 25th AIA Fluid Dynamics Conference.

[46] Oates, G. C. Aircraft propulsion Systems Technology and Design. American Institute of Aeronautic and Astronautics. Washington D.C. USA, 1989.

[47] Perceval, J. Cascade CFD analysis in windmilling condition. MSc Thesis, School of Engineering, Cranfield University. 2007.

[48] Peters, C.E. and S. Wehofer. Rocket Test Facility ARO, Inc. January 1962. AEDC TR-61/18

[49] Rasse, J. Sub-idle mixer modelling. MSc Thesis. Cranfield University. August 2005.

[50] Rebeske, J. J. and Rohlik, H. E. Acceleration of High-Pressure-Ratio Single-Spool Turbojet Engine as Determined from Component Performance Characteristics. I – Effect of Air Bleed at Compressor Outlet. NACA RM E53A09, March 10. 1953.

[51] Rasse, J. Sub-idle mixer modelling. MSc Thesis. Cranfield University. August 2005.

[52] Rowe, A. Conversation on data and extrapolation. Derby, Jan 2004.

[53] RRAP Synthesis Program BB50 CUG. CUG.BB50.21. Rolls-Royce PLC.

[54] Saravanamuttoo, H. I. H. Gas Turbine Theory. 5th Edition, Prentice Hall.

[55] Slack, N. et al. Operations Management. 4th Edition. Prentice Hall.

[56] Syed, C. 3 shaft turbofan starting synthesis program. CUGG. Rolls-Royce, report number CUGBD19, issue 2, 1996.

[57] Vincent, K. R. Huntley, S. C. and Wilsted, H. D. Comparison of lockedp-rotor and widmilling drag characteristics of an axial-flow compressor type turbojet engine. Lewis flight propulsion laboratory, Cleveland, Ohio, Naca RM E51K15, 1952.

[58] Walker, C. L. and Fenn, D. B. Investigation of Power Extraction Charactersitics and Braking Requirements of a Windmilling Turbojet Engine. NACA RM E52D30.

[59] Walsh, P. P. and Fletcher, P. Gas Turbine Performance.1998. Blackwell Science Ltd.

[60] Zedda, M. CD87: a tool to size combustion volume for relight and pullaway – engineering description. Rolls-Royce. 2005.

[61] Zwede, B. Gas turbine mixers during windmilling and starting. Report no. 51030. Rolls-Royce.